UiO : Department of Geosciences
University of Oslo

Ozone Above the Tropical Atlantic Ocean

Sigrid Marie Vildskog Auganæs

Master's Thesis, Spring 2023

Abstract

Ozone (O_3) plays a crucial role in the Earth's atmosphere, both in the stratosphere and the troposphere. This thesis investigates tropospheric ozone above the tropical Atlantic Ocean using observations, trajectories and the Norwegian Earth system model (NorESM). The research questions addressed include the presence of a minimum in tropospheric ozone over the tropical Atlantic, the comparison of ozone profiles between ship campaigns and land-based stations, the variability of ozone above the Atlantic compared to other ocean basins, and the performance of NorESM in representing observed ozone features.

Observations from the SO287 CONNECT ship campaign crossing the tropical Atlantic Ocean reveal no ozone minimum similar to that previously observed in the tropical West Pacific. Ozone concentrations over the tropical Atlantic ranged from 25 to 80 parts per billion (ppb), with an average of 45 ppb throughout the troposphere. The sampled air masses exhibited characteristics from different regions, indicating biomass burning and stratospheric influences. Comparisons with nearby SHADOZ stations confirmed the successful sampling of the same air mass by the ship campaign and the Paramaribo SHADOZ station.

Furthermore, the ozone concentrations from ship campaigns in different tropical ocean basins, revealed higher ozone concentrations above the tropical Atlantic compared to other tropical ocean basins. The NorESM model, newly including the MOZART-TS1 chemistry scheme, captures the expected patterns of surface ozone and wave-one distributions, with some deviations. However, the model simulates the abrupt increase to stratospheric ozone at lower altitudes than observed, likely due to coarse resolution in the upper troposphere and stratosphere.

Samandrag

Ozon (O_3) spelar ei avgjerande rolle i atmosfæren både i stratosfæren og troposfæren. Denne avhandlinga undersøker troposfærisk ozon over det tropiske Atlanterhavet ved hjelp av observasjonar, trajektoriar og den norske jordsystemmodellen (NorESM). Forskingsspørsmåla som blir svara på inkluderar tilstadeværet av eit minimum av troposfærisk ozon over det tropiske Atlanterhavet, samanlikning av ozonprofilar mellom skipskampanjar og landbaserte stasjonar, variasjonen i ozon over Atlanterhavet samanlikna med andre havbasseng, og kor godt NorESM modellen representerer observerte ozoneigenskapar.

Observasjonar frå SO287 CONNECT skipskampanjen som kryssa det tropiske Atlanterhavet, avslører ingen ozonminimum lik det som førre er observert i det tropiske vestlige Stillehavet. Ozonkonsentrasjonar over det tropiske Atlanterhavet varierte frå 25 til 80 delar per milliard (ppb), med eit gjennomsnitt på 45 ppb gjennom troposfæren. Dei analyserte luftmassane viste karakteristiske eigenskapar frå ulike regionar, som indikerer skogbrannar og stratosfæriske påverknader. Samanlikningar med nærliggande SHADOZ stasjonar bekrefta vellykka prøvetaking av dei same luftmassane av skipskampanjen og Paramaribo SHADOZ stasjonen.

Vidare er ozonkonsentrasjonar frå skipskampanjar i med ulike tropiske havbasseng samanklikna, og avdekkjer høgare ozonkonsentrasjonar over det tropiske Atlanterhavet samanlikna med andre tropiske havbasseng. NorESM, inkludert MOZART-TS1 kjemisystemet, fanger opp dei forventa mønstera av overflateozon og wave-one distribusjonar, med nokre avvik. Likevel simulerer modellen den brå økinga av ozon på lågare høgde enn det som er observert, sannsynlegvis på grunn av grov oppløysing i øvre troposfære og stratosfære.

Acknowledgements

I would like to express my deepest gratitude to my supervisors for their invaluable support and guidance throughout the completion of this master's thesis. Kirsten "Kicki" Krüger, I am incredibly grateful for your research expertise and insightful discussions. You provided me with the perfect master project and the opportunity to participate in a campaign and conduct my own measurements. Your dedication and attention to detail have been essential in shaping this thesis.

Birgit Quack, I extend my heartfelt thanks for not only taking me on board as a master student, but also on board the RV Sonne. Under your exceptional leadership, I had the time of my life and gained invaluable experiences.

Katrin Müller, I appreciate your assistance in providing the necessary resources for my ozone-sonde preparations during the campaign. Your helpful comments, guidance, and unwavering positivity have motivated me more than you can imagine. You will always be welcome back in my Overleaf documents.

Dirk Olivie, I am grateful that you have helped me to use the NorESM and for patiently addressing all my questions, never considering any of them as "stupid". Your support has been invaluable to the progress of this research.

I would also like to extend my thanks to the DWD Lindenberg, in particular Susanne Körner for teaching me how to prepare and launch ozone-sondes.

To the scientists and crew aboard the SO287 CONNECT campaign on RV Sonne, I am indebted to you for not only making my month at sea an unforgettable and enjoyable experience but also for your assistance in launching my ozone-sondes. Special thanks to Alexandra Rosa, Jesus Reis, and Claudio Cardosso for being an exceptional radiosonde team, and eating sauce like soup (still launching about it). Obrigado!

I would like to express my gratitude to my fellow master students creating a fun and good environment in our study room. Especially thanks to Ingrid and Anne Gro for the emotional support. Thanks to Thorbjørn and Carina, without you two I wouldn't have made it this far.

Thanks to my parents and brother (and those who act like substitutes for either one) for always supporting me, and never doubting me for a second.

Contents

List of Figures

List of Tables

PART I

Introduction and Background

CHAPTER 1

Introduction

1.1 Motivation

Ozone (O_3) is a naturally occurring gas that plays a crucial role in the atmosphere. Although ozone is typically associated with the stratosphere where it reaches its maximum concentration, it also exhibits important properties in the troposphere. In the stratosphere, ozone protects us against harmful high-frequency radiation from the sun through a photochemical cycle (Brasseur and Jacob, 2017). Meanwhile, in the troposphere, ozone is produced by reactions of emitted chemical compounds and is a greenhouse gas that is harmful to humans and plants (Schwela, 2000, Reich and Amundson, 1985). Additionally, ozone plays a vital role in controlling the oxidation or "cleaning" of tropospheric air by serving as a precursor to the hydroxyl radical (OH) (Brasseur and Jacob, 2017). While ozone has a lifetime on the order of days in the troposphere, the OH radical has an extremely short lifetime as it oxidizes hundreds of chemical species and hence "shields" the stratosphere from surface emissions (WMO, 2011). However, measuring the concentrations and variability of tropospheric OH is challenging and an ongoing research topic (Montzka et al., 2011). Since ozone is a major precursor of OH, ozone measurements can be used as a proxy for OH.

As presented by Rex et al. (2014), there is a pronounced tropospheric ozone minimum over the tropical West Pacific. This region is the main source of tropospheric air that reaches the stratosphere, due to the strong convective activity in the area and enhanced transport within the tropical tropopause layer (TTL) (Rex et al., 2014, Krüger et al., 2009). Low amounts of tropospheric oxidants in this area can contribute to ozone-depleting substances reaching the stratosphere. The ozone profiles used in Rex et al. (2014) were conducted on the 2009 TransBrom cruise from Tomakomai, Japan to Townsville, Australia onboard the research vessel (RV) Sonne, and showed very low tropospheric ozone values within the detection limit of the ozone-sonde instrument.

Electrochemical Concentration Cell (ECC) sondes are the most widely used ozone-sondes to measure ozone profiles in situ up to 35 km altitude (Smit, 2014, Smit et al., 2007). There are many land-based stations that launch regular ozone-sondes (Smit, 2014), including the network called the Southern Hemispheric ADitional OZone-sondes (SHADOZ) with 14 stations. Though such an abundance of vertical ozone data has not always been available (Smit et al., 1990). SHADOZ provides a long record of high-quality ozone-soundings starting in 1998 (Witte et al., 2017). Apart from data collected at stations close to marine environments, not a lot of vertical ozone data is available over the oceans, especially not long time series. Four ship campaigns onboard the old RV Sonne have conducted ozone measurements using ECC ozone-sondes over the tropical oceans, including the tropical East Pacific, tropical West Pacific, and the Indian Ocean. The SO287 CONNECT ship campaign in December 2021 to January 2022 was the first ship campaign on board RV Sonne that sampled ozone profiles over the tropical Atlantic Ocean.

Earth system models are models that simulate the interactions and dynamics of various components of the Earth system. They are complex models that combine multiple sub-models representing different aspects of the Earth, such as the atmosphere, oceans, land surface, ice, and biogeochemical cycles. Initiatives like the Coupled model intercomparison project (CMIP) coordinate and compare the output of climate models from different research institutions Eyring et al., 2016. CMIP has played a crucial role in advancing climate science, supporting the development of climate models, improving understanding of climate variability and change, and providing a scientific basis for the assessment reports of the Intergovernmental Panel on Climate Change (IPCC) (Naik et al., 2021) The NorESM is an Earth system model that is part of CMIP, and is currently under development to incorporate full chemistry.

The main objective of this thesis is to investigate tropospheric ozone above the tropical Atlantic Ocean, using observation and NorESM.

1.2 Objective

The thesis work includes training in ozone-sonde preparation and launches at the Deutscher Wetter Dienst (DWD) in Lindenberg, Germany, and a month-long ship campaign onboard RV Sonne crossing the Atlantic from December 2021 to January 2022. Ozone- and radiosonde data from this campaign are post-processed and analyzed to obtain an overview of the meteorological situation and ozone distribution in the sampled area and are compared to nearby land-based SHADOZ stations for validation. Data from four additional ship campaigns onboard RV Sonne in the tropical East Pacific, tropical West Pacific, and the Indian Ocean are compared to results from the SO287 CONNECT to investigate

the differences between the ozone concentrations above tropical oceans. In addition, case studies involving trajectories from the HYSPLIT model are utilized to better understand the unique characteristics of the observations from SO287 CONNECT.

In order to validate the performance of NorESM and its new chemistry scheme, the model's output will be evaluated by comparing expected or observed signatures in ozone against a historical run spanning the years 1980 to 2014. The model will also be used to aid the interpretation of observational results.

The following research questions will be addressed:

- Is there a minimum in tropospheric ozone above the tropical Atlantic?
- Did the SO287 CONNECT campaign sample the same air as the nearby SHADOZ stations?
- How does ozone in the troposphere vary above the Atlantic compared to other ocean basins?
- Does NorESM represent the expected and observed ozone features in the tropics?

1.3 Outline

The rest of the thesis is organized as follows:

Chapter 2 is the introduction to background material relevant to this study.

Chapter 3 provides an overview of the data used in this thesis.

Chapter 4 presents the methods used to obtain data and produce results for this study in regard to observations. It also includes information about the NorESM and the experiment used in this thesis.

Chapter 5 and **Chapter 6** feature the main results from observations and modeling, respectively.

Chapter 7 holds the discussion of main findings.

Chapter 8 draws the thesis to a close with a conclutson.

Appendix A features additional material, like individual radiosonde profiles.

CHAPTER 2

Background

This chapter aims to provide an overview of the key background theories that are relevant to this study. To begin with, the chapter introduces the structure of the atmosphere, with a focus on the troposphere and stratosphere. Subsequently, an overview of the general circulation of the atmosphere and its fluctuations are presented. Additionally, important and basic concepts of atmospheric chemistry that govern this study are introduced. Lastly, the chapter explains the workings and operation of an ECC Ozone sonde.

2.1 Structure of the atmosphere

The Earth's atmosphere can be vertically divided into distinct layers, with various criteria used to differentiate them, including temperature, gas composition, and electrical properties (Ahrens and Henson, 2016). The most prevalent method for characterizing these layers is by using the temperature profile and lapse rate. By determining whether the temperature decreases or increases with height, we can identify five different layers and spheres in the atmosphere. An illustration of the four lower spheres, their temperature properties, and their vertical placement is presented in Figure 2.1.

2.1.1 Troposphere

The troposphere is the lowest layer of Earth's atmosphere, extending from the surface up to an altitude of about 10 to 17 km (Ahrens and Henson, 2016). It contains roughly 75% of the atmosphere's total mass and is the sphere where all of Earth's weather occurs (Zell, 2015). Starting from the surface going upwards, the temperature decreases mainly due to the decrease in pressure. The word "troposphere" comes from the Greek word "tropein," meaning "to turn" or "to change," referring to the moving air masses in the layer. The movement of air masses is caused by incoming solar radiation, which warms the Earth's surface

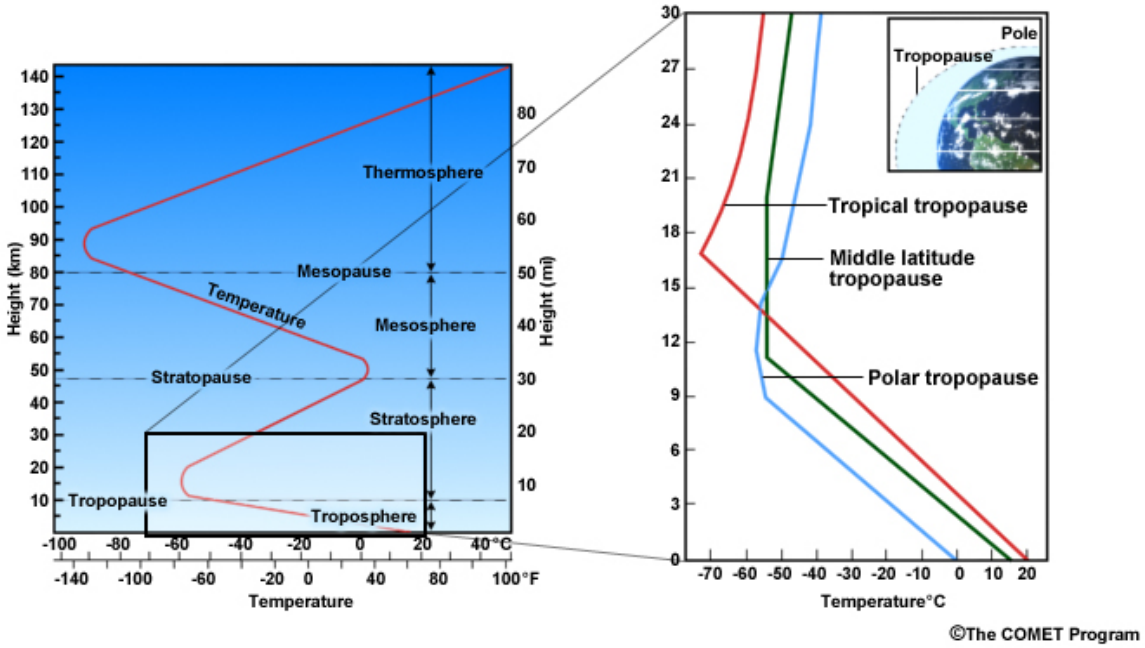

Figure 2.1: The vertical structure of the atmosphere is illustrated on the left, with a closer look at the troposphere and tropopause on the right. Figure from UCAR (n.d.).

and the air above it, resulting in convective activity and differences in surface pressure (Stevens, 2010).

The lower part of the troposphere, usually spanning 2-3 km altitude above surface, is the boundary layer (Ahrens and Henson, 2016). The boundary layer is influenced by the direct contact with the Earth's surface and its roughness, such as land with different properties or oceans. This layer is usually turbulent, and exchanges energy, mass, and momentum between the surface and the overlying air masses (Wallace and Hobbs, 2006).

After a distance of 10 to 17 km, the temperature in the atmosphere stabilizes and stops decreasing, marking the tropopause. This is the boundary that distinguishes the troposphere from the stratosphere. Various methods are used to define the tropopause, including the cold point and lapse rate. For the cold point tropopause (CPT), the lowest temperature in the profile determines the tropopause (Highwood and Hoskins, 1998). This method is suitable for regions like the tropics, where the temperature profile has a distinct cold point. However, in other regions, the CPT method may be challenging due to the presence of multiple or less-defined cold points, as shown in Figure 2.1. In such cases, the lapse rate tropopause (LRT) is used, where the tropopause is

the lowest point where the temperature lapse rate is 2°C/km or less and does not exceed this threshold within 2 km (WMO, 1957). This means that the tropopause is located where the temperature does not decrease significantly with altitude. Regions with a large separation between til CPT and LRT are associated with the extratropical upper troposphere, where atmospheric dynamical waves create the deviation (Pan et al., 2018, Munchak and Pan, 2014). These areas with large deviations of CPT and LRT do not need to be in the vicinity of the subtropical jets.

The height of the troposphere and tropopause exhibit latitude-dependent variations. As illustrated in the upper right corner of Figure 2.1, the troposphere's thickness varies significantly between high and low latitudes. The thickness variation is attributed to the Earth's rotation and thermal expansion (Wallace and Hobbs, 2006). The tropopause altitude is higher over the equator than the polar regions and is also present at higher altitudes in summer than in winter, also due to thermal expansion. However, locating the tropopause in subtropical regions can be extremely challenging, even with the CPT and LRT methods. In such areas, strong winds in the jet streams lead to a mixing of the tropospheric and stratospheric air masses, leading to a break in the tropopause (Ahrens and Henson, 2016).

Especially in the tropics, the concept of a clear separation between the troposphere and stratosphere does not hold. In the tropics, the Tropical tropopause layer (TTL) serves as the transition zone between tropospheric and stratospheric air in a couple of kilometers thick layer (Tegtmeier and Krüger, 2022, Folkins et al., 1999). The TTL shares dynamical properties with both the stable-layered stratosphere and the convective troposphere. The layer is on average located with a lower boundary near 14 km altitude, an upper boundary at 18.5 km altitude, and laterally constrained by the subtropical jets (Fueglistaler et al., 2009). Different approaches are used to identify the boundaries of the TTL. The lower boundary can be defined by the upper tropospheric ozone minimum, where the ozone mixing ratio reaches 90 ppb within the TTL. The upper boundary can be defined by the CPT (Fueglistaler et al., 2009).

2.1.2 Stratosphere

The stratosphere is a layer of the Earth's atmosphere situated just above the troposphere. Unlike the troposphere, which is well-mixed, the stratosphere is stratified, hence its name. This layer is characterized by stable layers of air that prevent the vertical mixing of gases, leading to a distinct layering of atmospheric components (Ahrens and Henson, 2016). The most well-known phenomenon of the stratosphere is the ozone layer, which plays a critical role in protecting life on Earth from the harmful effects of ultraviolet (UV) radiation (Section 2.3).

The temperature characteristic of this layer is the temperature inversion, meaning the temperature increases with altitude. The reason why the stratospheric temperature increases with altitude is due to the absorption of the maximum solar insolation by ozone at 15- 40 km altitude, a process that will be further explained in Section 2.3.

2.2 General circulation of the atmosphere

In the interest area of this thesis, the ozone abundance is affected by large-scale transport and the general circulation (GC) of the troposphere and stratosphere, in addition to meteorology (Lu et al., 2019). The predominant concepts of this large-scale overturning circulation will be introduced in this section.

The primary force of the GC of the atmosphere is the incoming solar radiation. This imbalance of energy between the warmer tropical regions and the cold poles has to be equalized and hence drives the dynamics in the troposphere. Radiative imbalance combined with the Coriolis effect resulting from the Earth's rotation creates three tropospheric overturning cells; Hadley, Ferrel, and polar cell. A visual representation of the zonally continuous cells is shown in Figure 2.2.

In the low latitudes near the equator, intense solar radiation causes the surface to heat up, resulting in warm air masses rising, generating low pressure at ground level. The ascending air expands and cools before descending back to the surface in the sub-tropics around 30 ° N/S. To balance the low pressure at the equator, air from higher latitudes flows towards lower latitudes, resulting in so-called "trade winds" that are deflected to the right in the Northern Hemisphere and left in the Southern Hemisphere due to the Coriolis effect. This thermally direct cell is known as the Hadley cell.

Between 60 and 90 ° N/S are the polar cells. These cells are also thermally direct, with sinking cold air at the poles that flow toward lower latitudes. Around 60 ° N/S, cold air meets warmer air from the lower latitudes, creating the polar front.

The Ferrel cell, located between the Hadley and polar cells, is unique in that it is thermally indirect, with air flowing in the opposite direction to the Hadley and polar cells. The reason why this cell circulates in a thermally indirect pattern is that it is influenced by the movement of the neighboring Hadley and Polar cells.

In the upper troposphere, forming at the boundaries between the different circulation cells, exists fast-moving, narrow bands of westerly winds. These winds, also known as jet streams, develop due to strong horizontal gradients in

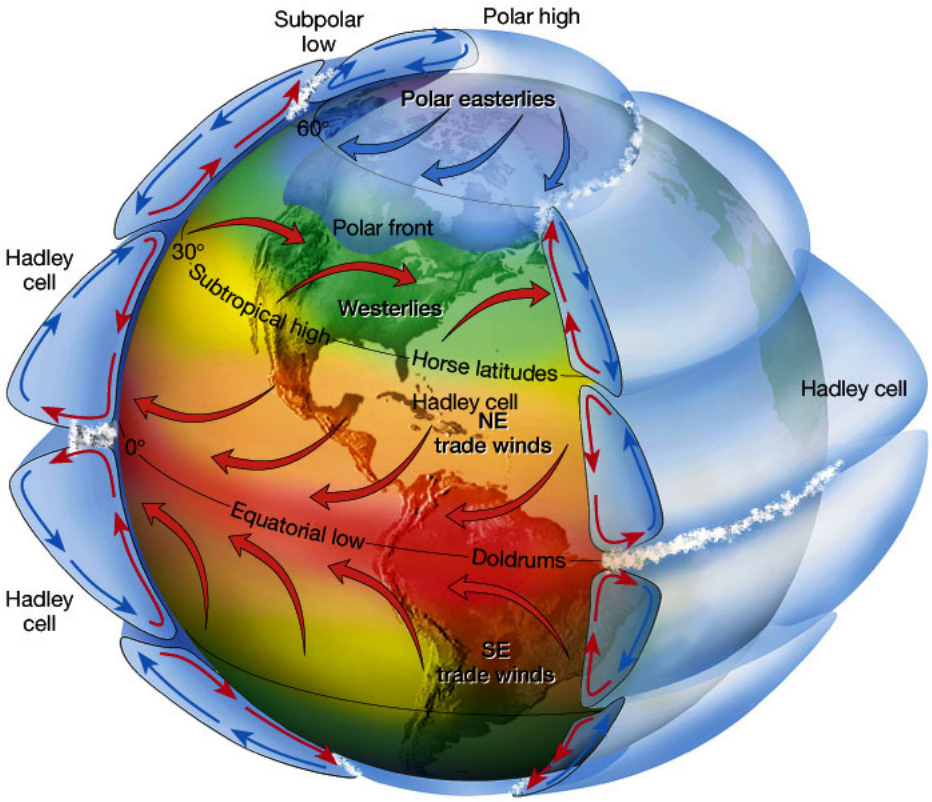

Figure 2.2: The general circulation of the troposphere and surface. Figure from Garrison (2014)

temperature and pressure and can reach wind speeds of up to 400 km/h (Ahrens and Henson, 2016). There are two major jet streams in each Hemisphere, the subtropical jet streams at around 30 °N/S and the polar jet streams around 60 °N/S. Both jet streams are located at an altitude where the strong winds cause tropospheric and stratospheric air to mix, often called a tropopause break or gap (Ahrens and Henson, 2016).

2.2.1 The Inter-Tropical Convergence Zone

Where the trade winds converge between the Hadley cells is called the Inter-Tropical Convergence Zone (ITCZ). The narrow area of the ITZC is usually very wet, due to strong convection leading to thunderstorms, lightning and heavy rainfall (Ahrens and Henson, 2016). The clouds along the ITCZ can form long continuous bands, making the zone easy to spot on satellite imagery. On average, the ITZC can be found at 6 °N but shifts seasonally towards the corresponding summer Hemisphere (Schneider et al., 2014).

Being the area where Northern and Southern Hemispheric air masses converge,

the ITCZ marks the boundary between the two different air masses. Atmospheric chemistry-wise, mixing between hemispheres is on a time scale of years (Jacob, 1999). Due to more land mass and higher population, emissions of pollutants and ozone precursors from combustion, industry, and biomass burning emissions are more prominent in the Northern Hemisphere (Brasseur and Jacob, 2017). This makes the ITCZ a boundary and an area of mixing between the clean Southern Hemispheric air, and the more polluted Northern Hemispheric air.

2.2.2 The Walker circulation

In the equatorial Pacific region, there is a zonal circulation driven by surface temperature differences and the lack of Coriolis force. The Walker circulation has a strong rising air branch over the tropical West Pacific, with low sea level pressure and the globally highest sea surface temperatures (SST). The air sinks again above the equatorial eastern Pacific, creating a descending branch. Trade winds transport the air back across the Pacific, while upper-level westerly winds connect the rising and sinking branches, creating a circulation cell. A schematic of the Walker circulation is illustrated in Figure 2.3a. During El Niño (see Section 2.2.3) the Walker circulation can weaken, shift or even reverse. A shifted Walker circulation can be seen in Figure 2.3b.

2.2.3 El Niño Southern Oscillation

The Equatorial Pacific phenomenon called El Niño Southern Oscillation (ENSO), is a coupled atmosphere-ocean phenomenon that has repercussions throughout the globe (Hakim and Patoux, 2018). The oscillation is described as low-frequency variations in SST, sea-level pressure, and surface-level wind patterns in a time frame of 2-7 years (Oman et al., 2011).

Under neutral conditions, there is normal Walker circulation and easterly trade winds which leads to coastal upwelling outside the equatorial West coast of South America. SSTs in the eastern Pacific are colder due to the upwelling and a constant high atmospheric sea level pressure due to descending cold air from the Walker circulation. The easterly trade winds blowing across the Pacific push the warm surface water towards the western Pacific, resulting in higher air temperatures, rising air, and low atmospheric sea surface pressure.

The cold phase, known as La Niña, is similar to the neutral conditions but amplified. It usually follows directly after the warm phase El Niño. Trade winds strengthen and amplify the coastal upwelling in the eastern Pacific. A visual representation of SST and the Walker circulation during a La Niña can be seen in Figure 2.3a.

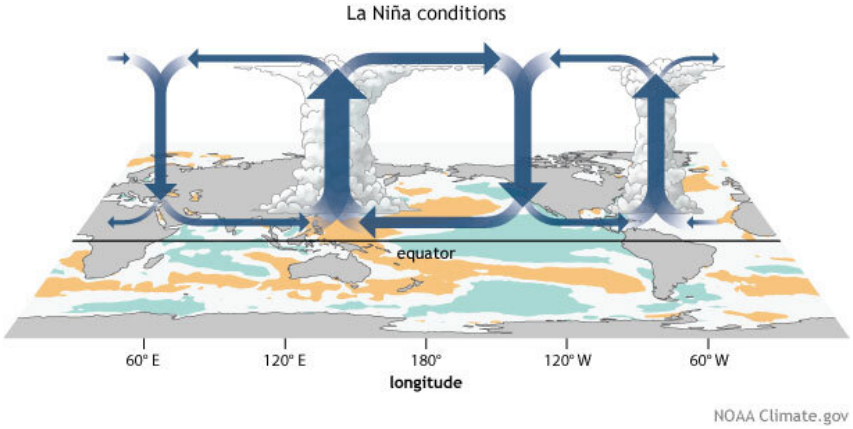

(a)

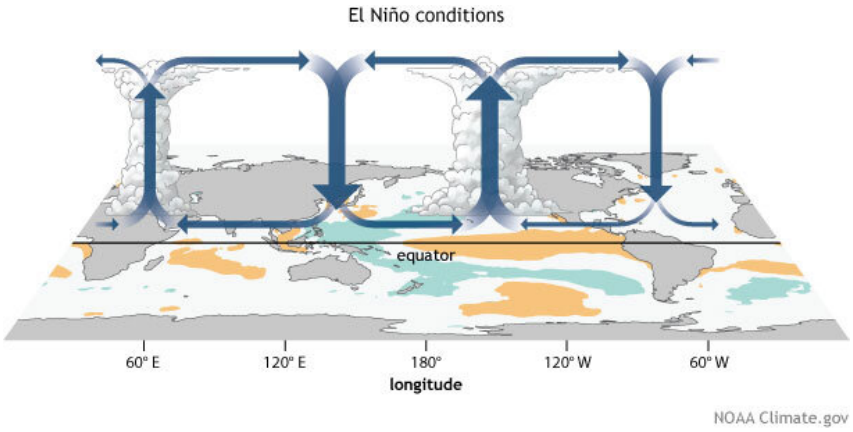

(b)

Figure 2.3: Schematic illustrating the La Niña (a) and El Niño (b) conditions. Blue and orange shading indicates cold and warm SST anomalies, respectively. Overlaying generalized visualization of the shift in the Walker circulation. Figure from NOAA, Downloaded 12.04.2023.

During an El Niño phase the conditions reverse. The trade winds weaken or turn westerly, prohibiting the coastal upwelling in the eastern equatorial Pacific. Warm SSTs are accompanied by convection and precipitation due to an eastward shift of the Walker circulation. Western equatorial Pacific SST turns cold, and atmospheric conditions turn dry due to the downward transport of dry air from the sinking branch of the Walker circulation.

There are several different ways to quantify and indicate what phase of ENSO the system is currently in. The most commonly used one is the 3.4 Oceanic Niño Index (ONI), which is defined by the SST temperature anomaly in a specific region of the equatorial Pacific Ocean. If the average SST is above or below the threshold of 0.5 K from the mean, it is an El Niño or La Niña, respectively

(Trenberth, 2023).

ENSO can affect atmospheric ozone concentrations (Oman et al., 2011). The response of tropical tropospheric ozone is consistent with changes in the Walker circulation. Positive anomalies in the 3.4 Niño index coincide with positive sensitivities in tropospheric ozone in the western Pacific and Indian Ocean. The opposite occurs in the eastern and central Pacific, where positive anomalies in 3.4 Niño index coincides with negative sensitivities in the upper troposphere (Oman et al., 2011).

2.2.4 Brewer-Dobson circulation

The Brewer-Dobson circulation is an atmospheric wave-driven meridional circulation in the stratosphere. This slow circulation moves air rising in the tropics towards the poles, with the strongest branch usually directed towards the winter pole. In the tropics, the rising branch of the Hadley cell pushes air from below and the BD circulation simultaneously works as a pump, sucking air upward, contributing to a higher tropopause, especially in the northern hemisphere winter (Butchart, 2014). Ozone-rich air from the tropical stratosphere is in this way transported to the polar regions, increasing the ozone concentration.

2.2.5 Quasi-Biennial Oscillation

The Quasi-Biennial Oscillation (QBO) is a variation of zonal wind direction in the tropical stratosphere. The QBO has a mean period of 28 months and causes most of the interannual variability of ozone above the altitude of 20 kilometers (Lee et al., 2010). The easterly phase contributes to Lower amounts of ozone in the lower stratosphere, because of more upwelling that enhances the transport towards the poles (Baldwin et al., 2001).

2.3 Atmospheric chemistry

The atmospheric chemistry and gas composition of the atmosphere is not only important for life on Earth but also for its properties and dynamics. There are many different ways of expressing the concentrations in the atmosphere, Mole fractions (mol/mol) are the most common and are also referred to as "mixing ratio" (Brasseur and Jacob, 2017). The mole fraction is the ratio of the number of moles of one substance to the total number of moles in the mixture (Brasseur and Jacob, 2017). Table 2.1 gives an overview of the gas abundance in the atmosphere. In addition to the main contributors to the atmospheric composition, we have an abundance of trace gases and aerosol particles. Tracers are gases or molecules that have mixing ratios below 10^{-3}

Table 2.1: Mixing ratios of dry air, excluding water vapor. Table and caption from Brasseur and Jacob, 2017.

Gas	**Mixing ratio (mol/mol)**
Nitrogen (N_2)	0.78
Oxygen (O_2)	0.21
Argon (Ar)	0.0093
Carbon dioxide (CO_2)	$400 \cdot 10^{-6}$
Neon (Ne)	$18 \cdot 10^{-6}$
Ozone (O_3)	$0.01 - 10 \cdot 10^{-6}$
Helium (He)	$5.2 \cdot 10^{-6}$
Methane (CH_4)	$1.8 \cdot 10^{-6}$
Krypton (Kr)	$1.1 \cdot 10^{-6}$
Hydrogen (H_2)	$500 \cdot 10^{-9}$
Nitrous oxide (N_2O)	$350 \cdot 10^{-9}$

mol/mol, while aerosols are solid or liquid particles with a size of 0.01 to 0.10 μm and are typically measured in particles per cm^3 (Brasseur and Jacob, 2017). Aerosol particles and trace gases do not contribute a lot to the total mass of the atmosphere but are important for atmospheric reactivity and environmental impacts (Brasseur and Jacob, 2017).

When a substance exists in low mixing ratios it is convenient to present them as a fraction, usually parts per million (ppm), parts per billion (ppb), or parts per trillion (ppt). This unit is often used when dealing with pollutants and trace gases and refers to the volume of one substance to the total volume of the mixture, expressed in the most suitable fraction. (Brune, 2020).

The major components listed in Table 2.1, trace gases and water vapor (H_2O) react and drive the chemical processes in the atmosphere. To attain fast chemistry, radical reaction chains are usually involved. Radicals are chemicals with unfulfilled electron orbits and are therefore seeking to fill that empty electron space, resulting in faster reactions (Brasseur and Jacob, 2017). A reaction involving a radical usually produces a new radical, starting a chain reaction. Photolysis can be the process that makes radicals, where high-energy solar insulation causes cleavage of non-radicals. Solar radiation is therefore crucial to driving the chemistry in the atmosphere, as the main component in photochemistry (Brasseur and Jacob, 2017).

The following reactions and information presented under Section 2.3.1 are from Brasseur and Jacob (2017), if not cited otherwise.

2.3.1 Ozone

Ozone, a molecule composed of three odd oxygen atoms, plays a vital role in the Earth's atmosphere, protecting us from harmful ultraviolet radiation from the

sun. The distribution of ozone is not uniform throughout the atmosphere. The stratosphere contains 90% of the planet's ozone. Ozone is a chemically active gas in the atmosphere with a large range of lifetimes, ranging from days to months in the troposphere. Although the troposphere has much lower concentrations of ozone than the stratosphere, ozone chemistry is still very important here. In the upper troposphere, ozone is a potent greenhouse gas (Mohnen et al., 1993, Naik et al., 2021). In the lower troposphere, ozone is a toxic gas that provides health risks for humans, animals, and plants (Schwela, 2000, Reich and Amundson, 1985). The chemistry of ozone in both the stratosphere and troposphere is complex and highly dependent on a range of factors, including solar radiation, temperature, and the presence of other atmospheric gases. The following sub-sections, the chemistry of ozone in both spheres and the factors that influence its formation and depletion will be introduced.

Stratospheric ozone

Production of ozone in the stratosphere starts in the following way; Molecular oxygen (O_2) gets photolyzed:

$$O_2 + hv \rightarrow O + O \tag{R1}$$

where hv refers to incoming solar radiation with a wavelength of 242 nm or shorter. The single oxygen atom can then react with molecular oxygen in a three-body reaction to form ozone (O_3),

$$O + O_2 + M \rightarrow O_3 \tag{R2}$$

where M is the third body, which can be for example N_2 or O_2. The third body is present in the reaction equation to prohibit the limitation of the kinetics of the reactions. In the case of reaction R2 the third body takes up internal energy, stabilizing O_3 in its ground state while releasing heat. This is the reason why the stratosphere has a temperature inversion in addition to the absorption of UV radiation.

Reaction R1 is considered to be the main source of O_3 in the stratosphere, as it is a crucial precursor for reaction R2 to take place. The rate of reaction R1 occurs increasingly less with decreasing height and is negligible below 20 km altitude.

O_3 is rapidly photolyzed due to its loose bonds by

$$O_3 + hv \rightarrow O + O_2 \tag{R3}$$

Radiation with a shorter wavelength than 1180 nm is included here as hv, though O_3 has three principal bands of absorption. The three bands are the Hartley band (200 - 290 nm), the Huggins band (310 - 400 nm), and the Chappius band (400-850 nm), resulting in different levels of excited single oxygen atoms. The ground state single oxygen produced by reaction R3 can produce O_3 by again reacting with O_2 in reaction R2, or it can react with O_3,

$$O + O_3 \rightarrow O_2 + O_2 \tag{R4}$$

In the stratosphere, the production and loss of O_3 are called the Chapman mechanism and are primarily driven by four reactions: R1, R2, R3, and R4. During the daytime, reactions R2 and R3 play a key role in maintaining equilibrium between O and O_3. Single oxygen atoms are rapidly interchanged between O and O_3 with a lifetime of around one second in relation to with reaction R2. Thus, reaction R2 is not a sink for O, while reaction R3 is not a true sink for O_3. The concentration of O_3 in the stratosphere is regulated by reaction R1, which produces more single oxygen atoms, and reaction R4, which removes both single oxygen atoms and O_3. The Chapman mechanism does not take into account ozone-depleting catalytic cycles.

The hydroxyl radical

The hydroxyl radical (OH) is a highly reactive molecule that plays a critical role in atmospheric chemistry. It is a key player in the oxidation of many pollutants in the atmosphere and thus cleaning the air we breathe in addition to tropospheric air entering the stratosphere, and is often referred to as the "detergent" of the atmosphere (Rex et al., 2014). The OH radical is also involved in the natural cycling of important atmospheric gases, including methane (CH4) and carbon monoxide (CO). The concentration of OH in the atmosphere is highly variable and is influenced by a wide range of factors. In addition, OH is very short-lived, which makes it difficult to measure in situ (Montzka et al., 2011).

OH is produced in a reaction between water vapor and an excited single oxygen atom originating from photolysis of O_3. This ozone loss mechanism is prominent in the tropics with warm and humid conditions near the marine boundary layer:

$$O^* + H_2O \rightarrow OH + OH \tag{R5}$$

The hydroxy radical then goes on to create a catalytic cycle:

$$O_3 + HO \rightarrow HO_2 + O_2 \tag{R6}$$

$$O_3 + HO_2 \rightarrow OH + O_2 \tag{R7}$$

Here, the OH reacts with O_3, producing a hyperperoxy radical (HO_2). The HO_2 also reacts with O_3 in reaction R7 returning to OH, creating a catalytic ozone-depleting cycle. Another possibility is for OH to react with a single oxygen atom, producing a single hydrogen atom and O_2, resulting in a different catalytic cycle for ozone loss. H, OH, and HO_2 are considered a chemical family called the HO_X-family and contribute to the HO_X-catalytic ozone loss in the troposphere.

The relationship between ozone and water vapour (relative humidity) in the troposphere is a topic of research (Shiotani et al., 2002, Thompson et al., 2000, Müller, 2020). Studies have found that ozone and relative humidity have an anti-correlation in ozone profiles that are "layered". In low ozone, humid conditions in the tropics, dry and high ozone layers are associated with advection, though ozone alone is not a good indicator of air mass origin (Müller, 2020).

Tropospheric ozone

Production of tropospheric O_3 is dependent on the oxidation of CO, CH_4 and volatile organic compounds (VOC) initiated by OH. For this process to take place, odd nitrogen oxide radicals (N or NO_2, commonly referred to as NO_X) needs to be present. In the case of CO,

$$CO + OH \rightarrow CO_2 + H \tag{R8}$$

followed by

$$H + O_2 + M \rightarrow HO_2 + M \tag{R9}$$

produces HO_2. Similarly for CH_4 the reaction

$$CH_4 + OH \rightarrow CH_3 + H_2O \tag{R10}$$

followed by

$$CH_3 + O_2 + M \rightarrow CH_3O_2 + M \tag{R11}$$

and

$$CH_3O_2 + NO(+O_2) \rightarrow NO_2 + HO_2 + CH_2O \tag{R12}$$

Where O_2 in parentheses indicates that it is needed for the reaction, but does not limit the kinetics. Nitrogen oxide radicals are emitted into the atmosphere mainly by combustion engines, lightning, biomass burning, or microbial activity in the soil. Due to its short lifetime, the NO_X concentration is more prominent over highly populated continental areas. In the presence of NO_X, formation of O_3 happens by

$$HO_2 + NO \rightarrow OH + NO_2 \tag{R13}$$

followed by

$$NO_2 + hv \rightarrow NO + O^* \tag{R14}$$

and

$$O^* + O_2 + M \rightarrow O_3 + M \tag{R15}$$

Providing the net reactions

$$CO + 2O_2 + hv \rightarrow CO_2 + O_3 \tag{R16}$$

where hv is radiation with wavelength below 320 nm, and

$$CH_4 + 4O_2 + hv \rightarrow CH_2O + H_2O + 2O_3 \tag{R17}$$

for CO and CH_4, respectively.

For regions with concentrations of VOC, which comes from biogenic, combustion, and industrial processes, the rate of O_3 production depends linearly on the concentrations of NO_X. CO and other non-methane hydrocarbons are also considered common markers for biomass burning (Blake et al., 1999). Ozone-rich layers in the mid-troposphere have been linked to biomass burning by several studies (Thompson et al., 2000, Oltmans et al., 2001). Similar to reaction R13, an organic peroxy radical RO_2 reacts with NO the same way HO_2 would and goes on to produce O_3. In high NO_X regimes, like highly populated areas, the extensive concentration of NO_X will contribute to reactions with OH, reducing OH availability needed for ozone production. This will usually result in low ozone concentrations in urban areas.

The above reactions are the main sources of O_3 in the troposphere. The dominant sink of O_3 however is photo-chemical loss. Photolysis in the presence of water vapor and HO_X yields

$$O_3 + hv \rightarrow O^* + O_2 \tag{R18}$$

$$O^* + H_2O \rightarrow OH + OH \tag{R19}$$

$$O_3 + OH \rightarrow H0_2 + O_2 \tag{R20}$$

$$O_3 + HO_2 \rightarrow OH + 2O_2 \tag{R21}$$

Where hv is under 320 nm.

2.3.2 Tropospheric ozone distribution: Wave-one

The zonal equatorial distribution of tropospheric ozone follows a wave-one pattern, as first described in Fishman and Larsen (1987). The wave-one does not refer to a dynamic wave in the atmosphere, but describe the difference in tropical tropospheric ozone as depicted in Figure 2.4. The wave-one is prominent in all seasons of the year, but stronger in September to November, with a varying tropospheric ozone burden of 10-20 DU (Thompson et al., 2003). The pattern shows that there is more free tropospheric ozone over the tropical Atlantic than the Pacific linked to the GC and seasonal pollution from biomass burning (Thompson et al., 2003). Due to a lack of sources of ozone precursors, the ozone in the troposphere over the open ocean is generally lower than over land (Brasseur and Jacob, 2017). The tropical Atlantic has higher levels of ozone compared to other tropical oceans due to being downwind from the European and African continents. The tropical Pacific is notorious for having low amounts of tropospheric ozone due to the lack of emissions of precursors, but also perfect conditions for tropospheric ozone depletion. In the tropical West Pacific troposphere very low concentrations of ozone are measured (Rex et al., 2014, Müller, 2020). Production of ozone is low here due to low concentrations of both NO_X and VOCs (Brasseur and Jacob, 2017). The conditions for the ozone loss mechanisms are also ideal, with low overhead ozone in the stratosphere letting through more radiation for photolysis in the troposphere, and high SST and boundary-layer temperatures resulting in high levels of humidity providing water vapor for reaction R19 (Rex et al., 2014). In the tropical East Pacific, production of ozone is also low, due to low concentrations of the precursors NO_X and VOCs. Tropospheric ozone depletion is not as dominating as in the West, because of lower SST due to upwelling, and more stratospheric ozone overhead. Here, a null-cycle starting with reaction R14 followed by R2, returns to NO_2 and ozone in a reaction between NO and ozone.

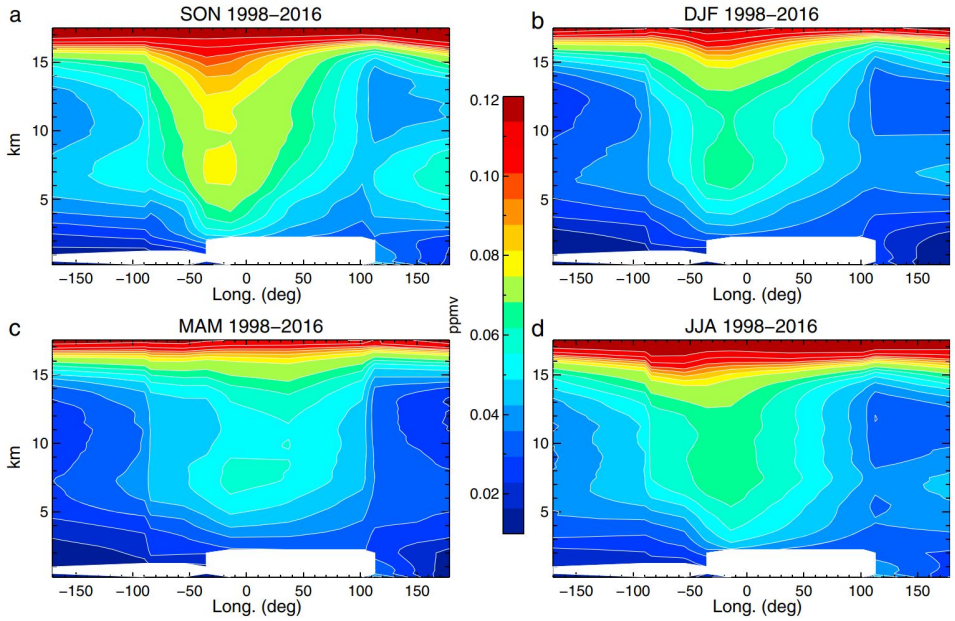

Figure 2.4: Longitudinal cross-section of O_3 mixing ratios (ppm), computed from 0.25 km averages of 1998–2016 reprocessed data, for the 10 tropical SHADOZ stations, in the troposphere to the lower region of the TTL. Four seasons illustrated: (a) SON; (b) DJF; (c) MAM; and (d) JJA. Data from 10 tropical stations within 15 °N/S. Figure and modified caption from Thompson et al. (2017).

2.4 Ozone-sondes

Meteorologists often utilize radiosondes, small instruments attached to balloons, to vertically measure atmospheric properties. These compact and lightweight instruments are connected to gas-filled balloons, allowing them to reach altitudes of up to 35 km (Ahrens and Henson, 2016). Radiosondes are equipped to measure temperature, pressure, and humidity, as well as wind direction and speed with the use of GPS positioning. These devices collect data every 1-5 seconds, transmitting it back to the ground station via radio signals.

In comparison to radiosondes, ozonesondes are also lightweight and compact instruments, but they are slightly larger in size and weigh approximately 1 kg. To measure ozone and other related variables, ozonesondes are paired with a radiosonde that relays the data to the ground station. Ozonesondes measure an electric current produced between a cathode and anode solution when the solutions come into contact with ozone, rather than measuring ozone directly. The detailed process of preparing an ozonesonde is described in section 4.1.

There are three primary types of ozonesondes currently in use, including the Electrochemical Concentration Cell (ECC), Brewer-Mast (BM), and Japanese Ozonesonde (KC96), each with its unique design (Smit, 2014). During SO287 CONNECT, ECC ozone-sondes were utilized, as well as all additional ozone-sonde data utilized in this thesis.

2.4.1 ECC ozone-sondes

There are two manufacturers that produce ECC ozonesondes, Science Pump and EN-SCI. During SO287 CONNECT EN-SCI model 2Z where used, together with GRAW DMF-17 radiosondes and GRAW ground station. Details about sondes used in the collection of additional ozone data used in this thesis can be found in Section 3.1.

From the outside, an EN-SCI ozonesonde is a 19.1 cm x 19.1 cm x 25.4 cm sized polystyrene box, as pictured in Figure 2.5. The polystyrene box, or the "flight box", is the outer shell that protects the ozone sonde from precipitation, radiation, and temperature change during its ascent. The instrument inside and its main component are illustrated in Figure 2.6. Attached to a lightweight aluminum frame are the air pump, sensing cells, and circuit board. The pump, powered by a 12 V battery, pumps air from the outside of the sonde, into the cathode cell. Every component in contact with the ozone should be treated with a material inert to ozone, like Teflon, not to disturb the chemical reactions and ozone measurement (Müller, 2020). The two sensing cells made of molded plastic, are mounted on the side of the sonde, and connected to the circuit board by two wires. The cap of the cathode cell has two tubes, the first one being the air sample intake tube from the pump, and the other one for exhaust. The anode cell only has one tube for exhaust. Both cells have a platinum mesh inside of different sizes, and an ion bridge connecting the two cells. The ion bridge is where the cables connected to the circuit board are attached, and where the measuring of the cell current that represents the ozone takes place.

When the instrument is placed in the flight box there are only three small holes in the polystyrene to get maximum insulating effect from the cold temperatures in the upper troposphere and stratosphere, as the cathode and anode solutions might freeze. These three small holes are for the air intake tube, exhaust, and cable connecting the circuit board with the radiosonde attached to the outside of the flight box.

Figure 2.5: Ozonesonde just before launch, 18.12.21. SO287 CONNECT sonde no. 13. Photo: Birgit Quack.

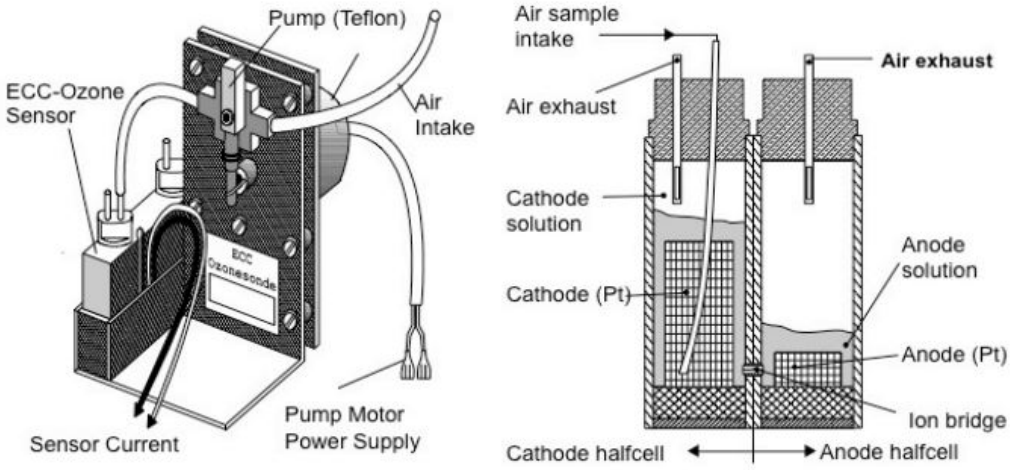

Figure 2.6: Schematic of ECC ozonesonde and sensing cell. Figure and caption from Smit (2014).

2.4.2 Chemistry of ECC ozone-sondes

The process of mixing the cathode and anode solution is described in Table 2.2.

The principle of measuring O_3 with an ECC is to convert O_3 into an electric current. Ambient air is pumped through the air intake pipe into the solution in the cathode cell. Here, a redox reaction takes place, which transfers electrons between chemical species (Zumdahl and Zumdahl, 2013).

$$2KI + O_3 + H_2O \rightarrow I_2 + O_2 + 2KOH \qquad \text{(ECC1)}$$

Table 2.2: Chemical components needed for 2L cathode solution

Chemical Formula	**Name**	**Amount**
KI	Potasium iodide	10.00 g
KBr	Potassium Bromide	25.00 g
$NaH_2PO_4 \cdot H_2O$	Sodium phosphate monobasic monohydrate	0.63 g
$Na_2HOP_4 \cdot 7H_2O$	Sodium phosphate dibasic 7-hydrate	1.87 g

The redox reaction turns all sampled ozone into molecular oxygen and iodide to iodine (I_2) (Smit, 2014). The iodine comes in contact with the platinum electrode in the cathode cell and is reduced back to iodide (I^-), taking up two electrons per I_2 molecule:

$$I_2 + 2e^- \rightarrow 2I^- \tag{ECC2}$$

The anode cell with saturated KI solution is connected to the cathode cell by an ion bridge. Here, I^- is converted to I_3^- by releasing two electrons:

$$3I^- \rightarrow I_3^- + 2e^- \tag{ECC3}$$

The electric current generated in the circuit connecting the cathode and anode cell is directly proportional to the partial pressure of ozone after correction of the residual background current discussed in Section 4.3. The conversion of the electrical current I_m [μA] to O_3 [mPa] is done by:

$$P_{O_3} = \frac{R}{2F} \cdot \gamma \cdot ((1-\alpha)I - \beta) \cdot T_{box} \cdot t_{100} \tag{2.1}$$

where the components of the equation is givven in Table 3.1

Table 2.3: Providing an overview of variables that go into the Equation 2.1

Variables	**Information**
R	Universal gas constant
F	Faraday constant (as a factor of two, 2 electrons per ozone molecule)
γ	Pressure dependent pump efficiency
I	Cell current
T_{box}	Temperature inside the pump [K]
α	Slope parameter ($\alpha = 0.024 \pm 0.009$
β	Modified background current ($\beta = 0.009 \pm 0.009$)

Equation 2.1 is derived from Vömel and Diaz (2010), and is automatically implemented in the GRAWMET ground-station software used during SO287 CONNECT and other ship campaigns (see Section 3.1 for research details). Correction of the cell current is a highly controversial topic in the community. Previously, the background current was subtracted from the measured current, but due to the later discovery that the background current continuously changes during flight research regarding why the background current changes, and how to treat it, is ongoing (Smit and Thompson, 2021).

2.4.3 Difference in ozone-sonde manufacturer

The data used to produce results in this thesis (see Section 3) is mainly sampled using two different types of ECC ozone-sondes; EN-SCI 2Z and Science Pump 6A. There is a long list of factors that can influence the performance of every single ozone-sonde launch, including the standard operating procedures (SOP) during preparation, the mixing ratio of the sensing solution, and the type of ECC ozone-sonde (Smit et al., 2007). The World Calibration Centre for OzoneSonde (WCCOS: https://www.wccos-josie.org/wccos) has a series of experiments named Jülich Ozone Sonde Intercomparison Experiment (JOSIE), where the different factors of uncertainty due to a list of influences, including the differences between the EN-SCI Z and Science Pump A ECC ozone-sonde models were assessed (Smit et al., 2007, Smit and Thompson, 2021). The JOSIE (2000) study found that the two model types performed within 5% of each other below the altitude of 20 km when being prepared in the same conditions. However, above 20 km the EN-SCI sonde measured 5-10% more ozone than the Science Pump (Smit et al., 2007). The background current measured during this JOSIE shows that the two types of ECC ozone-sondes have background currents of the same magnitude for different sensing solution types (Smit et al., 2007). The same results can be seen in Vömel and Diaz (2010), though the differences between the two sonde types were not the aim of the study and therefore not discussed and concluded upon in this paper.

PART II

Data and Methods

CHAPTER 3

Data

The following chapter provides an overview of data used to produce the results in this thesis. In addition to data collected specifically for this thesis, observational data collected in other geographical locations, time-frames, and using different instrumentation is used. It also includes information on HYSPLIT and the input used for generating trajectories. Further, details about the standard NorESM, and its new experimental additions will be described. This chapter aims to provide useful information about the available data.

3.1 Observational Data

3.1.1 SO287 CONNECT

The SO287 CONNECT campaign aims to investigate Pan-Atlantic connectivity of marine biogeochemical and ecological processes and the impact of anthropogenic pressures. Onboard the RV Sonne, the expedition crossed the Atlantic, casting off from Las Palmas de Gran Canaria 11.12.2021, transiting through the Panama Canal, and docking in Guyaquil, Equador 11.01.2022. The cruise track is depicted in Figure 3.1. The start of the cruise track is steadily going southwest, before diverting straight west along the 17 °N longitude. After reaching about 50 °W, the ship redirected for the Sargasso Sea, reaching the northernmost point at 30 °N close to Bermuda. The ship then headed souhtwest into the Caribbean Sea, passing between Puerto Rico and the Dominican Republic before reaching the Panama Canal. After transiting through the Panama Canal the cruise track crossed the Equator about 85 °W, and further docked in the Guayaquil harbor.

During the SO287 CONNECT cruise, a total of 45 balloons with radiosondes were launched, seven of which additionally carried ozone-sondes (Quack, 2022). Radiosonde profiles were delivered to the Global Telecommunication System. As seen on the radiosonde curtain plots in Section 5.1 some early radiosondes were shallow, this is likely due to interference between radiosonde and ground

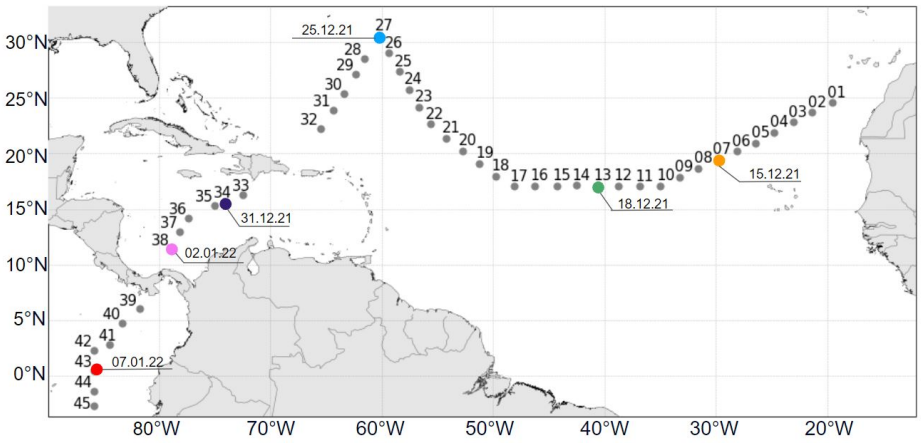

Figure 3.1: SO287 CONNECT cruise track visualized by radiosonde launches. Colored points indicate ozone-sonde launches.

station. The third ozone-sonde coupled with radiosonde number 19, was unable to record any ozone data due to a rough launch. Radiosonde data from sonde no. 19 is not affected. Thus 6 out of 7 ozone-sondes are available

3.1.2 Southern Hemispheric ADitional OZonesondes

Ozone-sonde data from three permanent stations and one temporary SHADOZ station is used in this thesis. The SHADOZ network was set up to aid the improvement of characterization of the vertical structure of ozone in the troposphere and stratosphere, besides validating ozone-monitoring satellites (Thompson et al., 2017). Observations of the vertical structure of ozone using ozone-sondes have previously been sporadic, and SHADOZ aid in the systematic collection of vertical ozone data at stations in the Southern Hemisphere tropics and subtropics, though some stations are located in the Northern Hemisphere (Thompson et al., 2003).

3.1.2.1 SHADOZ stations

SHADOZ stations are usually located distant from sources of ozone precursors (Thompson et al., 2003). The Paramaribo, Surinam station is located on the North coast of South America at 5.81 °N and 55.21 °W. The station is close to the city center of Paramaribo and lies 10 km from the coast. The average wind direction in this area is north-easterly trade winds (Ahrens and Henson, 2016). Located on the opposite side of the northern South American continent, is the Quito station in the heart of Ecuador. Situated at 0.20 °S and 78.44 °W, the station is inside the city center perimeter of Ecuador's capital. According to the station's latitudinal position, the average wind direction in this area is

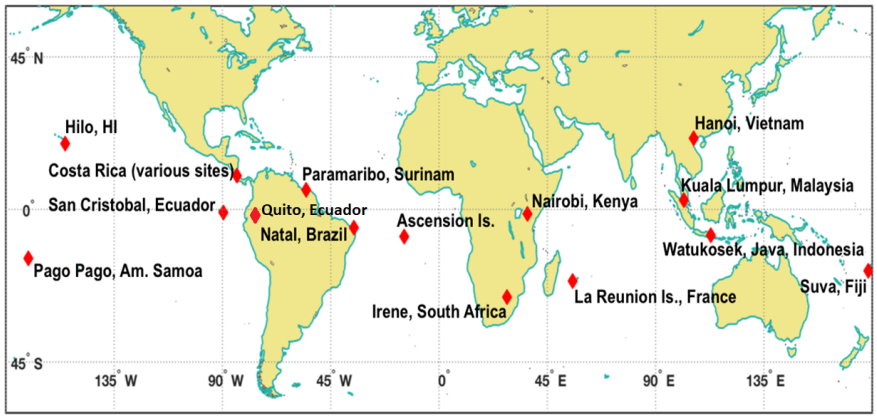

Figure 3.2: SHADOZ station locations. Figure modified to include the temporary Quito, Ecuador station, original from https://tropo.gsfc.nasa.gov/shadoz/

mainly easterly trade winds, but due to the station's high elevation of 2300 meters. This can vary as the near-surface winds may be affected by topography (Ahrens and Henson, 2016). Costa Rica is found in Middle America with the Caribbean Sea to the East, and the Pacific Ocean to the West. This SHADOZ station was established in the city of San Jose, 9.94 °N and 84.05 °W. This station, similar to the Quito station, is located within the city center of the city and at a high elevation above sea level, whereas San Jose is situated at 1240 m. The average wind direction is the North-eastern trade winds, and the station is set 50-70 km from either coast. The last of the four SHADOZ stations used in this thesis is found on the Galapagos islands, Ecuador, close to the town of San Cristobal at 0.90 °S and 89.61 °W. Since the station is located close to the Equator in the Pacific, the average wind in the region is weak easterly trade winds (Ahrens and Henson, 2016).

Table 3.1: Overview of SHADOZ data used in this study

	Paramaribo	**San Cristobal**	**Costa Rica**	**Quito**
Sampling period	September 1999 - Present	March 1998 - Present	July 2005- Pressent	October 2021- Present
Comment		No sampling 2006-2007, 2009-2012, 2017-2020		
Launches within or close to SO287	06.12.2021 14.12.2021 20.12.2021 03.01.2022 10.01.2022 17.01.2022 24.01.2022	11.12.2021 12.12.2021 17.12.2021 28.01.2022	08.12.2021 17.12.2021 13.01.2022 25.01.2022	17.12.2021 28.01.2022
Number of DJF files used in variability calculation	195	90	141	
Comments		Variability calculated using soundings from December 1999 to January 2016		Too short data set to calculate DJF variability
Radiosonde/ Ozone-sonde model	Vaisala RS41-SGP/ Science pump 6A	iMet-4 / Sience Pump 6A	Vaisala RS-80 or iMet-4 / EN-SCI 2Z	iMet -4 / EN-SCI 2Z
Comments	From December 2021 ECC ozone-sondes used in Paramaribo showed significantly higher background currents during preparation.		SHADOZ website says soundings from CR is from 'various sites'. Data shows launch altitude change, not position.	

3.1.3 Additional RV Sonne campaigns

Vertical ozone profile measurements have been conducted during four campaigns onboard the old RV Sonne from 2009 through 2015. These campaigns include TransBrom (Very short lived bromine compounds in the ocean and their transport pathways into the stratosphere) and SHIVA (Stratospheric Ozone: Halogens in a Varying Atmosphere) in the tropical West Pacific, SPACES-OASIS (Organic very short-lived substances and their Air-Sea exchange from the Indian Ocean to the Stratosphere) in the Indian Ocean, and ASTRA-OMZ (Air Sea interactions of TRAce elements in Oxygen Minimum Zones) in the tropical Eastern Pacific. An overview of the campaigns, their acronyms, time-frames, and sonde types is provided in Table 3.2. Their research area is indicated in Figure 3.3, while their individual cruise tracks are shown in Figures 3.4, 3.5, and 3.6.

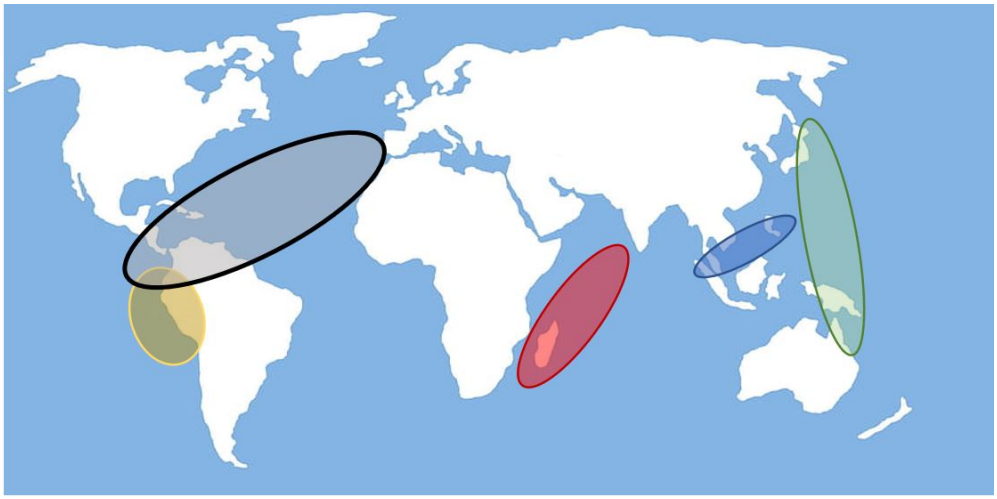

Figure 3.3: Map showing area sampled during the five cruises analyzed. Black: SO287 CONNECT, Yellow: ASTRA-OMZ, Red: SPACES OASIS, Blue: SHIVA, Green: TransBrom.

Table 3.2: Overview of ship campaigns onboard RV Sonne that conducted ozone profile measurements with ECC ozone sondes

Acronyme	**Title**	**Cruise no.**	**Time frame**	**Ozone sonde/ Radiosonde**
CONNECT	Pan Atlantic Connectivity of Marine Biogeochemical Processes / Impact of Anthropogenic Pressures	SO287	11.12.2021-11.01.2022	EN-SCI / GRAW DFM-17
ASTRA -OMZ	Air Sea interactions of TRAce elements in Oxygen Minimum Zones	SO243	05.10.2015-22.10.2015	EN-SCI / GRAW DFM-09
SPACES -OASIS	Organic very short-lived substances and their Air-Sea exchange from the Indian Ocean to the Stratosphere	SO234-2 / 235	23.07.2014-07.08.2014	EN-SCI / GRAW DFM-09
SHIVA	Stratospheric Ozone: Halogens in a Varying Atmosphere	SO218	15.11.2011-29.11.2011	EN-SCI / GRAW DFM-97
TransBrom	Very short lived bromine compounds in the ocean and their transport pathways into the stratosphere	SO202	09.10.2009-24.10.2009	EN-SCI / GRAW DFM-97

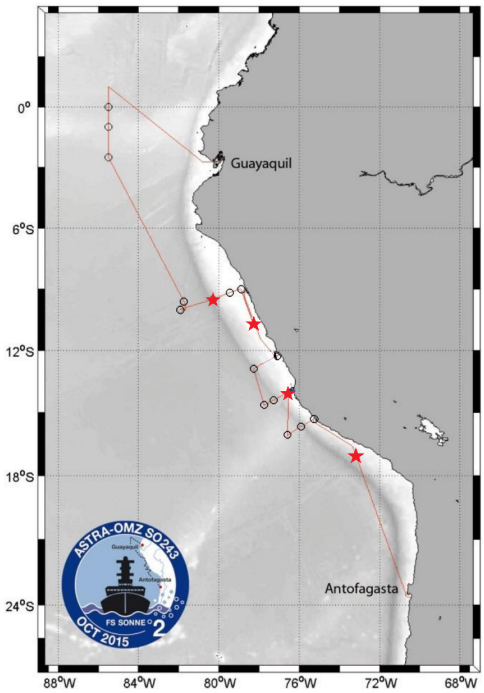

Figure 3.4: Cruise track for ASTRA-OMZ. Red stars marking ozone-sonde launches. Figure from Marandino (2016), has been modified.

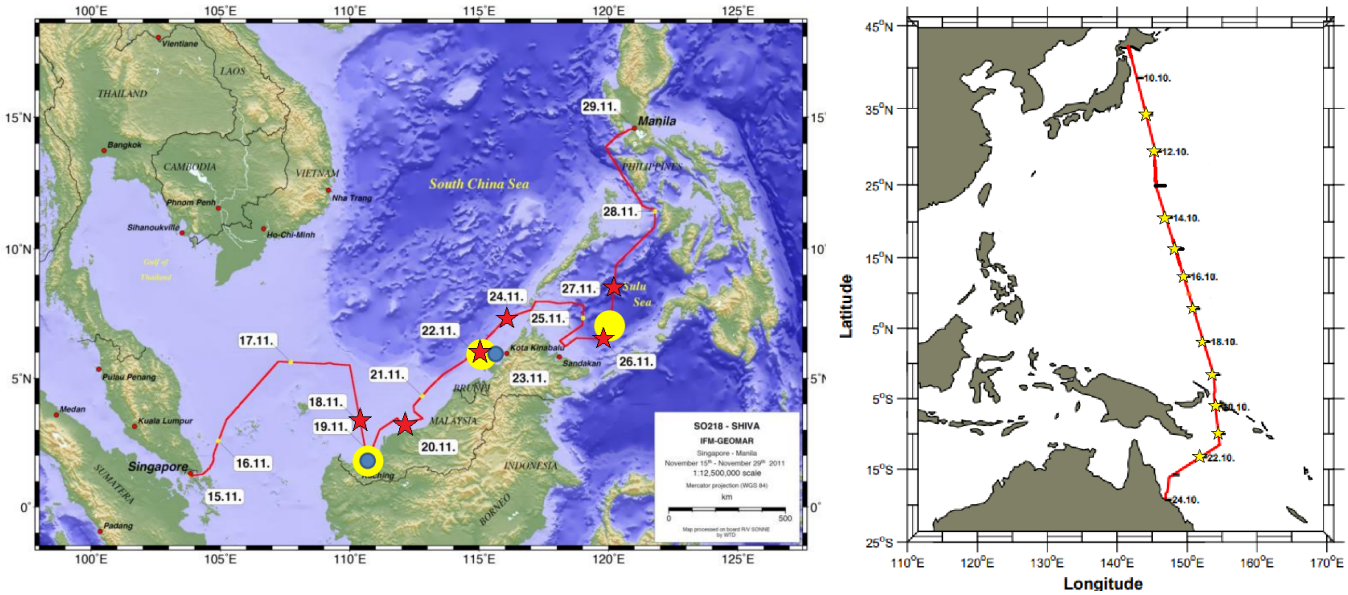

(a) SHIVA (b) TransBrom

Figure 3.5: Cruise track for the tropical West Pacific campaigns, TransBorm and SHIVA. Stars marking ozone-sonde launches. Figure from (a) Quack and Krüger (2013) and (b) Krüger and Quack (2013), has been modified.

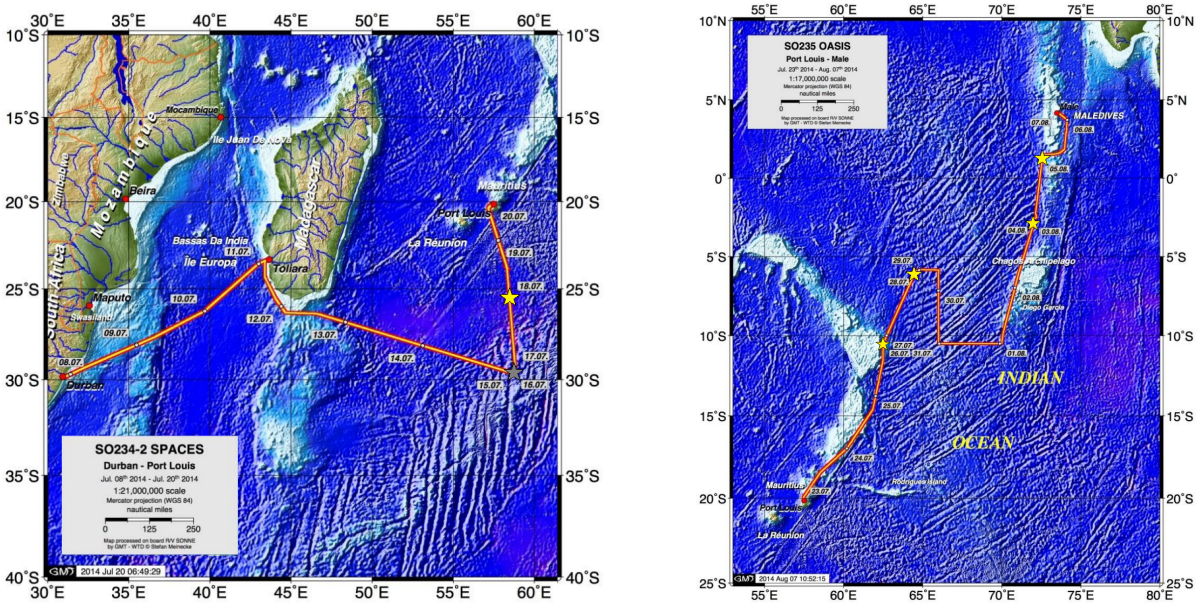

(a) SPACES-OASIS SO234-2 (b) SPACES-OASIS SO235

Figure 3.6: Cruise track for SPACES-OASIS. Yellow stars marking ozone-sonde launches. Figure from (a) Krüger et al. (2014a) and (b) Krüger et al. (2014b), has been modified.

3.2 The climate diagnostic bulletin

The climate diagnostic bulletin is a publication produced by the National Centers for Environmental Prediction (NCEP), which is part of the National Oceanic and Atmospheric Administration (NOAA). The bulletin provides an analysis of the Earth's climate system, including global climate patterns, anomalies, and forecasts (https://www.cpc.ncep.noaa.gov/).

The purpose of the Climate Diagnostic Bulletin is to monitor and analyze the state of the climate on a global scale. It combines observations from various sources and climate models to provide a comprehensive overview of the Earth's climate conditions each month. The bulletin focuses on understanding and predicting climate phenomena such as ENSO, and other deviations from the GC.

Selected figures from the climate diagnostic bullitin is modified and used to aid iterpertation of the meteorological and climatological conditions in the first part of Section 5.1.

3.3 HYSPLIT trajectory model

To investigate air mass origin for the case studies presented in Section 5.2 and 5.4, backward trajectories were calculated using NOAA's HYSPLIT model. The model uses a hybrid approach, including the Lagrangian moving reference frame and the Eulerian fixed reference frame (Stein et al., 2015). HYSPLIT is available as a downloadable program but is also available free to use online. In this thesis, the online HYSPLIT version was utilized, due to its ensemble feature. There is a wide range of meteorological data to choose from when generating trajectories, including the NCEP Global Forecasting System (GFS) data which is used in this study. The GFS data is global with a horizontal resolution of 0.25 degrees, 127 vertical level, model top at 13 km, and hourly output (https://www.emc.ncep.noaa.gov/emc/pages/numerical$_f orecast_s ystems/gfs.php$, $Downloaded$28.04.2032). An ensemble of backward trajectories with the input info in table 3.3 was calculated. HYSPLIT has a limitation of 27 ensemble members, and a time frame of about 8 days using archive meteorological GFS data.

Before utilizing HYSPLIT, the individual ozone profiles were studied to pinpoint the point of interest. For running backward and forward trajectories, HYSPLIT needs information about the point where the calculation starts. The inputs needed are coordinates (latitude and longitude), altitude, date, and time, as well as the number of hours you want to be calculated, in this study the maximum was chosen.

Table 3.3: Overview of input for all HYSPLIT trajectories presented in Section 5.4

Case study	**Date and time**	**Latitude [°N]**	**Longitude [°E]**	**Altitude [m]**	**Direction**
Double sampeled air masses (07)	15.12.2021 UTC 13:00	19.44	-29.89	1000	Forward
Double sampeled air masses (13)	18.12.2021 UTC 15:00	17.12	-40.65	1000	Forward
Double sampeled air masses (Q)	17.12.2021 UTC 12:00	-0.19	-78.44	2378	Backward
Double sampeled air masses (P)	20.12.2021 UTC 15:00	5.80	-55.22	1000	Backward /Forward
Tropospheric maximum (07)	15.12.2021 UTC 14:00	19.45	-29.74	7618	Backward
Tropospheric maximum (13)	18.12.2021 UTC 15:00	17.09	-40.56	7360	Backward
Extra-tropical sonde (27) under	25.12.2021 UTC 17:00	30.35	-59.22	10666	Backward
Extra-tropical sonde (27) nose	25.12.2021 UTC 17:00	30.24	-59.60	12829	Backward
Extra-tropical sonde (27) anti-nose	25.12.2021 UTC 17:00	30.21	-59.52	13636	Backward
Extra-tropical sonde SC	17.12.2021 UTC 14:00	-0.88	-89.61	10326	Bakward
East Pacific low	07.01.2022 UTC 18:00	0.46	-85.83	540	Backward

3.4 The Norwegian Earth system model

The Norwegian Earth System Model (NorESM) is a model developed by the Norwegian Climate Center. Earth system models (ESM) are valuable tools for studying the chemical processes in the atmosphere and the factors that influence them. These models simulate the interactions and processes that shape the Earth's climate, including physical, chemical, and biological aspects. They help us estimate past and future climate conditions. The model is constructed using the framework of the Community Earth System Model (CESM2) but with its own ocean and biogeochemistry coupling (Seland et al., 2020). The model has multiple versions, where this study uses the NorESM2-MM version, meaning that both atmosphere-land and ocean-sea ice is resolved on a 1° grid (Seland et al., 2020). The atmosphere component has a vertical resolution of 32 layers, arranged in hybrid sigma pressure coordinates from 992.5 to 3.6 hPa. Its components and couplings are illustrated in Figure 3.7.

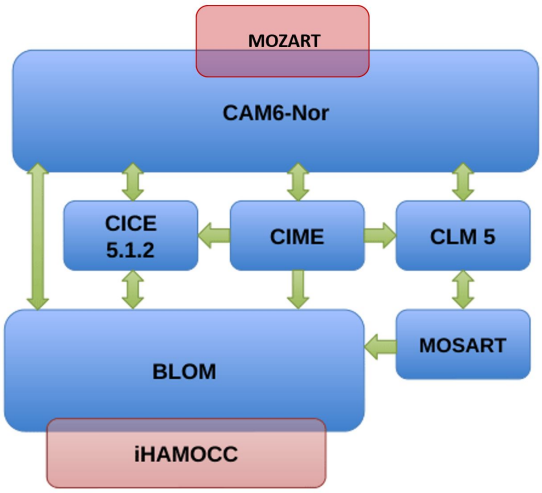

Figure 3.7: Overview of the different components in NorESM2 and their interactions (CIME: configuration handler; CAM6-Nor: atmosphere and aerosol; CICE5.1.2: sea ice; CLM5: land and vegetation, MOSART: river transport; BLOM: ocean; iHAMOCC: ocean carbon cycle; MOZART: full chemistry). Figure and caption have been modified, original from Seland et al. (2020).

The standard NorESM2 contains an elaborate aerosol scheme but has limited chemistry. The aerosol scheme describes dust, sea-salt, black carbon, organic matter, and sulfate. The model uses prescribed climatological 3D distributions of OH, ozone, NO_3, and HO_2. Additionally, 8 gas-phase tracers are explicitly modeled: sulfur dioxide (SO_2), dimethyl sulfide (DMS), sulfuric acid (H_2SO_4), hydrogen peroxide (H_2O_2), isoprene, monoterpene, and the semi- and low-volatile precursor of secondary organic aerosols (Kirkevåg et al., 2018). The

aerosols in this model version are represented by 21 tracers.

The model version used in this thesis has extended the chemical mechanism to include the gas-phase chemistry taking place in the troposphere and stratosphere. The new chemical mechanism is a combination of the standard aerosol scheme that exists in NorESM, in combination with the chemical mechanism MOZART-TS1 available in CESM2. MOZART-TS1 is an expansion of the Model of Ozone and Related Chemical Tracers (MOZART), which is a chemical transport model used to study the composition of the Earth's atmosphere, particularly the troposphere (Emmons et al., 2020). MOZART-TS1 in combination with the aerosol scheme from NorESM results in an aerosol and chemistry scheme described by around 200 tracers.

The model run utilized in this thesis is a historical experimental run. These runs are part of the larger collection of CMIP6 coordinated experiments, aimed at simulating the historical period spanning from 1850 to 2014. The historical simulation commences from the model's pre-industrial base state, known as the piControl experiment. The forcings in this simulation are determined using observational estimates, encompassing anthropogenic emissions, alterations in natural and anthropogenic atmospheric greenhouse gases, and solar forcing (Eyring et al., 2016). Variations in stratospheric ozone and aerosol concentrations are not prescribed but are calculated interactively due to the implementation of MOZART-TS1. The historical run included in this thesis spans a duration of 35 years, from 1980 through 2014, and has a free-running configuration with prescribed SSTs.

CHAPTER 4

Methods

This chapter describes the methods used to obtain and post-process data used to generate results in this thesis. Details about the precise process of preparing an ozone-sonde are introduced, following data post-processing methods.

4.1 Ozonesonde preparation procedure

The preparation of an ECC ozone-sonde is an important procedure that can potentially affect the measurements if not done carefully. ECC ozone-sondes need to be conditioned 3-7 days prior to launch. During SO287 CONNECT I prepared all 7 ozone-sondes on board, following the standard operating procedures outlined by the World Meteorological Organization's (WMO) Assessment of Standard Operating Procedures for Ozone Sondes (ASOPOS) in the Global Atmosphere Watch (GAW) report by Smit (2014) and Smit and Thompson (2021). The process was taught during training at the Deutscher Wetter Dienst (DWD) in Lindenberg in November 2021. The Vaisala RS41 SOP manual (Vaisala, 2019) was followed during the preparation of the ozone-sonde, with a few modifications.

4.1.1 Mixing of the sensing solutions

The first step in preparing ozone-sondes is mixing of the two different chemical sensing solutions used inside the sonde, the cathode and the anode (see section 2.4). Preparation of the sensing solutions took place the day before the preparation of the first ozone-sonde. The cathode solution was mixed with a 0.5 % KI content, as recommended by ASOPOS for EN-SCI ozonesondes. Two liters of cathode solution were mixed using pre-measured chemical components provided by Kartin Müller from the Alfred Wegener Institute (AWI) in Potsdam. The chemical components and their weights are provided in table 2.2. The preparation of the anode solution took place about 5 hours after the preparation of the cathode solution.

The different SOP manuals don't agree on the amount of time the sensing solutions should sit unused before being used inside an ozonesonde. EN-SCI claims the two sensing solutions need to be left unused for "a minimum of two weeks" before being used, while other manuals have no mention of such a long rest time. During SO287 CONNECT the sensing solutions were mixed the day prior to being used in the preparation of the first ozone-sonde (sonde no. 07).

The chemical components were dissolved one after the order listed in table 2.2 into one liter of distilled water from RV Sonne's MilliQ, and one more liter of distilled water was added before the solution was left to rest for three hours. After resting, the bottle of cathode solution was lightly shaken to make sure all components were dissolved before it was once again left to rest a couple of hours more before it was used to make the anode solution. 50ml of ready-made cathode solution was added to 90g of KI. The amount of KI to be used in the saturated anode solution is different across the various SOP manuals. As long as it is crystals present in the solution, indicating that it is KI saturated, the specific amount of KI can vary.

4.1.2 First preparation

The first preparation on an EN-SCI ECC ozone-sonde must be done 3 to 7 days prior to launch. The following 12 steps constitute the first preparation of the ozone-sondes launch during SO287 CONNECT, following the Vaisala SOP manual with minor adjustments advised by DWD Lindenberg:

1. Connect the ozone-sonde to the ozone testing unit (During SO287 CONNECT a clean pump corp. model TSC-1 was used).

2. Record pump pressure (>700 hPa) and vacuum (>500 hPa).

3. Condition pump and sensing cells with high-O_3 air from the ozone testing unit for 30 minutes.

4. After 10 minutes of high ozone, pump voltage (12 V) and pump current (<100 mA) can be recorded.

5. Run no-O_3 air through the sonde for 10 minutes, using an ozone destruction filter between the testing unit and the sonde.

6. Fill the cathode cell with 3 ml cathode solution, using a clean syringe.

7. 2 minutes after filling in the cathode solution, fill up 1.5 ml anode solution in the anode chamber using a new and clean syringe.

8. Run no-O_3 air through the sonde for 10 minutes, watching the measured sensor current.

9. Record the background sensing current (<1.5 μA). If the background current is too high one can wait for the current to steadily drop.

10. Condition the ozone sonde with ozone-rich air for 5 minutes, so that the cell current is steadily at around 5 μA the whole period.

11. Run no-O_3 air through the sonde for 10 minutes, and watch the cell current drop.

12. Switch everything off. Add 3 ml more cathode solution. Short circuit the cables from the sensing chambers, and store the sonde dark and cool (20-25 °C). Let the ozone sonde rest for 3-7 days.

4.1.3 Second preparation

On the day of launch, the ozone sonde is prepared a second time. During this preparation, one can see if the ozone sonde performed normally, and important parameters for the ground station software are recorded. The 5 step preparation is as follows:

1. Dump and change the cathode and anode solutions. 3 ml cathode, 1.5 ml anode.

2. Condition the sonde with no-O_3 for 10 minutes.

3. Connect the air-flow meter to the exhaust port of the pump. Record the time it takes for the pump to pump 100ml 5 separate times, and calculate the mean pumping time (around 30 s).

4. Repeat step 10 from the first preparation, this time recording the sensing background current after 0.5, 1, 3, 5, and 10 minutes after switching to no-O_3 air. The current recorded after 10 minutes should be used as the background current (<0.02 μA).

5. Prepare the ozone-sonde, radiosonde, and flight box for launch.

4.1.4 Launch

For the launch procedure, the EN-SCI ozone sonde was connected to a GRAW radiosonde and coupled with the GRAW ground station. The latex balloons (TORTEX brand) were then inflated at the rear deck of the ship, filling the balloon with helium to bring the sondes up to 35 km altitude with an ascending speed of about 5 m/s. Due to the balloon being about 2 meters in diameter, and being prepared out in the elements of the rear deck, a team of around 6 people helped during the launch to hold the balloon in place with a launch net as seen in Figure 4.1.

Figure 4.1: Ozonesonde just before launch, 07.01.22. SO287 CONNECT sonde no. 43. Photo: Isabella Zehender

4.2 Determining the launch positions

The launch positions of the radiosondes and ozone-sondes were decided upon considering a long list of factors. The SO287 CONNECT ship campaign had a fixed ship track with already decided stations for the oceanographic sampling. Stations were conducted twice daily with one station around zenith 12 local time, and the second around midnight local time. Due to the convenience, radiosonde launches took place at each station making the launch schedule about twice per day. 45 radiosondes were launched during this campaign, 7 of the radiosonde launches included the additional ozone-sonde and were only launched at noon stations for convenience.

When deciding the launch positions of the ozone-sondes, sampling over a wide range of latitudes and longitudes was desired. The first ozone sonde (radiosonde 07) was launched at the beginning of the cruise as far east as possible, considering the ozone-sonde preparation time. The following ozone-sondes were launched at about 10 longitudinal degrees apart. Ozone-sonde attached to radiosonde number 27 was launched on the northernmost point in the ship track. The two

ozone sondes launched in the Caribbean Sea (radiosondes no. 34 and 38) were mostly decided by what economic zones the campaign got permission to sample in. Two sondes were launched in the Caribbean Sea with the hypothesis that SST conditions there would be close to that of the tropical West Pacific. The last ozone-sonde was launched in the Eastern Pacific Ocean close to the equator and the San Cristobal SHADOZ station.

Radiosondes were launched twice daily starting from station 1 (noon station) until station 32 (midnight station). However, not all stations included a radiosonde launch, due to restrictions in the different economic zones. After the launch of radiosonde 32, the regular launch pattern was disrupted, and the radiosonde numbers no longer match the station numbers. In this thesis, the radiosonde numbers will be used for convenience, with an indication of location (see Figure 3.1) and launch date when needed.

4.3 Post processing of data

Post-processing of ozone data from ECC ozone soundings is a controversial topic. As mentioned in Section 2.4, ozone concentrations are not directly measured by the ECC ozone-sondes but rather calculated with a basis in a measured current occurring when ozone reacts with potassium iodide. The equation for calculating the ozone concentration in partial pressure (mPa) is also given in Section 2.4 as Equation 2.1. The treatment of the background current has long been a topic of controversy in the ozone-sonde community (Müller, 2020). Due to an unstable background current, with a proposed name change to "postpreparation current" by Vömel et al. (2020), a constant value should not be used in the calculation of partial pressure ozone (Vömel and Diaz, 2010). Due to the current usually decreasing with time, using the current recorded just before launch would lead to an overestimation during accent, and simply subtracting this current from the measured cell current causes too low ozone values, especially in areas with low amounts of ozone (Vömel and Diaz, 2010, Rex et al., 2014).

All ozone-sonde data used in this thesis have been corrected according to Vömel and Diaz (2010), apart from the 2009 TransBrom data. To aid the comparison between TransBrom ozone data and SO287 CONNECT ozone data the latter has been superimposed on top of Figure 4.2a from Rex et al. (2014).

The importance of appropriately reprocessing data for obtaining the accurate ozone partial pressure is highlighted in Figure 4.2. Figure 4.2a presents a visualization of ozone-sonde data acquired during the TransBrom after some post-processing by Rex et al. (2014). Regrettably, published the post-processed data is not available. On the other hand, the accessible data in Figure 4.2b has not undergone post-processing concerning the utilization of the post-preparation

current. Notably, Figure 4.2 reveals that merely deducting a constant post-preparation current from the measured cell current results in infeasible signals such as a negative ozone mixing ratio. Applying Equation 2.1 for post-processing would be uncomplicated, but the data and metadata necessary for computing the appropriate ozone partial pressure were unavailable for the TransBrom data for this thesis.

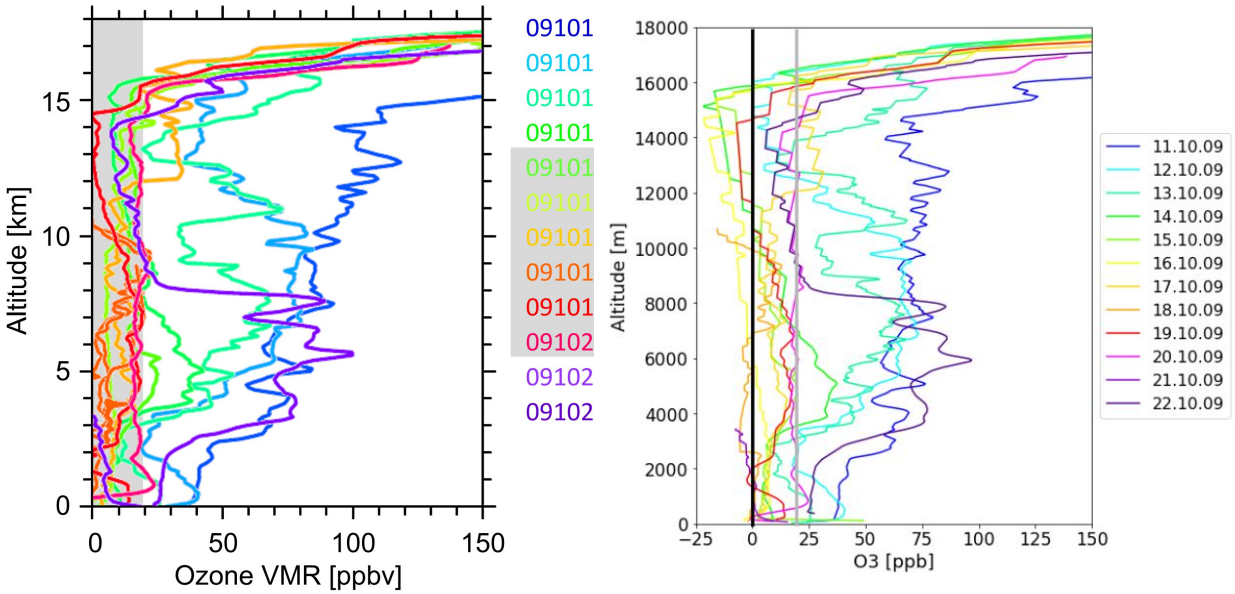

(a) (b)

Figure 4.2: (a) West Pacific during the TransBrom cruise in October 2009 tropospheric ozone mixing ratios from balloon sondes as a function of altitude. The legend shows the date and latitude of each sounding. Gray shading indicates the detection limit (left) and soundings with ozone abundances mostly below the detection limit (right). Figure from Rex et al. (2014). (b) Showing the same as the left panel but with available data (post-prosessed, but not according to Vömel and Diaz (2010)). The gray line indicated the same detection limit as the left panel.

4.3.1 Ozone unit conversion

Some ozone sonde data, including data from SO287 CONNECT, includes the calculated O_3 in mPa. The standard unit for ozone profiles is ppb in the troposphere and ppm in the stratosphere. Equation 4.1 is used to convert partial pressure to mixing ratio:

$$\frac{O_3[mPa] \cdot 10^{-3}}{p[hPa] \cdot 10^2} = O_3 \cdot 10^9[ppb] \tag{4.1}$$

Where p is pressure (Brasseur and Jacob, 2017).

4.3.2 Lapse rate tropopause

The LRT is calculated from sonde data using the definition given in Section 2.1.1. It is the point where the lapse rate in temperature reaches 2°C (or less) per kilometer, and does not exceed this threshold within 2 km altitude. This calculation is done by the Fortran code used by National Center for Atmospheric Research (NCAR) and translated to Python by Bunting et al. (n.d.). The Python code has further been modified to be used for the SO287 CONNECT radiosonde data.

4.3.3 Statistics

The variability box plots presented in Section 5.3 are calculated with the intent to analyze and compare local climatology to new observations. These plots are inspired by Oltmans et al. (2001). Data from long-existing SHADOZ stations were sorted into seasons, where the season used in this study is the winter season December to February (DJF). The ozone data were then binned according to altitude, with one bin every 250 meters. Within each of these bins a variability box plot where made, and plotted centered in their respective altitude range. The left and right whiskers represent the 10th and 90th percentile, respectively. The box itself represents 50% of the data, with its left and right edges marking the 25th and 75th percentile, respectively. The solid black line in each box portrays the median.

PART III

Results

CHAPTER 5

Results

The results chapter presents the key findings from both observational and trajectory data, in addition to the interpretation of the meteorology and climatology conditions. The chapter commences with an analysis of the meteorology during the SO287 CONNECT ship campaign, which is detailed in Section 5.1. The meteorology analysis comprises time-height cross-sections obtained from radiosonde data and an overview of the deviations from the GC; ITCZ location, ENSO phase, and QBO phase. The outcomes of the meteorology analysis are then used to characterize the air masses observed during the campaign. Following this, Section 5.2 introduces and examines the SO287 CONNECT ozone profiles, while Section 5.3 compares these ozone profiles to those from nearby SHADOZ stations. To further study these findings, case studies and trajectory analysis are conducted in Section 5.4. Lastly, the SO287 CONNECT ozone profiles are compared to other RV Sonne ship campaign ozone soundings in Section 5.5, presenting an overview of the difference in tropospheric ozone over the tropical ocean basins.

5.1 Meteorology

To approximate the location of the ITCZ, depicted in Figure 5.1, the estimated monthly mean precipitation is used. During the trans-Atlantic and Caribbean leg of SO287 CONNECT in December 2021, the cruise track remained North of the ITCZ. However, during the East Pacific leg of the cruise, the ship appears to have crossed the ITCZ. Consequently, all ozone-sondes were launched in Northern hemispheric air, with the exception of the ozone-sonde no. 43, which was released South of the ITCZ and hence in southern hemispheric air, considering the interpretation based upon monthly averages.

The ITCZ is found to be in close proximity to the four SHADOZ stations utilized in this study, as showcased in Figure 5.1. In December 2021, Paramaribo (P), Surinam, appeared to be situated within the ITCZ or in its immediate vicinity but further North during January 2022. A similar pattern is observed for the

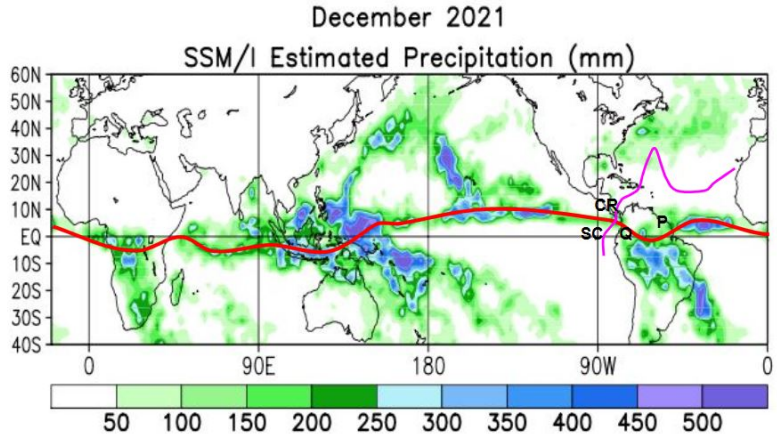

(a)

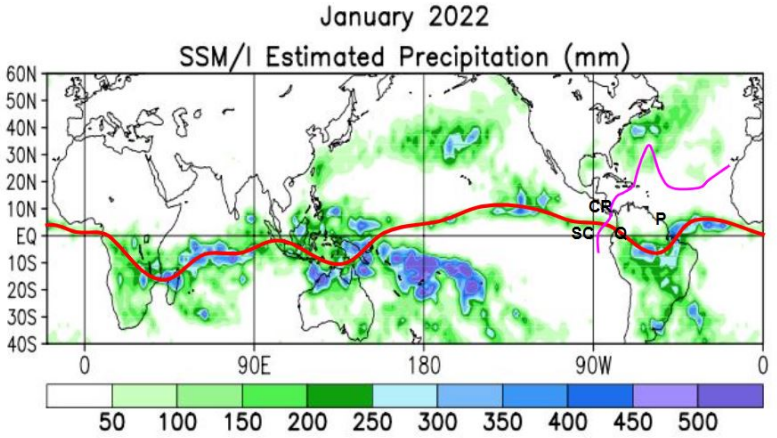

(b)

Figure 5.1: December 2021 and January 2022 estimated precipitation (mm), based on the Special Sensor Microwave/Imager (SSM/S) precipitation index (Ferraro, 1997). The red line indicates the ITCZ, the magenta line marks SO287 CONNECT cruise track, initials mark the SHADOZ stations. Figure modified, caption and original figure from L'Heureux and LaJoie, 2021 and L'Heureux and LaJoie, 2022.

Costa Rica (CR) station. Quito (Q) is also found to be in close proximity to the ITCZ but was slightly south in both December and January. San Cristobal (SC), Ecuador, located on the Galapagos Islands, is also close to the ITCZ but was located further south of it than the other stations in both December 2021 and January 2022. As a result, all four SHADOZ stations being in close proximity to the ITCZ, it is challenging to infer whether the stations will sample Northern or southern hemispheric air in December and January based solely on the estimated monthly mean ITCZ's location.

The December 2021 and January 2022 sea surface temperature (SST) anomalies displayed in Figure 5.2a reveal that a La Niña event persisted during most of the SO287 CONNECT cruise. This result is in agreement with other sources, such as NOAA, who reported an ONI of 1.0 for both December 2021 and January 2022 (.

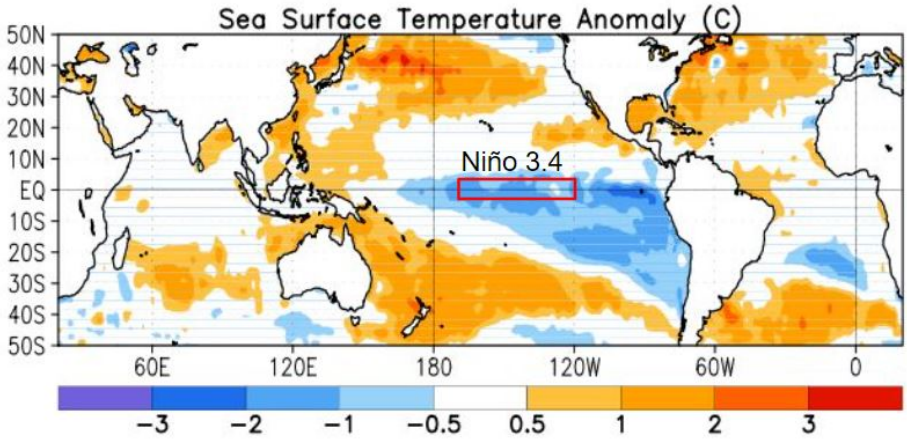

(a) December2022

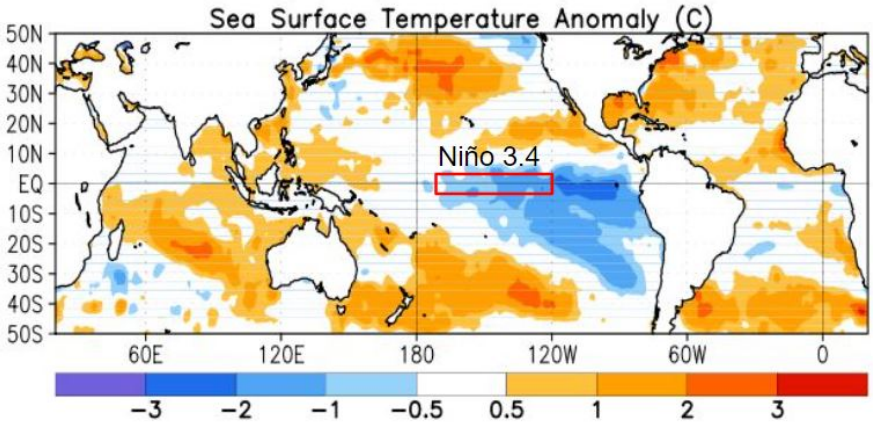

(b) January 2022

Figure 5.2: SST anomaly (°C). Anomalies are departures from the 1991-2020 base period monthly means, using ERA5 data. The red box marks the Niño 3.4 area for calculating the ONI. Figure is modified, original is from L'Heureux and LaJoie (2021).

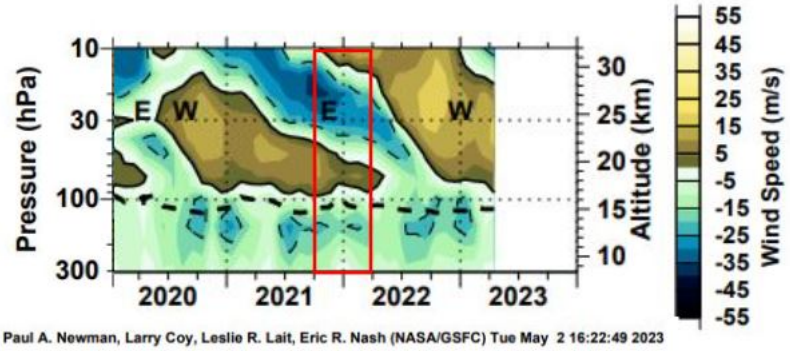

Figure 5.3: Zonal wind speeds derived from radiosoundings in Singapore (01.34 °N, 103.89 °E), in monthly averages. The dashed black line indicates the LRT. The red box marks October 2021 to March 2022. Modified Figure from https://acd-ext.gsfc.nasa.gov/Data$_s$*ervices*/*met*/*qbo*/*qbo.html*, *Downloaded*24.04.23.

The QBO phase during the SO287 CONNECT ship campaign is presented in Figure 5.3, using data from radiosoundings in Singapore. The QBO phase is in the midst of transitioning from Easterly to Westerly winds during the campaign period. Westerly winds are observed above 30 km altitude, followed below by strong Easterly winds above 20 km altitude that are propagating downward toward the tropopause later in 2022. Westerly winds remain dominant between the LRT and approximately 20 km altitude, with a thin layer of weak Easterly winds just above the LRT.

The temperature profiles obtained with radiosondes during SO287 CONNECT, displayed in Figure 5.4a, show that the cold point tropopause was observed at an average altitude of 17 km across the cruise track. In the first half of the cruise, the CPT and LRT stay separated by a couple of km. The largest separation can be seen in and around the Northernmost station no. 27, where the deviation is around 10 km and hence exhibit extratropical features. The LRT and CPT are more co-located in the East Pacific and Caribbean Sea than over the Atlantic, though the latitude of the radiosonde launch must be taken into consideration here (see lower panel in Figure 5.5). Radiosondes over the tropical East Pacific Ocean and the Caribbean Sea identified a more well-defined CPT than those launched over the tropical Atlantic.

Figure 5.4b displays a prominent pattern of strong Westerly winds centered around 15 km altitude, with wind speeds reaching up to 60 m/s in the first 19 radiosonde profiles. The altitude and latitude of the zonal wind maximum suggest that this is a subtropical jet, and should be the lateral boundary of the TTL. The separation of the CPT and LRT in this region can therefore be due to the mixing associated with the subtropical jet. On the cruise track diversion

North to the Northernmost station no. 27, a different wind regime was observed with Westerly winds throughout the whole sampled column. The wind speeds here are not as strong as the subtropical jet that was encountered previously during the cruise. This fits with the description of extra-tropical signals like large separation between CPT and LRT that does not necessarily need to be in the vicinity of the subtropical jet. For sondes no. 33-45 in the Caribbean Sea and the East Pacific Ocean, Easterly winds were observed directly over and following the tropopause, for the co-located CPT and LRT. Comparing the expected QBO signal from Figure 5.3 we see a thin layer of Easterly winds directly over the tropopause followed by a Westerly signal before turning back to Easterly with increasing height in both figures. As the QBO is a tropical feature, signals of it indicate that tropical air masses were sampled.

Comparing Figure 5.4a displaying temperature profiles to Figure 5.4c depicting ozone profiles one can detect that the tropopause is usually located near the abrupt shift from low to high mixing ratios of ozone in the upper troposphere or lower stratosphere. Sonde no. 27 also shows an abrupt increase of ozone co-located with the LRT rather than CPT. The low LRT and shift from high to low ozone in sone no. 27 may suggest a tropopause break. However, comparing Figure 5.4c and 5.4b, the ozone concentration in the upper troposphere observed by sonde no. 07 and 13 are not affected in the same way as in sonde no.27, even when experiencing higher wind speeds.

Defining a TTL from Figure 5.4 is challenging. Using the ozone profiles, signals of the TTL are possible to see in sonde no. 07, where the ozone minimum and CPT are not co-located, though this sonde also observed the subtropical jet which suggests that it's located on the boundary of the areas with a TTL. The same can be said for sonde no. 13, though the ozone minimum and CPT is more co-located here. As previously established, sonde no. 27 is extra-tropical and has therefore no TTL. The remaining three sondes have co-located ozone minimums and CPT and would therefore need additional input to be able to define a TTL. Radiosonde plots including temperature, humidity, wind speed and direction are included in Appendix A.

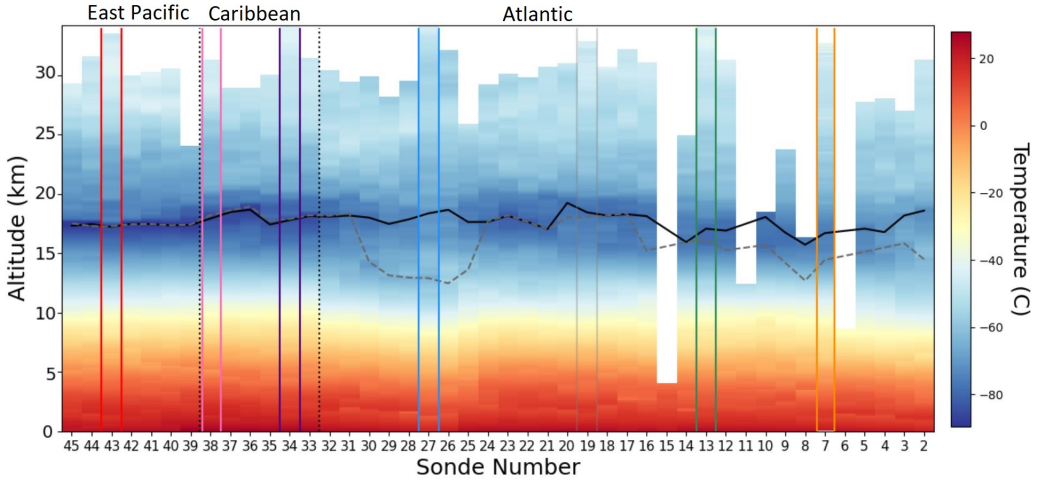

(a) Temperature (°C)

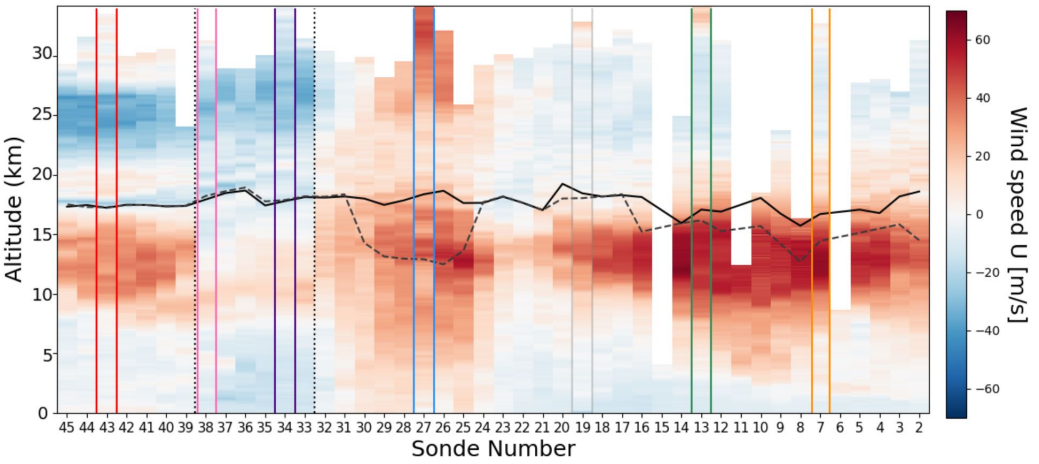

(b) Zonal wind speed (m/s)

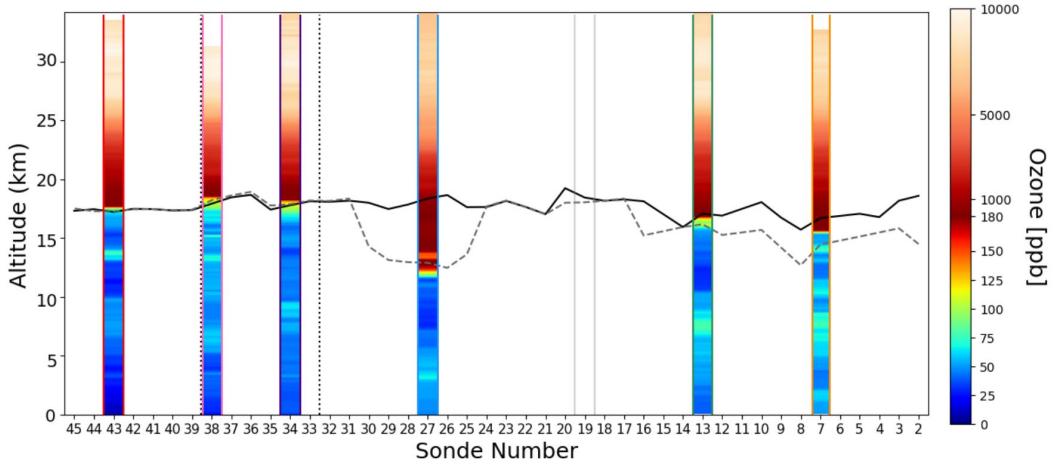

(c) Ozone (ppb)

Figure 5.4: Time-height cross-sections from radiosonde data. Black line marks the CPT, gray dashed line marks LRT. Colored vertical bars mark the ozone sondes. Dotted vertical lines mark different ocean basins; the left of the dotted line is the Pacific, the middle of the dotted lines is the Caribbean, and the Atlantic is right of the dotted line. Note that the x-axis has been inverted.

5.2 SO287 CONNECT ozone profile overview

The ozonesonde profiles sampled during the SO287 CONNECT cruise are presented in Figure 5.5. For a continuous view of the profiles on a logarithmic x-axis, please see Figure A.1 in Appendix A. In the troposphere, the ozone values are around 45 ppb on average, with a minimum of about 25 ppb, and a maximum of around 80 ppb in the free troposphere. In the stratosphere, the ozone maximum among the sondes is between 8 and 10 ppm, and is located between 29 and 31 km altitude. Going through the ozone profiles chronologically from the surface to the stratosphere, the sonde no. 07 launched East in the Atlantic exhibits the highest boundary-layer ozone mixing ratios of the ozone-sondes. There is a local maximum in profile no. 07 just above 7.5 km altitude, with smaller local maximums at 11 km and 14 km. The sharp increase in ozone takes place at 15km altitude, reaching its maximum of about 8 ppm in the stratosphere. Continuing, ozone-sonde no. 13 exhibits a lower amount of boundary-layer ozone compared to sonde no. 07, but exhibits a similar local maximum at around 7.5 m altitude. The profile reaches its minimum at 12.5 km altitude, with about 25 ppb ozone mixing ratio. The upper troposphere or lower stratospheric ozone increase happens at a higher altitude compared to sonde no.07, at approximately 16 km. The ozone maximum for sonde no. 13 is at 9 ppm. Sonde no. 27 was launched much further North than the other sondes and exhibits a different pattern compared to the other ozone-sondes. Boundary-layer ozone-levels of about 50 ppb, before coming to a brief local maximum of 70 ppb at 3 km altitude. Instead of steadily rising into a local maximum in the middle troposphere, the profile reaches its minimum of 25 ppb at 7.5 km altitude, the same altitude as the two previous ozone-sondes reach their local maximum. The profile then features a sharp increase in ozone as low as 12 km altitude, reaching a local maximum of 180 ppb at 13 km altitude. Sonde no. 27 then reaches the loWest stratospheric maximum, compared to the other sounding from this campaign, reaching 7.5 ppm at 29 km altitude. The first of the two Caribbean ozone-sondes, no. 34, exhibits the straightest ozone profile from this campaign, indicating mixing due to convection. The ozone mixing rations stay mainly within the 35-40 range, with a brief local maximum at 9 km, and a local minimum at 13.5 km. The sharp ozone increase takes place above 16 km altitude, ending in a stratospheric maximum of about 9 ppm at 30 km altitude. The seccond of the Caribbean sondes, no. 38, has similar characteristics to sonde no. 34, though this ozone profile meanders between local minima and maximum points with greater variability than the previous sonde. The upper troposphere or lower stratosphere sharp ozone increase takes place above 17.5 km. Sonde no. 38 features an ozone maximum in the stratosphere that is close to 10 ppm at 31 km altitude. The last ozone-sonde launched during the SO287 CONNECT campaign exhibits the loWest boundary-layer and lower

troposphere ozone mixing ratios of all profiels displayed in Figure 5.5. The ozone steadily increases with height, before reaching a local minimum at 11 km, followed by a local maximum at 14 km. Sonde no. 43 starts its sharp increase in ozone above 17.5 km altitude and reaches the highest stratospheric maximum in both altitude and ozone at 31 km with 10 ppm.

Case studies exploring the unique features in the SO287 CONNECT ozone-sondes will be conducted in Section 5.4. The first case study will be on the near-surface ozone of sonde no. 07 and 13, and their relation SHADOZ stations. The second case study will investigate the mid-tropospheric maximum observed by sondes 07 and 13, in relation to biomass burning. The third case study will explore the "nose" from sonde no. 27, referring to the sharp increase of ozone at 12 km altitude. And lastly, the fourth case study will examine the low near-surface ozone values seen in sonde no.43.

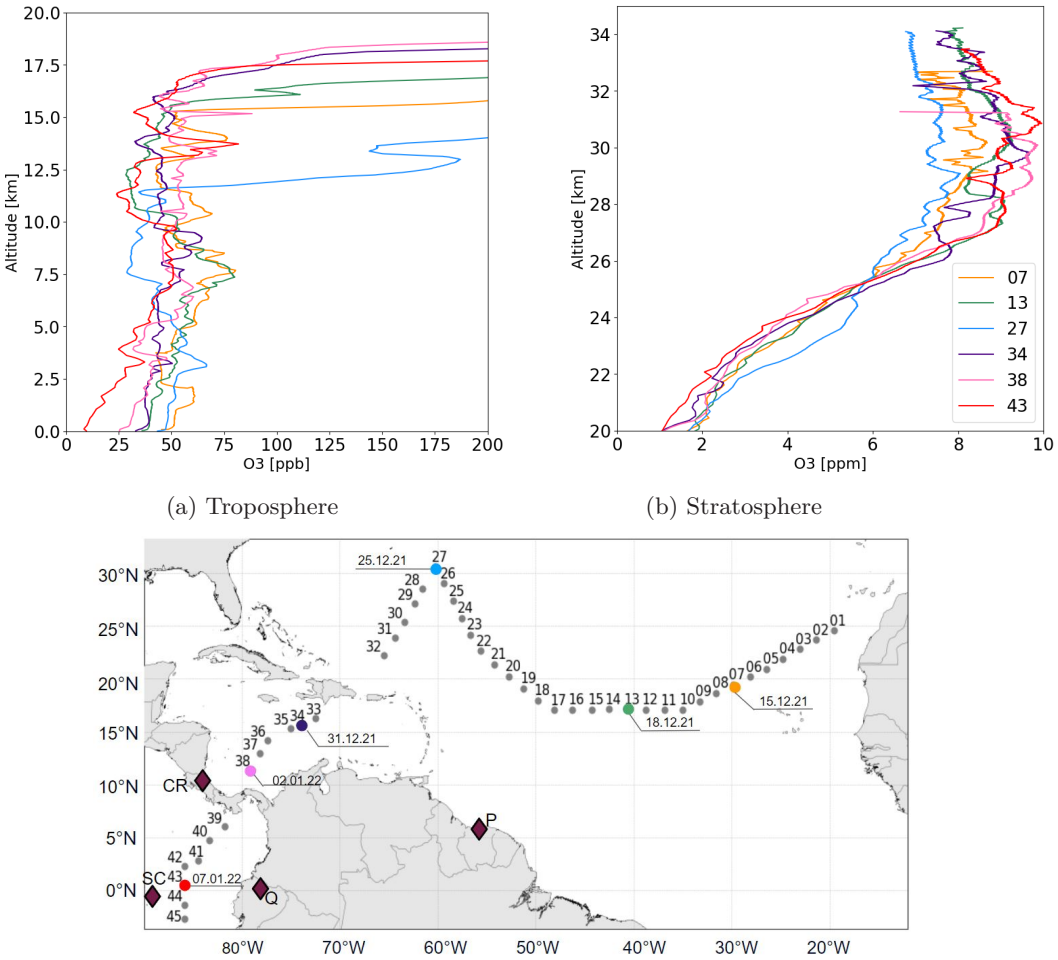

(a) Troposphere (b) Stratosphere

Figure 5.5: Ozone-sonde profiles. Map shows radiosonde launches, ozone sonde launches (colored) and SHADOZ station locations.

5.3 Comparison to SHADOZ

To analyze the ship-based ozone soundings from SO287 CONNECT, data from the network of land-based SHADOZ stations close to the cruise track in has been used for comparison. An overview of the average ozone variability in winter (December to February) for the three permanent SHADOZ stations used and their locations are comprised in Figure 5.6, in addition to two launches at the temporary Quito station.

During December 2021 and January 2022, seven ozone-sondes were launched from the SHADOZ station in Paramaribo, Surinam. In the troposphere, the ozone profiles stay above the 10th percentile of the climatology, as illustrated in Figure 5.6a. However, a few ozone profiles exceeded the upper boundary of the 90th percentile at different altitudes. Ozonesondes launched on December 14. 2021 and January 17. 2022, shows ozone values above the 90th percentile from about 12 km altitude up to the tropopause at 17 km altitude. Additionally, ozonesondes launched on December 20. 2021 and January 17. 2022, exhibited a brief local ozone maximum at an altitude of 2.5 to 3 meters. Another local maximum was observed in ozone-sondes launched on January 10. 2022 and January 24. 2022, at an altitude of 6 to 7.5 km, with the latter not having ozone values exceeding the local 90th percentile. Together, these profiles suggest that ozone at Paramaribo during the cruise period was on average slightly higher than the climatology, indicating an increased abundance of ozone in the region.

The SHADOZ station in Costa Rica is situated at an altitude of approximately 1.2 km (see Section 5.3). During the December 2021 to January 2022 period, four ozone-sondes were launched at the Costa Rica SHADOZ station. There is a local minimum in several of the ozone profiles below about 4 km, but due to missing ozone values and glitches in the data, these profiles are best interpreted above 4 km altitude in Figure 5.6b. All four ozone-sondes remained mostly within the local variability between 4 and 10 km altitude, except for the sondes launched on December 17 2021 and January 13 2022. The first exhibited a slight deviation outside the lower boundary of the 10th percentile around 6 km altitude, and the latter has a brief local maximum of 10 ppb above the local 90th percentile around 8 km altitude. The ozone-sonde launched on January 13. 2022, shows a local ozone maximum between 10 and 12.5 km, which reoccurs in magnitude between 12.5 and 15.5 km altitude. The first of the two maxima exceeds the local 90th percentile reaching 80 ppb, while the second one partially exceeds the upper 90th percentile while reaching the same ozone mixing ratio. The ozone-sonde launched on December 17, 2021, also displayed a local maximum between 12.5 to 14 km altitude, slightly lower in altitude than the second maximum of the January 13. 2022 profile. However, due to its lower position, the maximum ozone value is about 30 ppb higher than

(a) Paramaribo, Surinam
Data from 1999-2020, with 195 profiles.

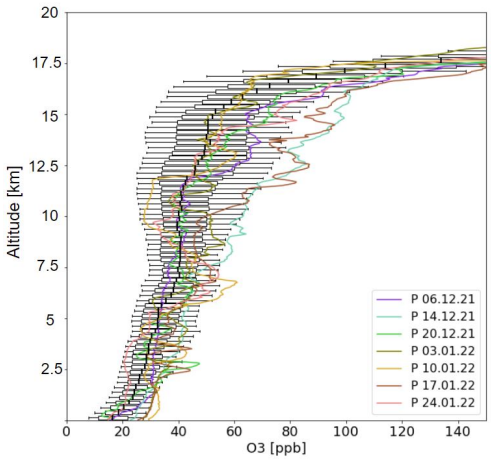

(b) Costa Rica.
Data from 2005-2020, with 141 profiles.

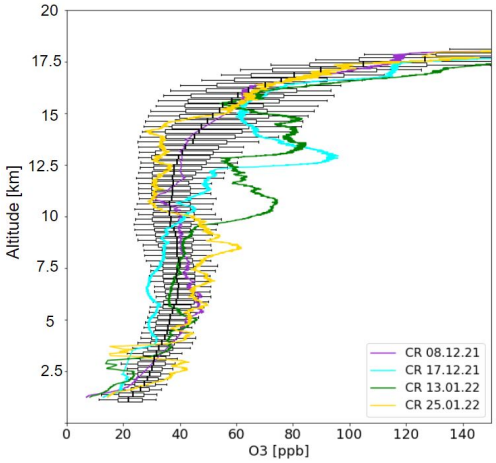

(c) San Cristobal, Ecuador.
Data from 1998-2016, with 90 profiles.

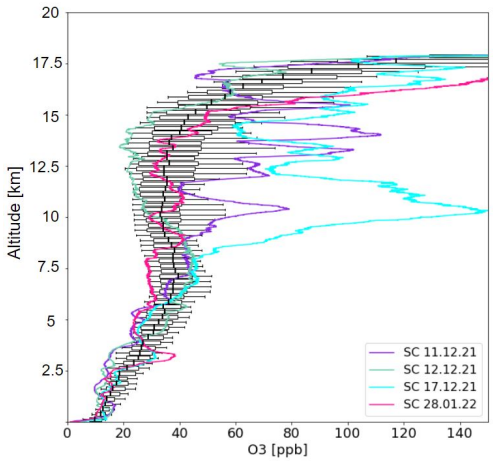

(d) Quito, Ecuador.
Single sondes.

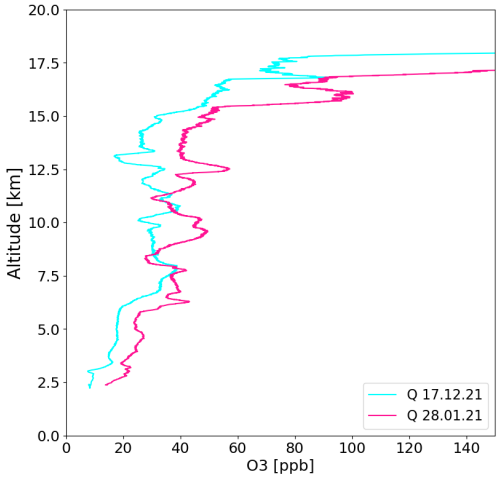

Figure 5.6: Average ozone profile variability for 250 m layers sampled at three SHADOZ stations in December through February. The box represents 50% of the data with the edges marking the 25th and 75th percentile. The right and left whiskers indicate the 90th and 10th percentile, respectively. The black vertical lines within the boxes highlight the median. Colored profiles show ozone profiles sampled in December 2021 and January 2022 and are not included in the box plot calculations.

the 90th percentile in this region, reaching close to 100 ppb. The ozone-sonde launched on December 8 2021, remains well within the central range throughout the troposphere.

The box plots representing the seasonal variability for the ozone profile at the San Cristobal SHADOZ station in Figure 5.6c have a narrower shape than those in Figures 5.6a and 5.6b, indicating lower variability. However, this may partly be due to a shorter time-series with a reduced number of profiles used in the calculation of the climatology. Despite the seemingly lower variability, this station exhibits the largest variability in ozone concentration among ozone-sondes launched by SHADOZ around the time of the SO287 CONNECT cruise. The first two ozone-sondes, launched on December 11. and 12. 2021, demonstrate a significant contrast at altitudes between 9 km and the tropopause at 17 km. The latter remained mostly within the variability whiskers throughout the troposphere, with brief dips below the 10th percentile at approximately 4 and 14 km altitude. The first ozone-sonde shows multiple layers of 80-110 ppb, which is a 20-40 ppb higher ozone concentration than the upper boundary of the 90th percentile. The ozone sonde launched on December 17. 2021, displays the most significant deviations from local variability in the mid-troposphere above 10 km. This local maximum exceeds 150 ppb, which is 110 ppb higher than the upper 90th percentile average variability in this region, season and altitude.

All the permanent SHADOZ stations have soundings in the period from December 2021 to January 2022 that exhibit higher ozone than the respective variability in the middle to upper troposphere. Increased levels of ozone in the upper troposphere in this region have been related to the cold phase of ENSO by Oman et al. (2011), but due to the limited number of profiles being analyzed such a relationship cannot be established here. Some stations have common launch dates, f. e. the launch at both Costa Rica and San Cristobal December 17. The two soundings from this date both reveal high ozone outside their respective variability, suggesting that this signal comes from the same source. The Paramaribo station has a different launch schedule with no common launch dates with the other stations, making it difficult to compare to other stations on an individual profile basis due to the pronounced day-to-day variability.

In contrast to the other SHADOZ stations, Quito does not have a long time-series of ozone profiles (see Table 3.1). Similar to the Costa Rica station, the Quito station is also located at a high altitude, which is the reason why the ozone profiles in Figure 5.6d start at around 2.5 km altitude. There were two launches in Quito close in time to the SO287 CONNECT campaign. Despite Quito being a land-based station, it also exhibits lower-than-expected mixing ratios of ozone close to the ground similar to the other continental-based stations Paramaribo and Costa Rica. Quito had two common launch dates with San Cristobal, one of which coincides with the San Cristobal and Costa Rica common launch date 17 December 2021. Surprisingly, Quito does not show any common tropospheric maximum on 17 December like the two other SHADOZ stations.

5.3.1 Paramaribo and SO287 CONNECT comparison

Referring back to Figure 5.5, the closest ozone-sonde launches to the Paramaribo SHADOZ station are sonde 07 and 13. It was hoped to sample an air mass that later in time would be sampled by the Paramaribo station. Interestingly, Figure 5.7 shows the two sondes launched during the SO287 CONNECT campaign recorded higher concentrations of ozone in the lower to middle troposphere compared to single Paramaribo launches and the variability within the season. Paramaribo is located on land and therefore in closer proximity to anthropogenic sources of short-lived ozone precursors compared to the sondes launched in the middle of the Atlantic Ocean, but is additionally impacted by airflow and the GC. Both the Atlantic SO287 CONNECT sondes exceed the Paramaribo variability in the uppermost troposphere above 15 km altitude, where the two sondes experience the abrupt shift from low to high ozone within the tropopause at lower altitudes compared to the Paramaribo variability. Due to the almost 15 latitudinal degrees difference in launch position, the difference in tropopause height is likely the cause of this slightly premature increase of ozone in the two SO287 CONNECT profiles compared to the Paramaribo soundings.

To investigate whether the same air mass was sampled both by SO287 CONNECT and the Paramaribo SHADOZ station, trajectories in Section 5.4 will be analyzed. This will not only determine if the same air mass was sampled twice but also potentially find out why the lower to mid-tropospheric ozone values are so different.

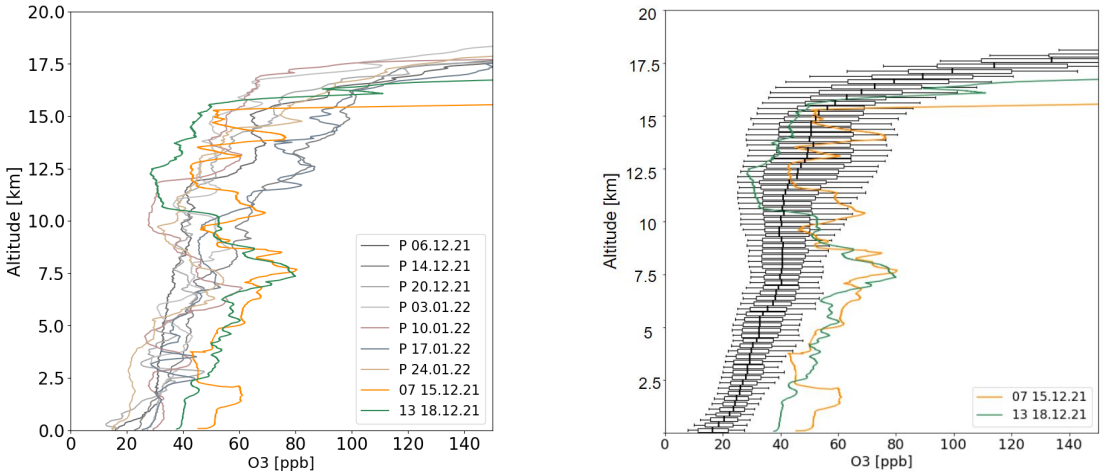

(a) (b)

Figure 5.7: (a) Ozone profiles from Paramaribo during December 2021 and January 2022 (gray), two first Atlantic ozone-sondes from SO287 (colored). (b) Average variability box plots from Figure 5.6a, displayed with the two first Atlantic ozone-sondes from S0287 CONNECT.

5.3.2 Costa Rica and SO287 CONNECT comparison

From Figure 5.8 one can see that the SO287 CONNECT ozone-sondes launched in the Caribbean Sea show slightly higher ozone values in the lower and mid-troposphere compared to the local variability in Costa Rica. Compared to the sondes launched in December 2021 and January 2022 at this station, the "Caribbean" SO287 CONNECT sondes do not appear to be too different, despite being launched over the ocean. Similar to Paramaribo, where there is more ozone over the ocean than land, though with smaller differences compared to Paramaribo. The Caribbean Sea might also be affected by pollution from shipping traffic which is a source of ozone precursors. Given that the Costa Rica station is located at 1.2 km elevation, in addition to glitching data in the lower 4 km of the profiles, a meaningful comparison is not possible in the lower-most troposphere between the SO287 CONNECT sondes and the Costa Rica sondes. Both SO287 CONNECT sondes has local maximums exceeding the 90th percentile of the Costa Rica climatology, at 9 and 7 km for sonde no. 34 and 38, respectively.

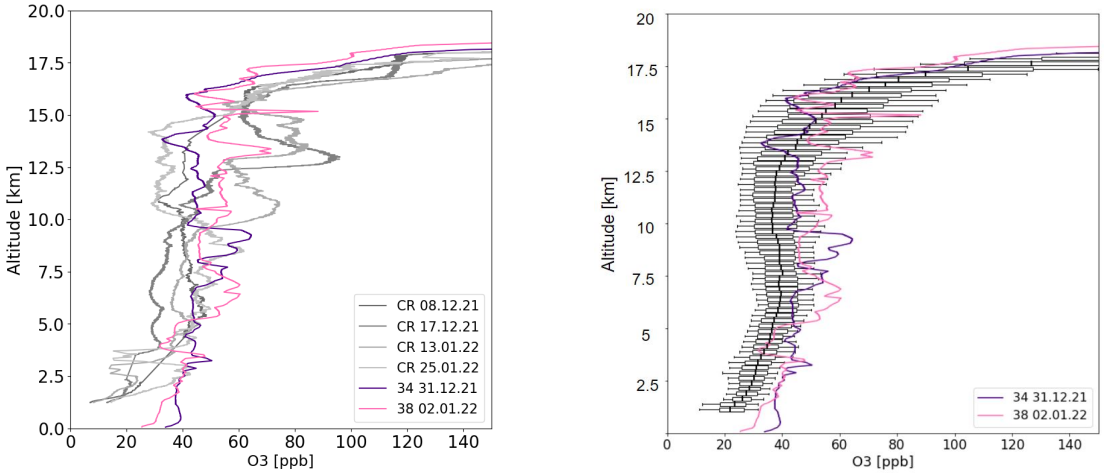

(a) (b)

Figure 5.8: (a) Ozone profiles from Costa Rica during December 2021 and January 2022 (gray), two Caribbean ozone-sondes from SO287 CONNECT (colored). (b) Average variability box plots from Figure 5.6b, displayed with the two Caribbeanc ozone-sondes from S0287 CONNECT.

5.3.3 San Cristobal and SO287 CONNECT comparison

SO287 CONNECT sonde no. 43 is well within the variability at San Cristobal, in contrast to half of SHADOZ sondes launched from San Cristobal during the campaign, as seen in Figure 5.9. The only similarity sonde no. 43 has with the SHADOZ sondes launched in December 2021 and January 2022 is the nose marking high concentrations of ozone outside the variability at around 13 km altitude, apart from low ozone values in the lower 8 km. The low ozone mixing ratios near the surface of about 15 ppb seem normal compared to both the variability box plots and the individually visualized sondes in Figure 5.9.

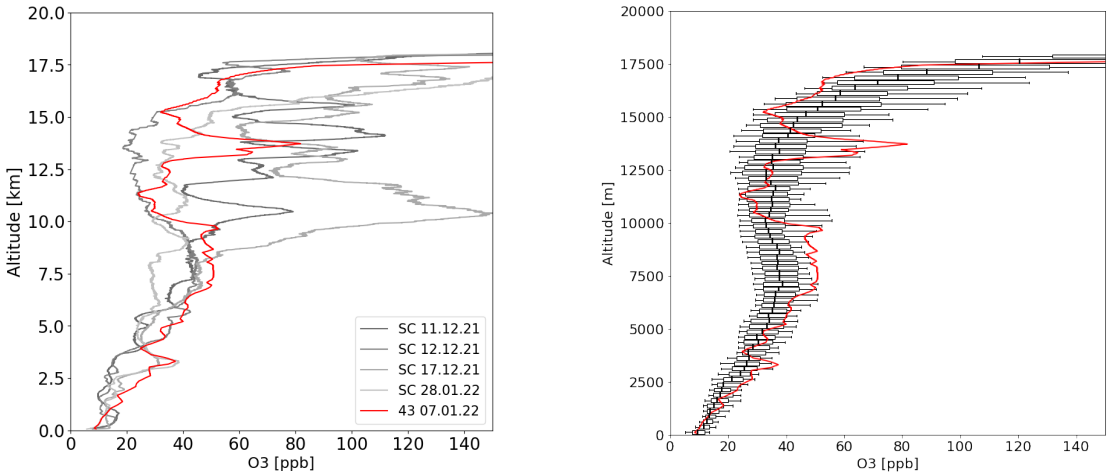

(a) (b)

Figure 5.9: (a) Ozone profiles from San Cristobal during December 2021 and January 2022 (gray), the Eastern Pacific ozone-sonde from SO287 CONNECT (red). (b) Average variability box plots from Figure 5.6c, displayed with the Eastern Pacific ozone-sonde from SO287 CONNECT.

5.3.4 Quito and SO287 CONNECT comparison

Comparing the two launches in December 2021 and January 2022 from the Quito SHADOZ stations to sonde no. 43 from SO287 CONNECT reveals that the observed tropospheric ozone values at Quito are even lower than in the Eastern Pacific. The low ozone mixing ratios suggest that Quito is sampling southern hemispheric air. Analysis of air mass origin will be discussed in Section 5.4.1.

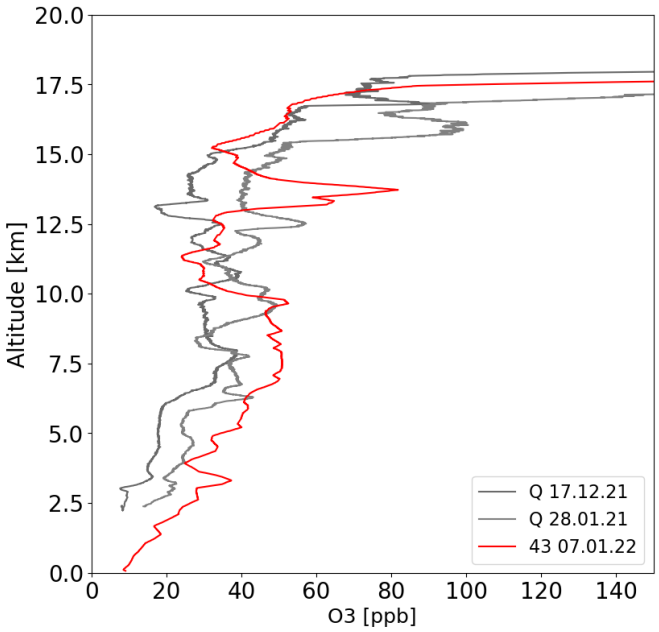

Figure 5.10: Quito ozone-sonde profiles launched during December 2021 and January 2021 (gray), and sonde no. 43 from SO287 CONNECT (red).

5.4 Case studies

In this Section, the four case studies introduced in Section 5.2 will be explored further. First, the Atlantic SO287 CONNECT sondes no. 07 and 13 will be explored with regard to their relation to nearby SHADOZ stations, followed by their local mid-tropospheric maximum. The big deviation in ozone of the Northernmost SO287 CONNECT sonde (no. 27), named the "nose", is being investigated by studying backward trajectories and radiosonde data. Lastly, the low near-surface ozone mixing ratios in SO287 CONNECT sonde no. 43 launched in the Eastern Pacific will be examined.

5.4.1 Double sampled air masses

In Section 5.3 it was highlighted that the Atlantic sondes show higher ozone mixing ratio in the lower and middle troposphere than at the Paramaribo SHADOZ station in the period of the SO287 CONNECT ship campaign. The Atlantic sondes were launched at a position and time so that the same air mass might be sampled by the SO287 CONNECT ozone sondes before being advected and sampled again by the SHADOZ sondes in Paramaribo. Figure 5.11 displays 8 days forward trajectories calculated from SO287 CONNECT sonde no. 07, within the boundary layerat 1000 m altitude. Rather than reaching Quito, the majority of this trajectory ensemble flows close to or over the SHADOZ Paramaribo station 4 to 5 days after the launch of sonde no. 07. Conveniently, sonde no. 07 was launched on 15.12.2021, while there was a launch on 20.12.2021 at Paramaribo, granting the possibility that the same air mass was measured twice.

Figure 5.12 displays SO287 CONNECT sonde no. 07 together with Parmaribo sonde launched 20.12.2021. In the lower troposphere, there is considerably less ozone observed over Paramaribo than SO287 CONNECT sonde no. 07. The lower ozone values in Paramaribo stay between 10-30 ppb lower than the SO287 CONNECT no. 07 sonde. Considering both launch locations with regard to the monthly mean ITCZ position (Figure 5.1), Where the SO287 CONNECT

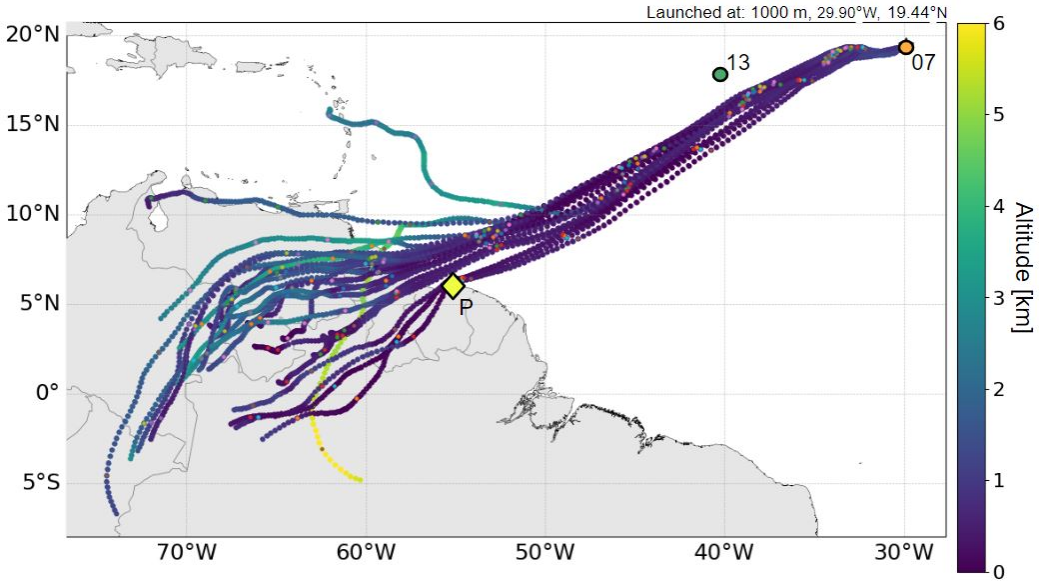

Figure 5.11: 27 member ensemble 8 days forward trajectories generated using HYSPLIT, with meteorological data from GFS. Colorbar shows altitude, colored points mark every 24 hours.

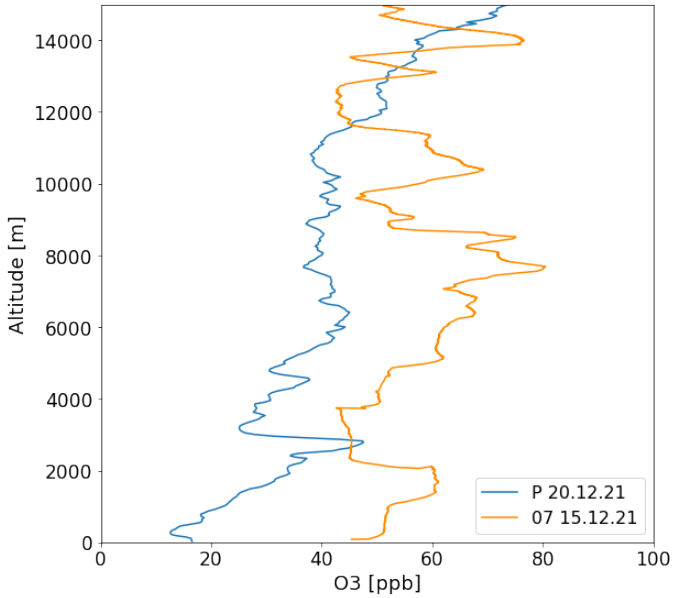

Figure 5.12: Ozone profiles from SO287 CONNECT sonde no 07 (orange), and SHADOZ Paramaribo 20.12.2021 (Blue).

was North of the ITCZ and Paramaribo was close to the ITCZ, there should be less ozone in the lower troposphere over the Atlantic Ocean compared to land due to sources of short-lived ozone precursors being emitted from for example anthropogenic activity or biomass burning, however, we observe an opposite signal.

Calculated backward trajectories from Paramaribo visualized in Figure 5.13 suggest that air masses observed at Paramaribo on the 20th of December 2021 originate both from the NorthEast and SouthEast of Paramaribo, with the majority coming from the SouthEast. None of the trajectories pass over the exact point of the SO287 CONNECT sonde launch position, but at lEast 10 out of 27 trajectories originate in the general vicinity. The Backward trajectories splitting into a Northern and a southern branch indicate that the Paramaribo station is located within the ITCZ. The lower ozone values in Paramaribo seen in Figure 5.12 can therefore be due to mixing with cleaner southern hemispheric air in the ITCZ. Hence, The Paramaribo ozone-sonde reveals signatures of southern hemispheric air, while ozone-sonde no. 07 is of Northern hemispheric origin.

Continuing this case study, Figure 5.14 displays forward trajectories from sonde no. 13 at 1000 m altitude. The sonde no. 13 was launched specifically to be able to sample the same surface air mass as Paramaribo, but the forward trajectories reveal that the air mass reaches Quito rather than Paramaribo. The trajectories mostly stay close to the ground, a few ascending after passing Quito. Instead of following the general Easterly flow of the trade winds near the equator, most trajectories pass the equator and continue south, along the prominent Andes mountain ridge.

Changing the perspective, back trajectories from Quito on the 17 December 2021 (Figure 5.15) and flow the expected general direction of the trade winds. These trajectories show that the air masses likely passed both the launch positions of SO287 CONNECT sondes 07 and 13 about 7 and 6 days prior to reaching Quito. Unfortunately, the timing of the launches during the SO287 CONNECT campaign and the launches at Quito does not match up perfectly for the air masses to be sampled two or three times.

All three SO287 CONNECT sondes show higher ozone values than those sampled in Quito during December 2021 and January 2022 in Figure 5.16. The back trajectories suggest the air masses sampled over Quito come from the Northern Hemisphere (Figure 5.15), in addition to passing over the South American

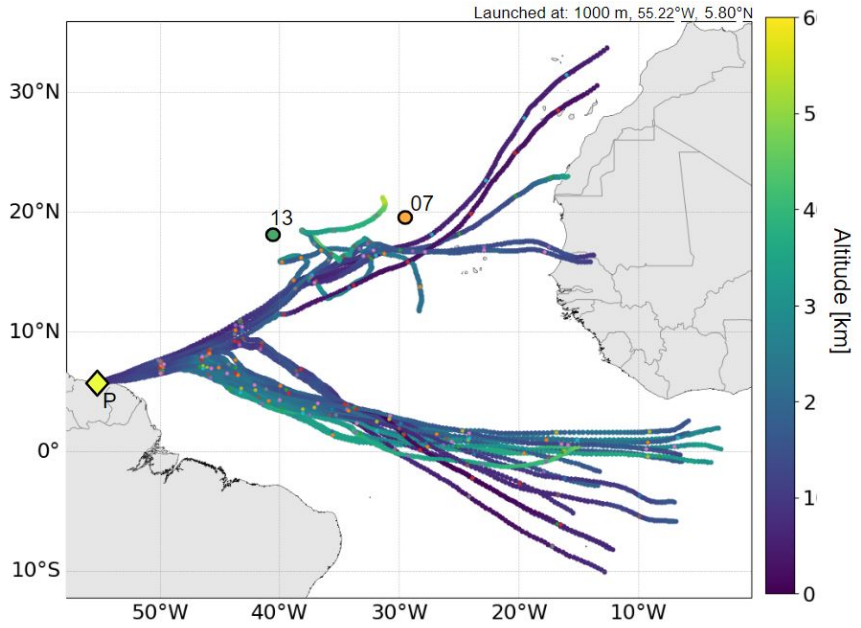

Figure 5.13: 27 member ensemble 8 days backward trajectories generated using HYSPLIT, with meteorological data from GFS. Colorbar shows altitude, colored points mark every 24 hours.

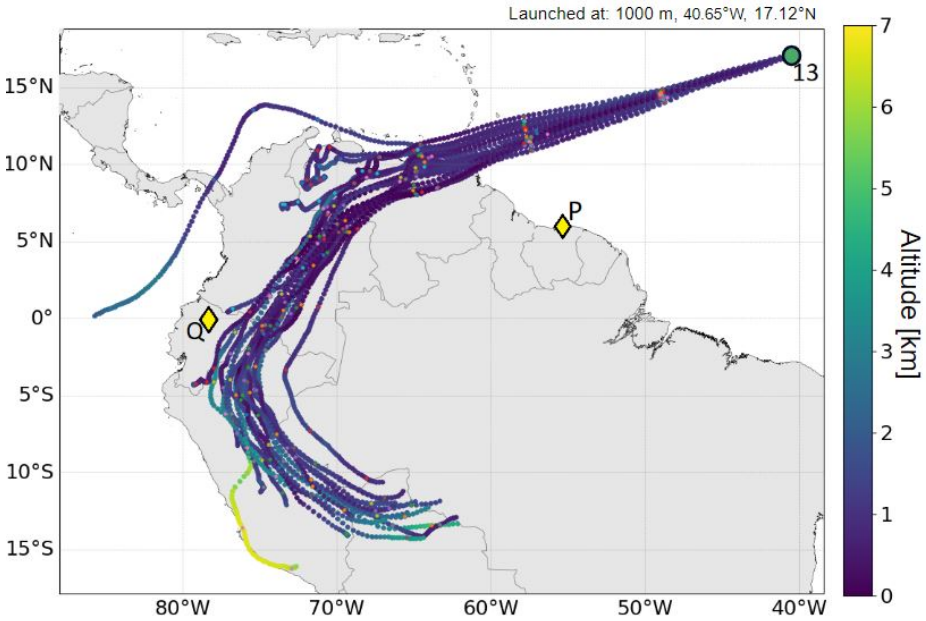

Figure 5.14: 27 member ensemble forward trajectories generated using HYSPLIT, with meteorological data from GFS. Colorbar shows altitude, colored points mark every 24 hours

continent close to the ground, and should exhibit elevated ozone mixing ratios near the surface. However, it is difficult to properly compare the single soundings from Quito with the sondes from SO287 CONNECT because the launch at Quito was the day prior to SO287 CONNECT sonde no. 13.

Considering the low ozone values from the SHADOZ sondes at Quito, compared to the sondes of SO287 CONNECT, the sampled air mass seems to have a signature of clean southern hemispheric air. The forward trajectories from SO287 CONNECT sonde no. 13 in Figure 5.14 indicate that the air masses are redirected south by the Andes mountain range, and no trajectories pass directly over Quito. This supports the theory that the mountain range blocks the Quito station from experiencing Northern hemispheric air masses, hence sampling southern hemispheric air. The back trajectory from Figure 5.15 shows the opposite. Taking into account that both the SO287 CONNECT sonde no 43. and the SHADOZ sounding at San Cristobal, Galapagos all experienced southern hemispheric air during the same time frame raises concerns about the accuracy of the backward trajectories from Quito. Revealed in Figure 5.6, Quito does not have the tropospheric maximum signature seen on the same date in both San Cristobal and Paramaribo, suggesting that Quito experienced an air mass different from the air masses observed at the two other SHADOZ stations.

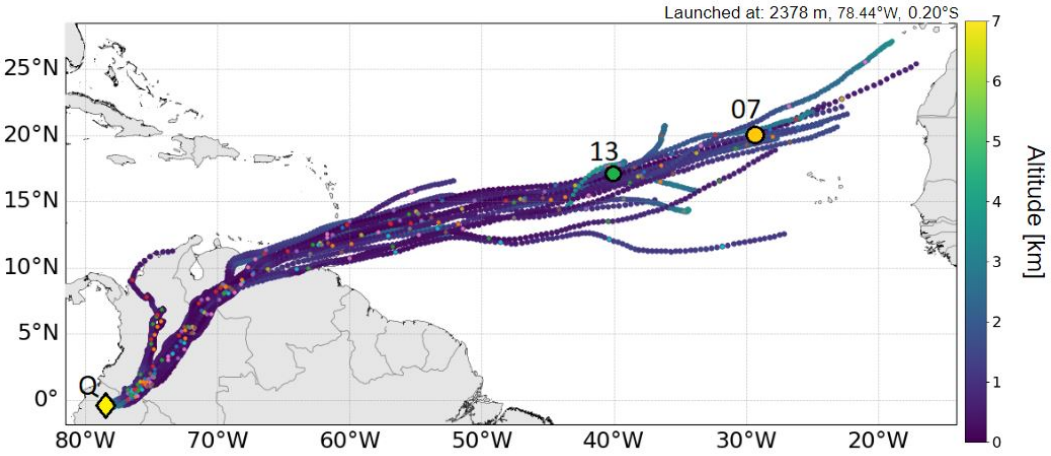

Figure 5.15: 27 member ensemble 8 day backward trajectories generated using HYSPLIT, with meteorological data from GFS. Colorbar shows altitude, colored points mark every 24 hours.

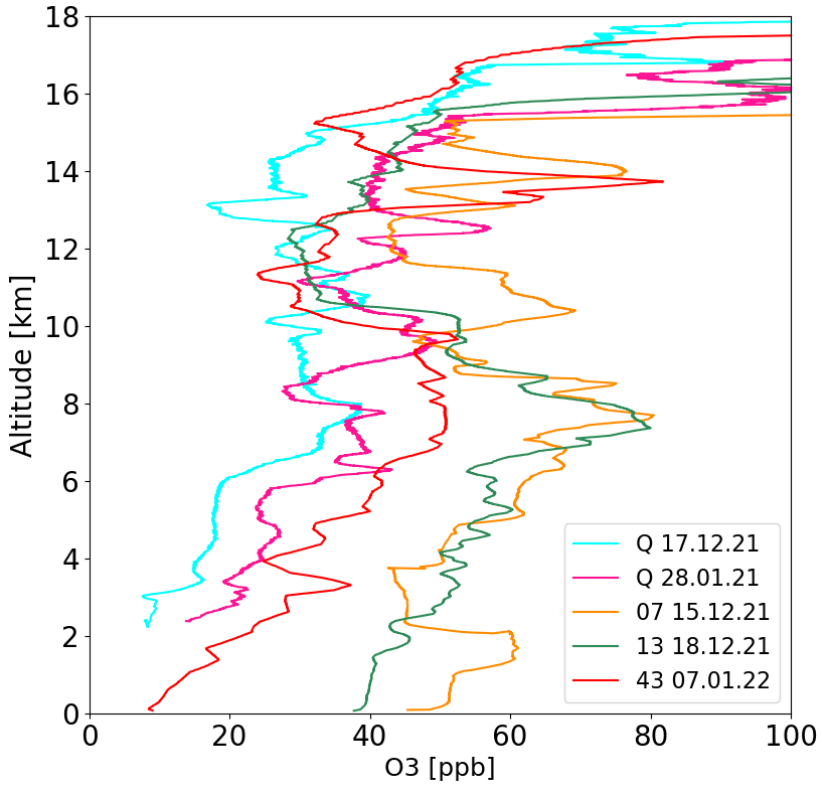

Figure 5.16: Quito ozone-sonde profiles launched during December 2021 and January 2021, SO287 CONNECT sondes no. 07, 13, and 43.

5.4.2 Mid-tropospheric ozone maximum

Figure 5.17 visualizes backward ensemble trajectories started from the mid-tropospheric maximums seen in SO287 CONNECT sonde no. 07 and 13. The majority of the ensemble members pass over North America before reaching the point where it was observed. Not many ensemble members show air-mass origin close to the ground, but a couple of members from each ensemble show close-to-ground air masses West off the coast of Mexico, probably related to convection. The majority of all ensemble members in both trajectories originate from either the same altitude as it was sampled during SO287 CONNECT, or above. Most trajectories also begin in the North-East Pacific, apart from some outliers, where the 07 trajectories have thee outliers originating from China, southern-middle Pacific, and one originating from close to the surface not far away from the cruise track in the Atlantic.

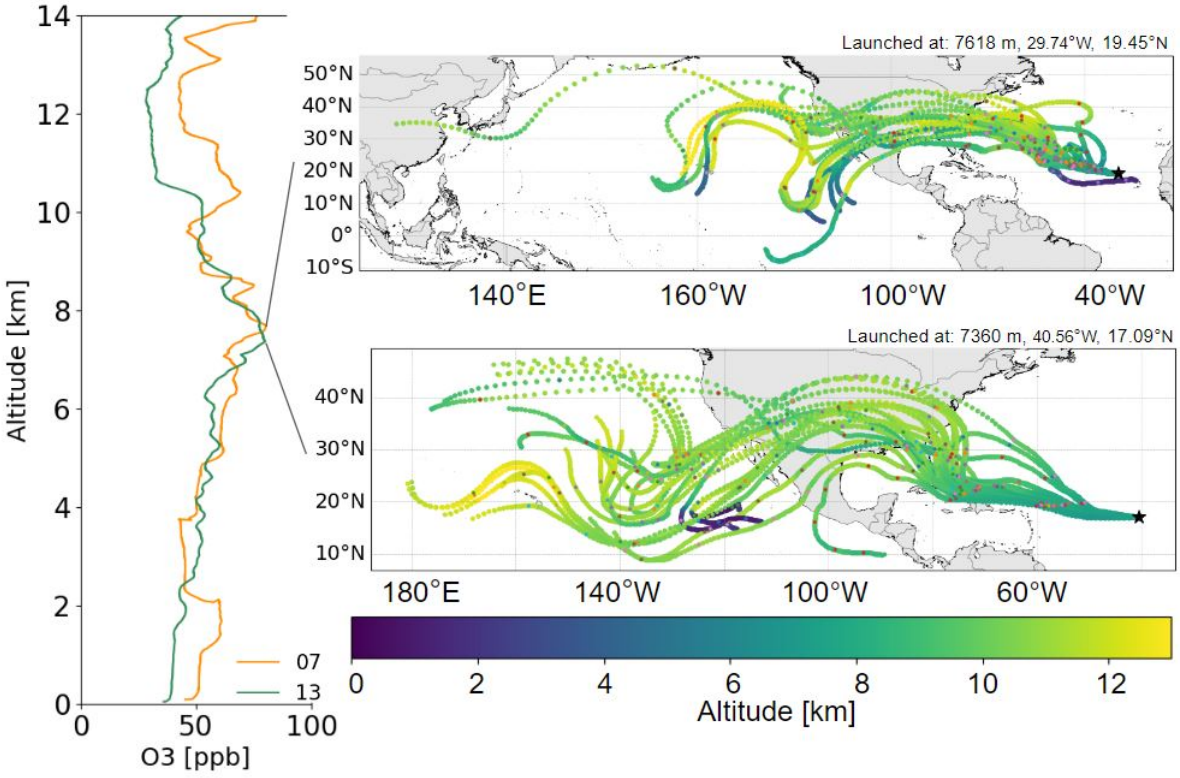

Figure 5.17: 27 member ensemble 8 day backward trajectories generated using HYSPLIT, with meteorological data from GFS. Colorbar shows altitude, and colored points mark every 24 hours.

Figure 5.18 displays active forest fires over the North American continent in the time frame related to the trajectories in Figure 5.17. The amount of biomass burning shown in Figure 5.18 supports the suspicion that these tropospheric

Figure 5.18: Active forest fires from 08.12.21 to 17.12.21, figure modified, original from https://firms.modaps.eosdis.nasa.gov/, Downloaded 13.05.2023.

ozone layers in SO287 CONNECT sondes 07 and 13 stem from biomass burning. Although this layer may fit the description of an ozone-rich tropospheric layer affected by biomass burning from Thompson et al. (2000), the altitudes of the trajectories do not support this because they saw air mass origin not close to the surface.

Examining the radiosonde profile data available for the two sondes in Figure 5.19, one can see a layered relationship between ozone and relative humidity. Both mid-tropospheric noses occur when the relative humidity is very low. Signals with low relative humidity and local ozone maximums are associated with filaments of dry stratospheric air, suggesting that these layers may have stratospheric origin rather than emissions of ozone precursors like biomass burning. Further investigations using other trace gases could be useful to establish the origin of the layer.

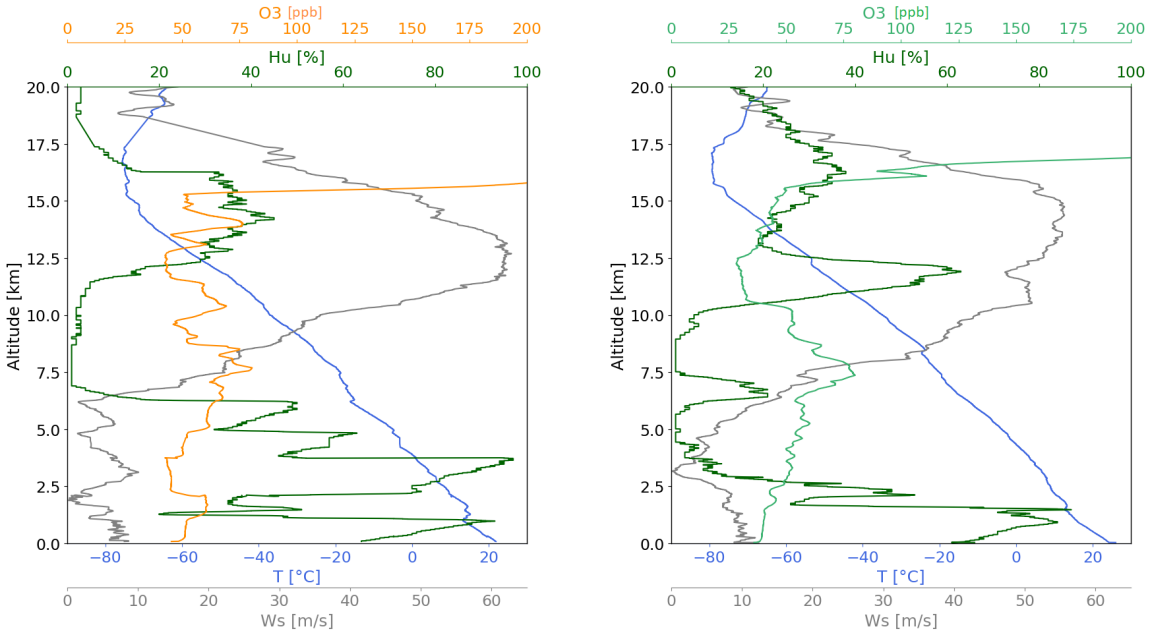

(a) (b)

Figure 5.19: (a)SO287 CONNECT sonde no. 07 and (b)SO287 CONNECT sonde no. 13 radiosonde profiles showing ozone [ppb], relative humidity [%], temperature [°C] and zonal wind speed [m/s].

5.4.3 Extra-tropical profile

This case study aims to investigate the nose of around 185 ppb at about 13 km altitude for SO287 CONNECT sonde no. 27 (Figure 5.2). Figure 5.20 shows 27 backward trajectories launched at location, altitude, and time when SO287 CONNECT sonde no. 27 observed the abrupt peak in ozone mixing ratios. In addition, two more trajectory ensembles were launched at a lower level below the nose, and in the little "anti-nose" just above it. From this plot, it is apparent that the air mass sampled is greatly affected by the subtropical jet because of the large wind speeds and thus distance traveled in just over 8 days.

All three trajectory ensembles derived from various altitudes exhibit similar outcomes. Going forward in time, all three trajectory ensembles indicate that the air mass has been at an approximate altitude equivalent to the sampling height for the duration of the trajectory, beginning over the Northern African continent or Mediterranean area. The lower trajectory ensemble in the lower panel of Figure 5.20 follows a seemingly straight path along the 30-40 °N latitude across Asia. They then divert from their straight path into a wave-like shape over the Northern Pacific Ocean where a few trajectories reach as far as 50 °N at 170 °W, followed by all trajectories reaching 20 °N at 150 °W.

This wave-like behavior can be recognized in the upper and middle panels of Figure 5.20 as well, where the diversion from the previous straight path gets larger with decreasing altitude. In the lower trajectories launched at 10666 m, the majority reaches above 50 to 60 degrees North. For trajectories launched at 12829 m, the majority of trajectories remain on a straight Eastward path, while a few trajectories exhibit a deviation further North compared to the trajectories that were launched at a lower altitude. Judging by the trajectory flow pattern, this wave-like deviation from the Westerly flow might be due to the synoptic situation, resembling the shape of a high-pressure system. As presented in Section 5.1, the average tropopause was located around 17 km altitude throughout the SO287 CONNECT campaign, though due to deviations in LRT and CPT for sonde no. 27 the exact height of the tropopause is hard to determine. The tropopause in the tropics is generally at higher altitudes than in mid-latitudes and polar regions. While the backward trajectories generally stay within the same altitude as the endpoint, they move into regions where the tropopause might be significantly lower when they swing North. This would mean the air mass enters the stratosphere when going North, explaining the high ozone mixing ratios observed by sonde no. 27. With this line of thinking, the trajectories that reach the furthest North should show more ozone, given that the ozone has a similar lifetime in all three altitudes. This means, however, that the trajectory launched at 10666 m should show the most ozone, while it

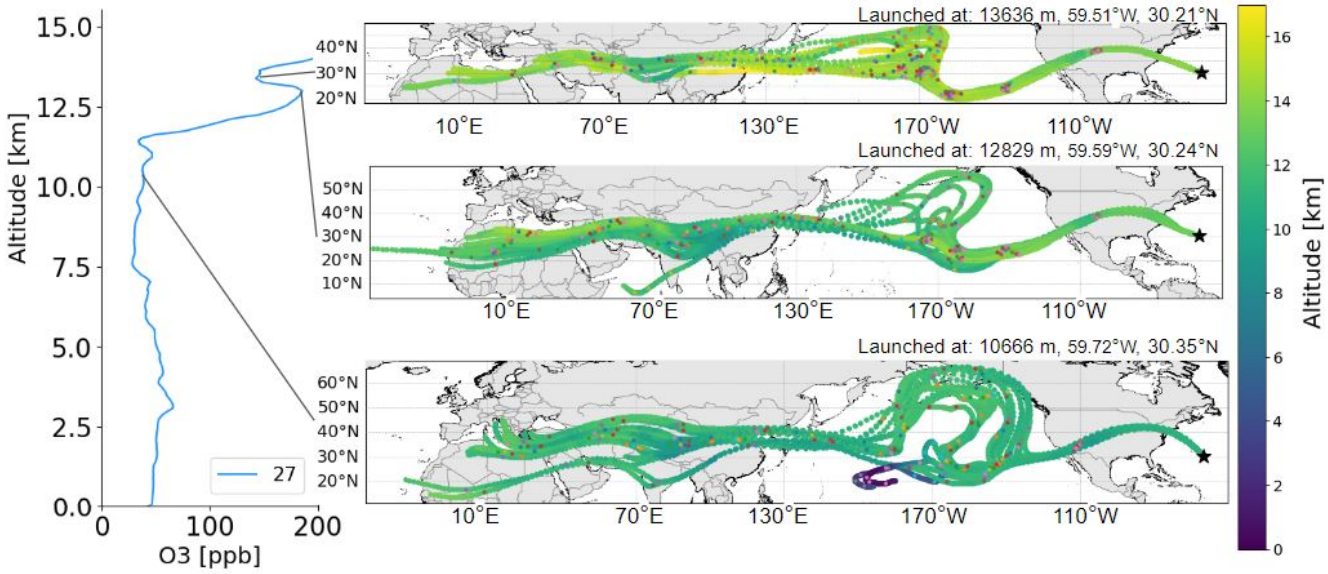

Figure 5.20: 27 member ensemble 8 day backward trajectories generated using HYSPLIT, with meteorological data from GFS. Colorbar shows altitude, colored points mark every 24 hours.

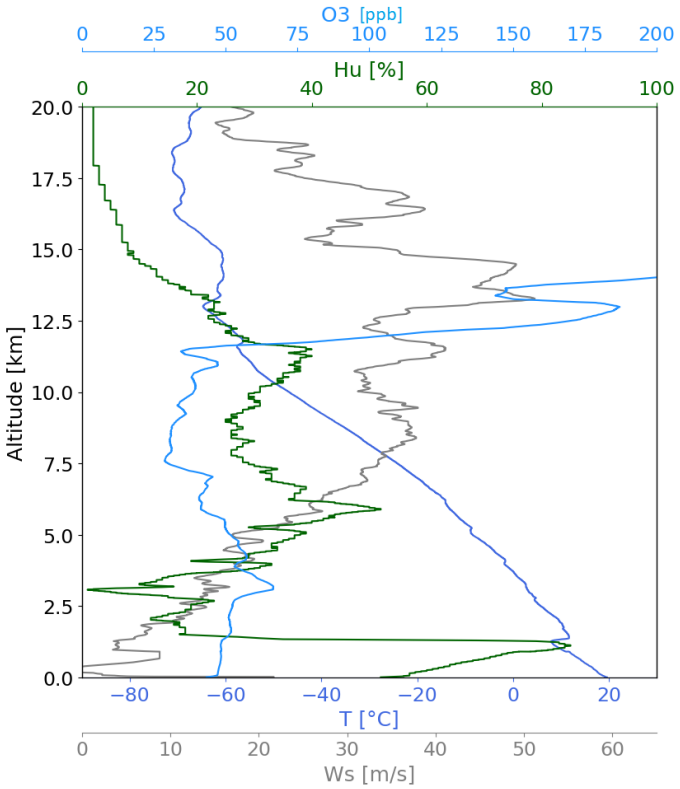

Figure 5.21: Vertical radiosonde profile from SO287 CONNECT sonde no. 27. Showing ozone [ppb], relative humidity [%], temperature [°C] and zonal wind speed [m/s].

certainly does not. The radiosonde profile in Figure 5.21 shows that the relative humidity is about 40% at 10666 m, while at the level of the nose and anti-nose the humidity is 20% and 10%, respectively. The low humidity observed above the sharp increase in ozone at around 12 km indicates that the nose observed as a result of an intrusion of dry ozone-rich stratospheric air.

A large nose is also seen in the 17.12.21 SHADOZ sonde launched at San Cristobal, though this nose is further down in the troposphere and exhibits ozone values of 150 ppb. In contrast to the nose in SO287 CONNECT sonde no. 27, its trajectories do not show that the air mas has been affected by the subtropical jets, as Figure 5.22 reveals. The majority of the trajectories originate in the tropical West Pacific off the NorthEast coast of Australia in the Salomon Sea. Some trajectories show starting points close to the surface, being lifted rapidly due to convection before being advected Northward and then across the Pacific.

Due to the location of the station, this peak in ozone in the middle troposphere is

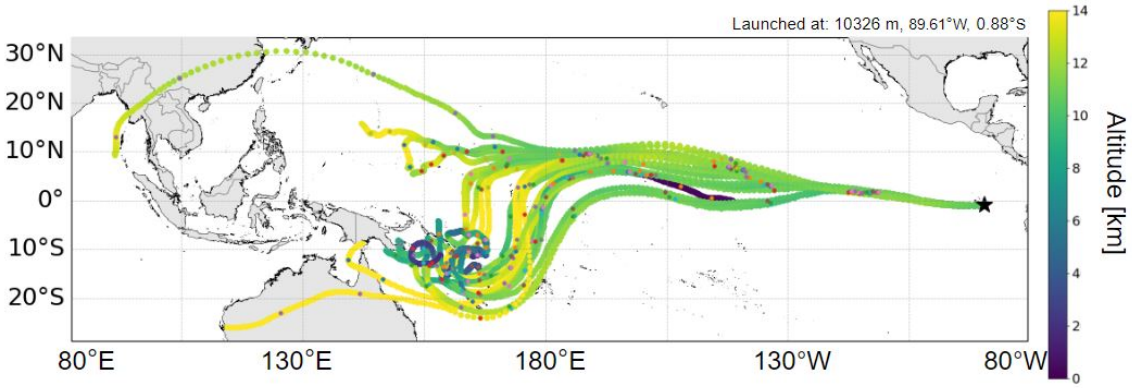

Figure 5.22: 27 member ensemble 8 day backward trajectories generated using HYSPLIT, with meteorological data from GFS. Colorbar shows altitude, colored points mark every 24 hours.

unlikely caused by stratospheric intrusion with regards to the GC and convective activity along the ITCZ. Local production of ozone due to NO_X influx from lightning is also implausible due to both low lightning activity over the ocean and limited NO_X production associated with lighting (Müller, 2020). The backward trajectories show air mass originating from the tropical West Pacific, but this is a region with low ozone concentrations throughout the troposphere (Rex et al., 2014,Müller, 2020). A possible source of ozone for this high ozone peak observed at San Cristobal (and other SHADOZ stations) may be a large local emission of ozone precursors from the Pacific islands where most trajectories have their origin. Figure 5.23 reveals an abundance of forest fires on the NorthEast coast of Australia, as well as Papua New-Guinea. Though these emissions might be disrupted by the humid conditions in the area causing ozone depletion.

The different results from the trajectories started in the two biggest tropospheric peaks seen in this thesis reveal that ozone-rich layers or 'noses' in profiles are not always caused by the same conditions. Further investigations looking into other trace gases are needed to better understand the causes of these layers. There is an ongoing debate about the origin of such high ozone layers, and whether they are stratospheric or due to biomass burning (Müller, 2020, Anderson et al., 2016)

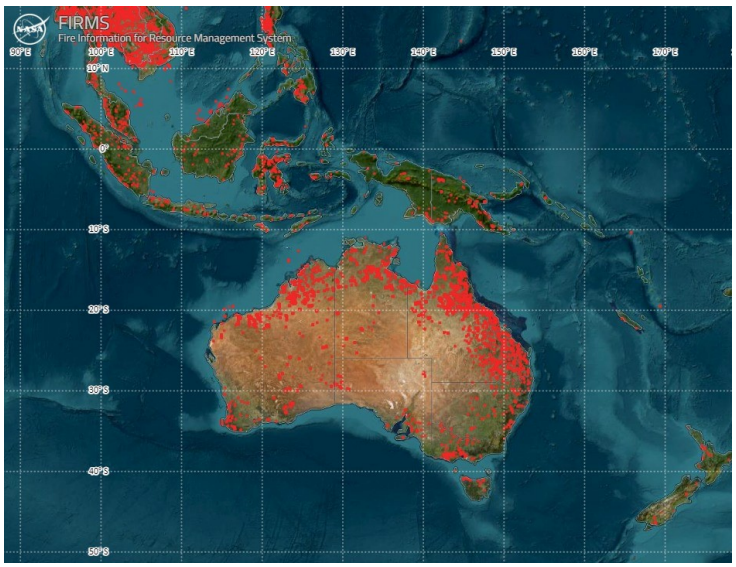

Figure 5.23: Active forest fires from 08.12.21 to 17.12.21, figure modified, original from https://firms.modaps.eosdis.nasa.gov/, Downloaded 14.05.2023.

5.4.4 Tropical East Pacific profile

As seen in Figure 5.24 the low ozone in the SO287 CONNECT profile no. 43 agrees with the local variability within the season. In this case study, the origin of the air sampled will be investigated to better understand what influences lower-tropospheric ozone in the tropical East Pacific. As expected, the majority of the trajectories originate from the clean southern Hemisphere. Few trajectories originate from over land, while the majority comes from over the East Pacific Ocean in the vicinity of where it was sampled by SO287 CONNECT sonde no. 43. According to the GC, and neglecting topography, this sonde should most likely have experienced elevated levels of ozone from being downwind of the southern American continent where anthropogenic and biomass burning emissions are high. This is, however, not the case, as it seems like the Andes Mountain range blocks transport from the trade winds in the area, contributing to the development of these ozone-poor conditions observed both by the SO287 CONNECT sonde no. 43 and the nearby SHADOZ station at San Cristobal. Convection may also play a role in creating this low ozone environment near the surface.

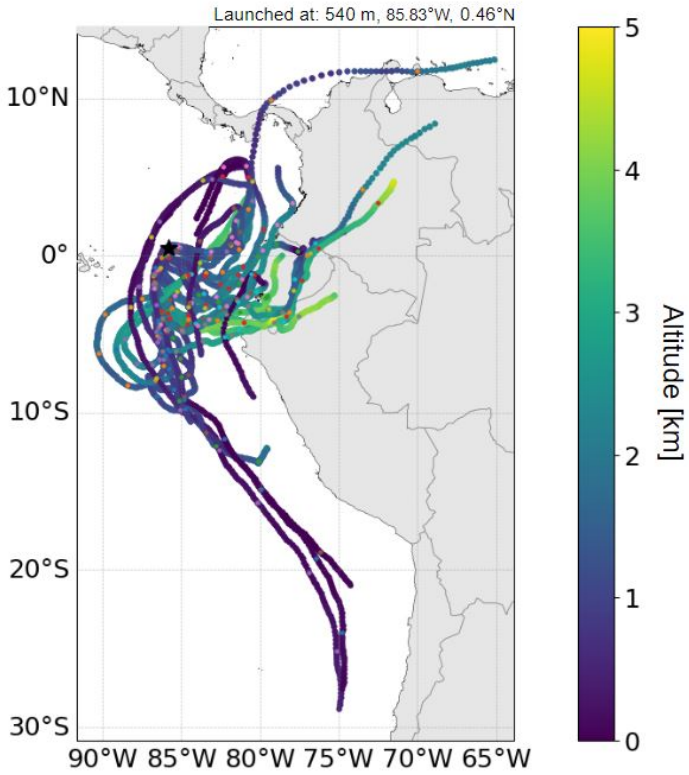

Figure 5.24: 27 member ensemble 8 day backward trajectories generated using HYSPLIT, with meteorological data from GFS. Colorbar shows altitude, colored points mark every 24 hours.

5.5 Comparison to other campaigns

In the following Section, ozone profile data from four additional ship campaigns onboard the RV Sonne will be presented to create an overview of the differences between vertical ozone profiles above the different tropical ocean basins. Data from each ship campaign will be individually examined and compared to the ozone profiles obtained during SO287 CONNECT, starting with ASTRA-OMZ in the tropical East Pacific, continuing with SPACES-OASIS in the Indian Ocean, ending with SHIVA and TrandBrom in the tropical West Pacific. Further, the results will be viewed together to better see their differences and to be used for Wave-one analysis.

5.5.1 Tropical East Pacific

During the ASTRA-OMZ cruise in October 2015, four ozone sondes were started and launched in the tropical East Pacific close to the coast of Ecuador, Peru and Chile. At this time, the ENSO was in its warm El Niño phase. The ASTRA-OMZ profiles show similar ozone mixing ratio near surface and a similar increasing rate with height as the SO287 CONNECT ozone profiles seen in Figure 5.25. SO287 CONNECT sonde no. 43, also launched in the tropical Eastern Pacific, shows even lower ozone mixing ratios than all profiles sampled during ASTRA-OMZ in the lower 5 km. A reason for this is that the ASTRA-OMZ sondes were launched between 10 °S and 18 °S, further south than sonde no. 43 at 0.45 °S (see cruise track in Figure 3.4), or the difference in the ENSO phase. Throughout the rest of the troposphere the ASTRA-OMZ and SO287 CONNECT ozone profiles stay within the variability of each other, apart from a nose at 11 km altitude in the ASTRA-OMZ 20.10.2015 sonde of about 80 ppb, in similar strength as the noses in SO287 CONNECT sondes 07 and 13 at 7.5 km altitude.

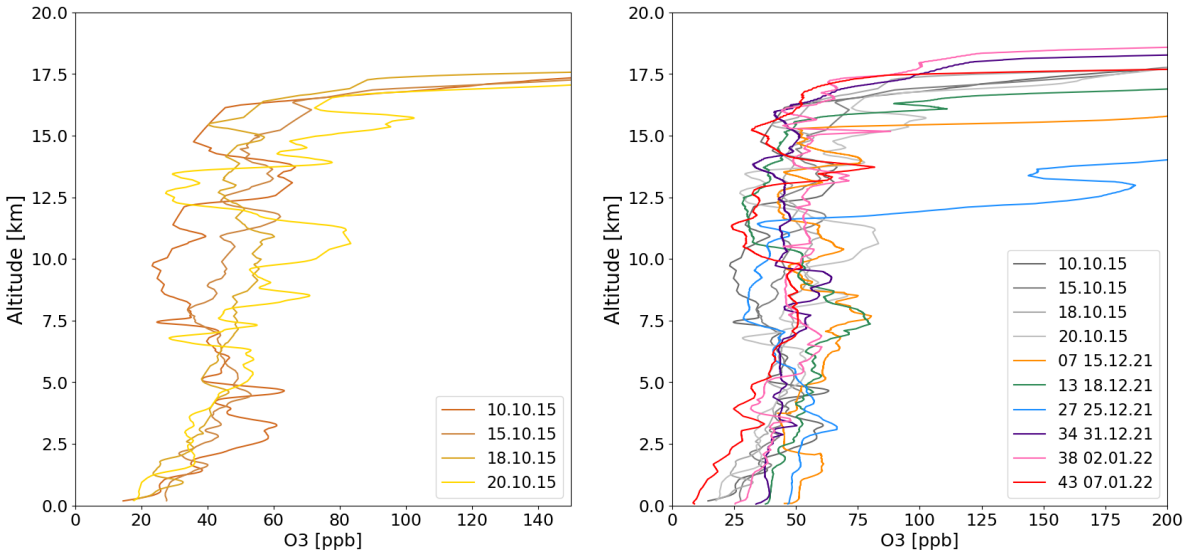

(a) (b)

Figure 5.25: ASTRA-OMZ ozone profiles (a), and SO287 CONNECT ozone profiles (colored) with ASTRA-OMZ(gray) (b).ASTRA-OMZ data is smothered with a rolling mean of 15 data rows per point.

5.5.2 Indian ocean

Five ozone-sondes were launched during the SPACES OASIS campaign over the Indian Ocean in July of 2014, and can be seen in Figure 5.26. The campaign had two separate legs, which is clearly distinguishable just from the ozone profiles in Figure 5.26a, where the sonde launched 18.07.14 was launched further south during the first leg (see cruise track in Figure 3.6). Starting with the SPACES OASIS ozone-sonde launched 18.07.14, this profile shows much higher ozone concentration throughout the entire troposphere compared to the rest of the ozone-sondes launched during this campaign. It has a broad local maximum between 5 and 7.5 km altitude, around the same altitude that the rest of the sondes reach their mid-tropospheric maximum. The ozone profile reviels a sharp nose at around 13 km altitude where it reaches just under 125 ppb. This upper tropospheric nose is reminiscent of the similar, but higher concentration nose of the SO287 CONNECT sonde no. 27, at a similar altitude. Another similarity between these two sondes is the launch latitude and season, where the SO287 CONNECT no.27 was launched in boreal winter around 30°N and SPACES OASIS sonde 18.07.14 were launched just south of 25°S, also in the during austral winter.

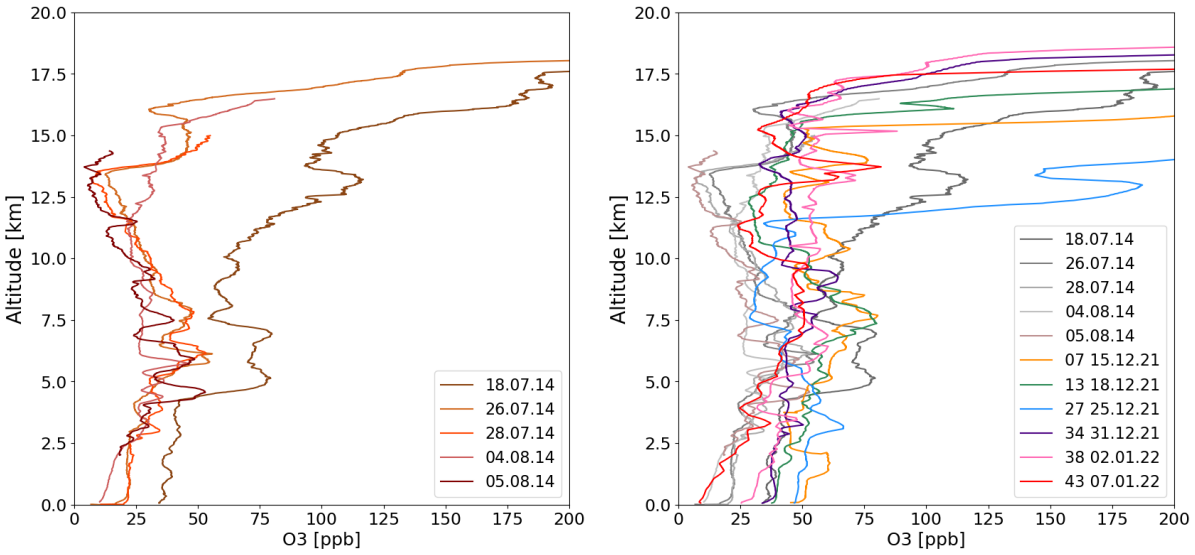

(a) (b)

Figure 5.26: SPACES OASIS ozone profiles (a), and SO287 CONNECT ozone profiles (colored) with SPACES OASIS(gray) (b).

For the second half of the SPACES OASIS campaign the ozone-sondes had more similar values throughout the troposphere. Only one of the sondes from this leg reached the stratosphere. Close to the surface, the ozone concentration for the SPACES OASIS sondes is closer to what was observed in the same altitudes for

the Eastern Pacific during SO287 CONNECT, with an ozone mixing ratio below 25 ppb in southern hemispheric air, which agrees with analysis and trajectories from Fiehn et al. (2017). Ozone mixing ratios stay lower than the majority of the SO287 CONNECT ozone-sondes in the upper troposphere, above 8 km altitude.

5.5.3 Tropical West Pacific

The six vertical ozone profiles obtained during the November 2011 campaign SHIVA in the South China Sea are displayed in Figure 5.27, accompanied by an overlay of the SO287 CONNECT ozone profiles. In the lower 8 km of the troposphere, the profiles start off with similar values near the surface, but diverge into two distinct patterns going upwards; either keeping the same mixing ratio throughout the whole troposphere or slowly increasing the mixing ratio before it remains constant throughout the upper troposphere. The straight signatures in both patterns are likely caused by a well-mixed tropospheric column due to convection, where the tropical West Pacific exhibits the highest level of convective activity worldwide. The first four sondes keep a steady mixing ratio through the whole troposphere, apart from the first sonde launched on 18.11.2011 which only reached 10 km altitude and is therefore difficult to categorize. The two last sondes launched 26th and 27th of November 2011 are the only two sondes that exhibit the latter pattern. The steady increase in ozone up to 10 km altitude is likely due to differences in advection, where the two last sondes are not shielded by the Borneo island like the other ozone-sondes. this agrees with trajectories from Fuhlbrügge et al. (2016). The "steady" mixing ratio sonde pattern is not observed in the ozone profiles obtained during the SO287 CONNECT cruise, as seen in Figure 5.27b. The SHIVA sondes with this nearly straight ozone profiles throughout the troposphere are not only not reciprocated in the SO287 CONNECT profiles but also exhibit much lower ozone mixing ratio above 2km altitude than observed during SO287 CONNECT.

As post-processed data from the October 2009 TransBrom campaign (discussed in section 4.3) is unavailable, Figure 5.28 was produced by superimposing SO287 CONNECT ozone-sonde profiles on top of the published Rex et al. (2014) ozone-sonde data (Figure 4.2a). The majority of the TransBrom sondes exhibit ozone values below the detection limit of the EN-SCI ECC ozone-sonde, while the SO287 CONNECT profiles demonstrate no such outcome except for sonde no. 43 in the lower 2 km. Most tropical TransBrom sondes exhibit straight ozone profiles, indicating an influence of convection. Ozone-sondes launched further North during TransBrom show more similar signatures to SO287 CONNECT ozone profiles, with tendencies of bigger local mid-tropospheric maximums.

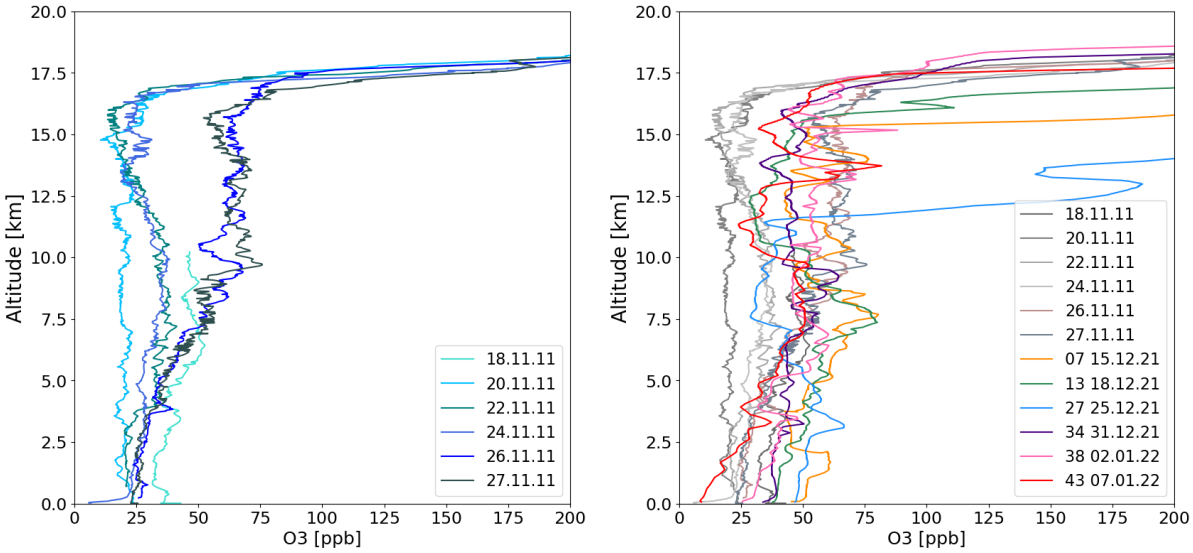

(a) (b)

Figure 5.27: SHIVA ozone profiles (a), and SO287 CONNECT ozone profiles (colored) with SHIVA(gray) (b).

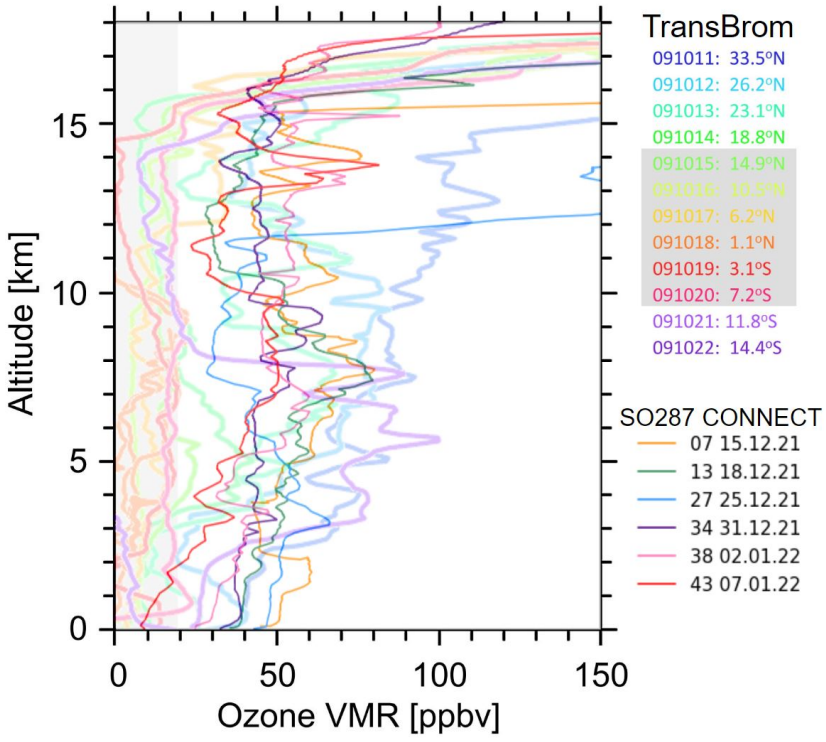

Figure 5.28: Figure displaying TransBrom ozone-sonde data in ppb from Rex et al., 2014 (faded), overlaid by SO287 CONNECT ozone-sonde profiles in ppb.

5.5.4 Wave-one analysis

As seen in previous Sections, there is high variability in tropospheric ozone over the different tropical ocean basins. Sorted by longitude, Figure 5.29 depicts all available ship-based ozone profiles. A pattern reminiscent of the wave-one presented in Figure 2.4 can be interpreted from Figure 5.29, but with many notes of caution. Firstly, Figure 2.4 is made using a seasonally averaged long time-series of SHADOZ data, whereas Figure 5.29 is compiled of single in situ profiles launched in different years, seasons, and other climatological conditions, as well as not covering the whole domain. Secondly, several profiles from the Indian Ocean and TWP do not cover the whole troposphere. Thirdly, two outliers with low tropopauses in ozone due to being extra-tropical and can be seen as the profile first SPACES OASIS profile at 58 °E, and third SO287 CONNECT sonde at -60 °E 2.4 (their similarities discussed in Section 5.5.2). Similar outliers were found when assessing the SHADOZ stations, though a few sub- or extra-tropical stations did not exhibit subtropical character (Thompson et al., 2017).

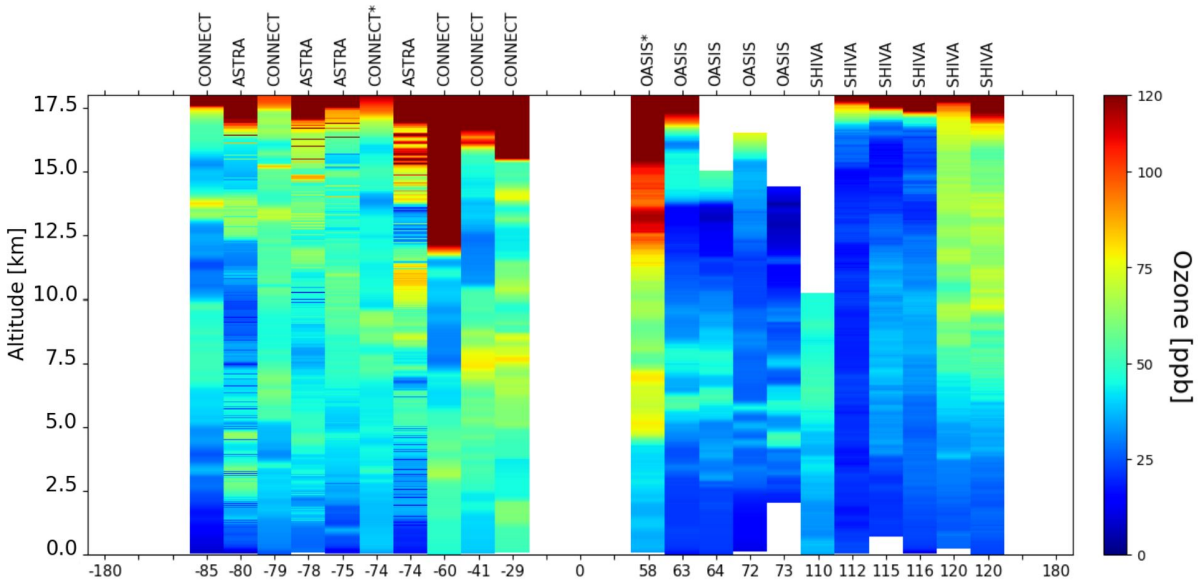

Figure 5.29: Longitude-height cross-section of tropospheric ozone (ppb) with data from (left to right) SPACES-OASIS, SHIVA, ASTRA-OMZ, and SO287 CONNECT.

From Figure 2.4, the left part of the figure depicting data from SO287 CONNECT and ASTRA-OMZ shows more tropospheric ozone than the rest of the profiles in the figure. While the ASTRA-OMZ profiles tend to start off with low ozone concentrations close to the surface, both ASTRA-OMZ and SO287 CONNECT profiles keep a high level of ozone, while exhibiting band-like

features oscillating in between local minima and maximums with increasing altitudes. This kind of band structure is not prominent in the SHIVA profiles, that mostly show well-mixed tropospheric nature in the ozone columns. The two Western-most (120 °W) profiles from SHIVA show higher ozone mixing ratios above 7.5 km altitude. If the TransBrom profiles from Figure 4.2a were to be added to Figure 5.29, the profiles would mostly support the theory that wave-one can be interpreted. Low ozone mixing ratios are prominent in all profiles launched within the tropics during TransBrom, as discussed in Section 5.5.3. Though it is hard to conclude with great confidence that the wave-one-like characteristics in Figure 5.29 is a wave-one signature, a notable difference in tropospheric ozone columns over the different ocean basins can be established.

CHAPTER 6

Model results

This chapter presents the key findings from a full cHemistry simulation using the NorESM. Findings are further validated with respect to expected signals from background theory and observations.

6.1 Surface ozone

Patterns close to the expected difference in surface ozone between Hemispheres is represented by NorESM and displayed in Figure 6.1. Both the annual mean climatology and the single-month climatologies depict distinct differences between the Northern and Southern Hemisphere surface ozone, with a stronger contrast in the boreal winter months of December and January. The Northern Hemisphere features higher levels of ozone, reflecting that the Hemisphere consists of more land mass and a higher population and therefore higher levels of emissions of ozone precursors. The Southern Hemisphere has less land mass, lower population, and therefore lower surface ozone than the Northern Hemisphere. The contrasting Hemispheric air masses stay separated at the ITCZ, agreeing with the theory that the mixing of Northern and Southern Hemispheric air happens on a timescale of years, in addition to the short lifetime of surface ozone on a time-scale of less than a week. The placement of the ITCZ solely based upon the surface ozone displayed in Figure 6.1 is more difficult to pinpoint due to less defined in the annual mean than the single-month panels. Generally, the ITZC would be placed in the darker blue part of the ozone gradient happening within the tropics, the reasoning for this being that ozone is convected away from the surface in addition to convection contributing to the depletion of ozone due to water vapor. Another feature likely caused by the GC is the sinking of ozone-rich air to the surface at 30 °N/S, seen especially in the single-month climatologies in the Southern Hemisphere. The signal here is stronger over land than over the ocean and is likely caused by ozone depletion in the presence of water vapor over the oceans. In the Northern Hemisphere, this feature has a different signal with lower ozone values over the continental

areas experiencing sinking of air compared to the rest of the Hemisphere. The ocean area, in this case, has higher ozone concentrations than land. One reason for this could be that in Borial winter there is less solar insolation that causes less photolysis of ozone, and also less heating off the ocean making the surface have less water vapor.

In both the annual mean displayed Figure 6.1a, and single-month means in Figures 6.1b and 6.1c, locations with higher elevations exhibits more ozone, f. e. the Rocky Mountains, Greenland, the Himalayas, The Mongolian Plateau, and Antarctica. This may be due to the vertical model coordinates being hybrid sigma pressure levels and therefore following the terrain in the lower troposphere, where higher ozone mixing rations are expected at higher elevations. High ozone can also be slightly North of the Equator over Africa, with this signal being more pronounced if Figure 6.1c depicts the January climatology. This signal is likely due to ozone production where high lightning activity in the ITCZ provides NO_X. A feature that is stronger during the single-month climatologies is the effect of low ozone environments over populated areas in winter, seen especially on the East Coast of North America, Europe, and China. This signal shows that the model represents the lack of ozone production in high NO_X regions. Minimas in ozone is also pronounced in the summer Hemisphere rainforests, in the Amazonas rainforest, Congo rainforest, and the Australasia Oceania rainforests. This suggests that the full chemistry used in this version of NorESM includes special chemistry regarding the relationship between ozone and vegetation, MOZART-TS1 was f. e. developed motivated by a better understanding of isoprene (Emmons et al., 2020). Prosesses like ozone deposition to the raiforest might also be a factor that can produce a strong signal in the model, as more ozone deposition should occur during during the wet season from December to May (Rummel et al., 2007)

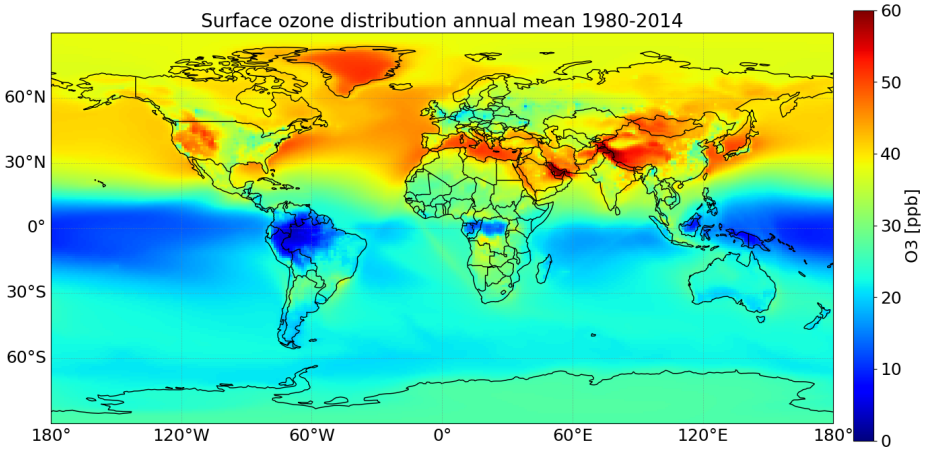

(a) Annual mean climatology

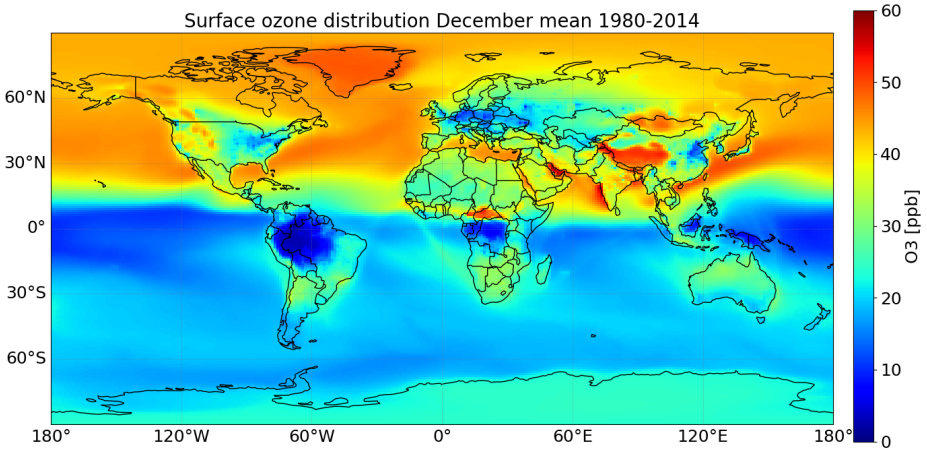

(b) December mean climatology

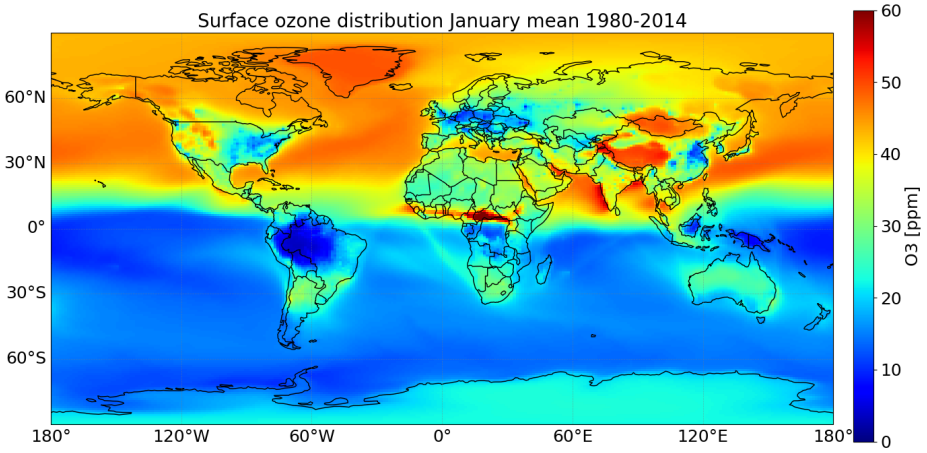

(c) January mean climatology

Figure 6.1: Surface ozone distribution simulated by NorESM. Lowest model level of 992.5 hPa is depicted. Climatology is from 1980 to 2014.

6.2 Climatology of SO287 CONNECT area

The difference between the SO287 CONNECT ozone profiles and the NorESM monthly mean December/January climatology is displayed in Figure A.9. The model profile does not exhibit any unique features like the observed profiles. This may partly be because the model output data is in monthly means, and in addition has been averaged over 35 years, but may also be due to its vertical resolution.

Overall, the model profiles match up quite well with the observed profiles throughout the troposphere. The largest deviation between the NorESM climatology and the SO287 CONNECT profiles is presented in Figure 6.2a, depicting sonde no. 07. Here, the model climatology from the nearest grid-box to the launch position of sonde no. 07 shows lower ozone mixing ratios throughout the troposphere. The abrupt increase of ozone in the upper troposphere or lower stratosphere, the tropopause, of the model also happens on a pressure level below the observed in this case. The signal, with underestimation of ozone throughout the troposphere, can be seen to some degree between all model profiles and their respective observed profile. The signal where the model portrays a shallow increase in ozone near the tropopause can be seen for all profiles, with the exception of sonde no. 27. The abrupt increase of ozone in the upper troposphere happens at about the same pressure level for the model and the observed no. 27 profile, at around 200 hPa. This is also at a lower level compared to the other profiles where this increase takes place at around 100 hPa, and may indicate that the model takes extra-tropical stratospheric intrusions like the one observed by SO287 sonde no. 27 into account. The upper tropospheric ozone minimum is also overestimated by the model due to the lower abrupt increase in ozone. Both the overestimation of the ozone minimum and the lower ozone increase might be doe to the vertical model resolution in the lower troposphere and stratosphere. If both the ozone minimum and the sharp increase in ozone happens in the same model layer, their characteristics may be lost.

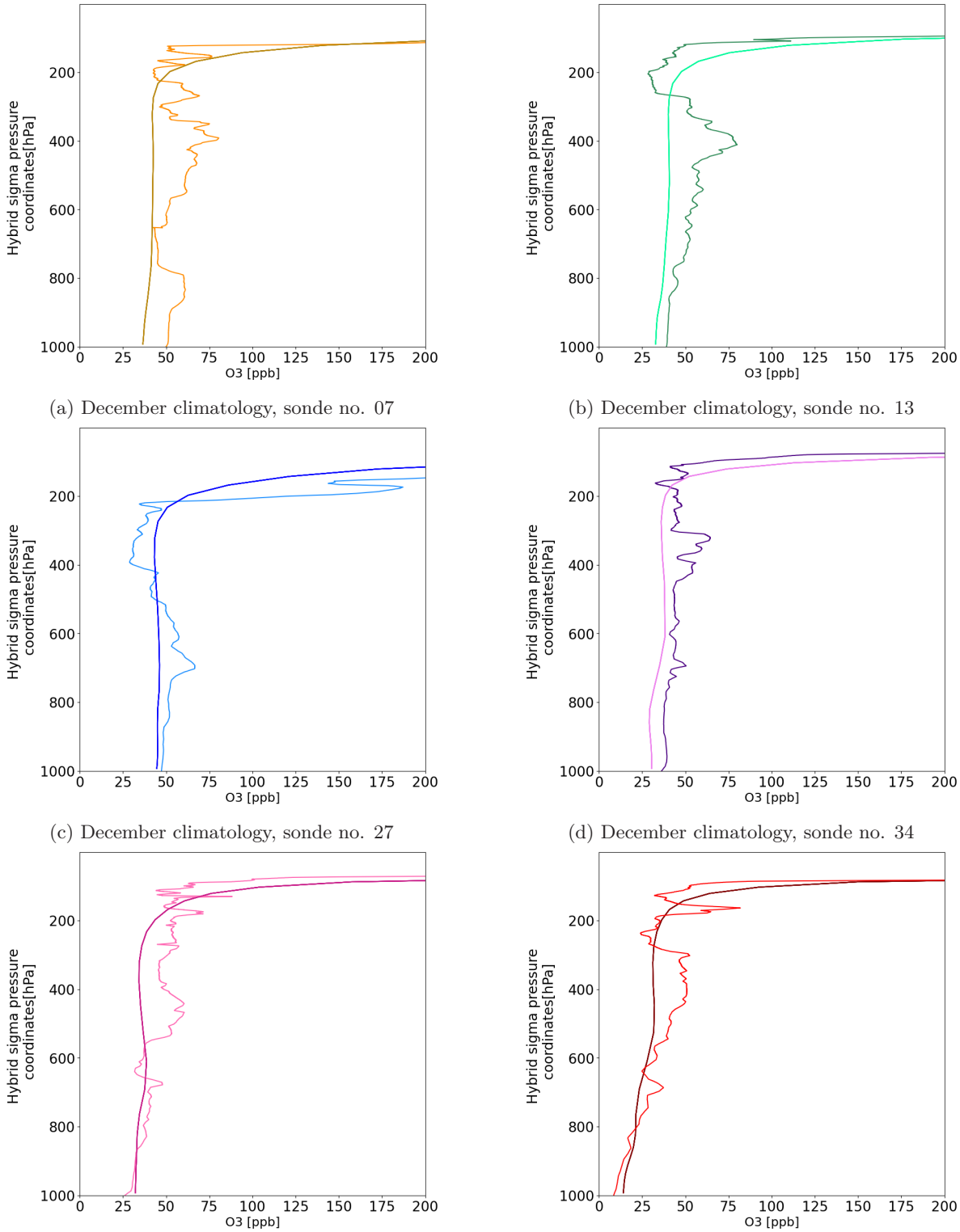

(a) December climatology, sonde no. 07

(b) December climatology, sonde no. 13

(c) December climatology, sonde no. 27

(d) December climatology, sonde no. 34

(e) January climatology, sonde no. 38

(f) January climatology, sonde no. 43

Figure 6.2: SO287 CONNECT ozone profiles shown together with their respective monthly NorESM Climatology. Model profiles are calculated from the nearest grid-point to the launch positions of the SO287 CONNECT sondes. Model profiles showing December or January monthly means averaged over 1980-2014.

6.3 Wave-one

The wave-one signature derived from ozone soundings at SHADOZ stations in Figure 2.4 is recognizable in the NorESM depicted in Figure 6.3. The seasonal differences in wave-one had similar features in both SHADOZ and NorESM data, with the strongest signal being in SON, followed by JJA and DJF, with the weakest signal in MAM. The peak of tropospheric ozone from SHADOZ observations is located between 0 and 50 °W in SON, JJA and DJF, but is more centered ad 0 °E during MAM. This feature is skewed in the NorESM modeling results where the tropospheric ozone peak is located mainly between 0 and 50 °E for SON and JJA, while a distinct peak can be challenging to detect in DJF and MAM. A possible explanation for the shift in ozone peak between the observations and the model output might be due to large distances between the SHADOZ stations, while the model is on a 1 ° horizontal grid. therefore, the model might show features that the SHADOZ observations miss due to their locations. Alternatively, this result can also be due to a misrepresentation of the transport and advection of ozone in the model. The tropospheric ozone peak in SON of Figure 2.4 coincides with observations from Ascension Island at around 20 °W (see Figure 5.3). This station experiences higher ozone values than f. e. Niarobi, Kenya on the African continent at about 40 °E. Overall, the signals in the SHADOZ observations seem to have more pronounced maximums and minimums compared to the model output. In general, the modeled tropopause is located in the layer at approximately 320 hPa. The ozone signal here appears seasonally reversed compared to the SHADOZ observation in Thompson et al. (2017). According to the observations, the abrupt shift from low to high ozone should be located at lower altitudes over central longitudes in SON, while this season exhibits the lowest ozone at this level in the model. Additionally, the model shows the highest ozone in this level during MAM, the season that according to the SHADOZ observations exhibits an elevated abrupt increase of ozone, and therefore lower ozone values at this level. As seen in Figure A.9, the model has a lower tropopause than the observations, especially in the tropics. The model might underrepresent the observed features in this upper tropopause region due to the coarse vertical resolution in the upper troposphere and stratosphere.

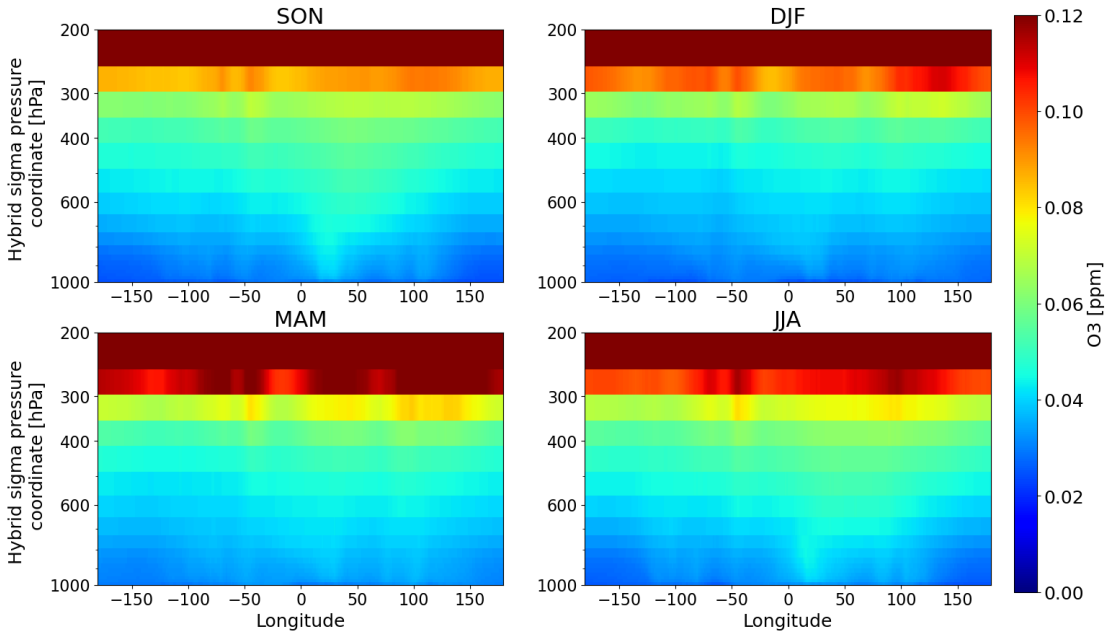

Figure 6.3: Longitude-height cross-section of monthly mean ozone [ppm] from NorESM divided into seasons, averaged in time (1980-2014) and spatialy between 15 °N and 15 °S.

PART IV

Discussion and Conclusion

CHAPTER 7

Discussion

Results show that the SO287 CONNECT ship campaign observed ozone mixing ratios of about 45 ppb on average throughout the troposphere, ranging between 25 ppb to 80 ppb in a "banded" or "layered" structure. Local ozone maxima layers in the troposphere are often associated with the advection of different air masses into an otherwise low ozone column and can have their origin in polluted areas with biomass burning or anthropogenic emissions of ozone precursors, or with stratospheric origin (Müller, 2020, Anderson et al., 2016, Oltmans et al., 2001, Thompson et al., 2000, Shiotani et al., 2002, Section 2.3). Possibilities for both stratospheric and biomass-burning signals were detected in the case studies. The extra-tropical ozone-sonde shows ozone maximums related to stratospheric intrusions, while the subtropical Atlantic sondes show local ozone maxima with the possibility of both biomass burning and stratospheric air origin.

The air masses sampled with balloon-borne instruments during the SO287 CONNECT ship campaign show typical characteristics of tropical, sub-tropical, and extra-tropical air masses. The two first ozone-sondes (no. 07 and 13) feature characteristics of being sub-tropical due to the presence of the subtropical jet as seen in their radiosonde zonal wind speed data, visualized in Figure 5.4b. Sonde no. 27 is, as established, extra-tropical due to both its lateral launch position and typical characteristics like low troposphere altitude interpreted from temperature, ozone and relative humidity data in Figure 5.21. The three last ozone-sondes launched in the Caribbean Sea and Eastern Pacific sampled tropical air masses. The Caribbean sondes no. 34 and 38 exhibit the straightest ozone profiles compared to the rest of the campaign, where uniform ozone profiles imply a well-mixed tropospheric ozone column likely due to convection, and strong convection can be a typical signal in the tropics. Sonde no. 43 in the Eastern Pacific, and together with the Caribbean sondes show typical tropical signals, especially with regards to their tropopause height, about 2 to 3 of km higher than the majority of the SO287 CONNECT ozone-sondes. These three sondes also observed the tropical QBO signal with changing zonal wind directions throughout the stratosphere, as seen in Figure 5.4. These

tropopause features are also reflected in the NorESM climatology, though the model shows 100 hPa lower tropopause heights than those observed during SO287 CONNECT. The difference between model and observations here can be du to either vertical model resolution, or the difference in vertical coordinates where the model uses hybrid sigma pressure levels and the observation has standard pressure levels. Even though the tropopause in NorESM is lower than observed, there is still a noticeable difference in tropopause heights for the tropics, sub-topics, and extra-tropics in the model. The tropics exhibit the highest tropopause at around 100 hPa, the extra-tropics have the lowest at 200 hPa, and the sub-tropics in between.

The Atlantic ozone profiles from SO287 CONNECT do not exhibit as low ozone values as observed by the 2009 TransBrom campaign in the tropical West Pacific. There, low amounts of ozone precursors presist due to a lack of emission sources, globally the highest SSTs, high relative humidity, strong convection, and low overhead ozone, leads to perfect conditions for tropospheric ozone depletion (Rex et al., 2014,Müller, 2020). The dominating wind direction near the surface being Easterly in the Northern Hemisphere tropics also prohibits the advection of ozone or precursors from remote emission sources as the Pacific Ocean is large, and the lifetime of ozone is only 5 to 10 days in the lower to mid-troposphere and therefore not long enough to survive the transport across the tropical Pacific. This contrasts with conditions over the tropical Atlantic Ocean. Though the launch sites over the ocean itself are remote from emissions of ozone precursors, it does exhibit higher ozone concentrations due to being downwind from the highly populated European, or African continents with biomass burning. The majority of the Atlantic sondes also experienced Northern hemispheric air due to being North of the ITCZ that separates the hemispheres and controls transport between the Hemispheres (Browell et al., 2001). This was confirmed by comparisons to nearby SHADOZ stations. The SO287 ship campaign took place during boreal winter which is the season with higher ozone concentrations on the Northern hemisphere, especially near the surface. This is also confirmed by the climatology for December and January simulated by NorESM, seen in Figure 6.1.

It is apparent that the Atlantic sondes experienced higher ozone mixing ratios than the ones launched in other tropical ocean basins. One reason for the distinct differences might be that the Atlantic SO287 CONNECT ship campaign is the only one of the 5 campaigns that stayed mainly in the Northern Hemisphere, and in addition took place in boreal winter. The pattern in Figure 6.3 resembles the wave-one pattern described first by Fishman and Larsen (1987) and by Thompson et al. (2017)(see Figure 2.4). A similar pattern is also apparent in the NorESM results in Figure 6.3. The height of the tropopause in Figure 6.3 might also be too low, as results showed when comparing the model to the

observations from SO287 CONNECT in Figure A.9. Taking this into account, a higher vertical resolution in the upper troposphere and stratosphere might improve the model's simulation of the tropopause and its ozone properties. The models experimental runs used in this thesis uses a free running atmosphere, meaning it is not nudged to simulate the true meteorological conditions at any given time-step. A nudged model run including observations from ozone sondes might inprove the models performance in terms of tropospheric ozone.

NorESM also reveals an ozone minimum over the Earth's major rain forests, agreeing with observations from for example Bela et al. (2015). Observations investigated in this thesis might also validate this model result, as both Paramaribo and Quito experienced lower ozone mixing ratios than expected according to their locations. The Paramaribo SHADOZ station is located close to the city of Paramaribo, and should therefore experience higher surface ozone concentrations due to emissions of precursors from anthropogenic emissions. The Paramaribo station is also downwind from the North Atlantic that, as we established, has high ozone concentrations. Trajectories from Figure 5.13 show that the lower mixing ratios experienced at Paramaribo may be due to the effect of the location of the ITCZ, where Paramaribo is located within the ITCZ and experience, therefore, lower ozone values than observed over the Atlantic by SO287 CONNECT. As seen in Figure 6.1 Paramaribo should also be affected by the ozone minimum generated from the Amazon canopy. NorESM simulation also show this effect in the Congo rain forest in Africa, which is located further East than where the southern trajectories in Figure 5.13 end, suggesting that this rainforest may have an influence on the air masses downwind from it in the Southern Atlantic. The Quito SHADOZ station is located close to the ozone minimum of the Amazon rainforest. Like Paramaribo, the Quito station is located near the city center of its respective city, a highly populated city with expected emissions of anthropogenic ozone precursors, but does, like Paramaribo, sample lower amounts of ozone than the SO287 COONECT ozone-sondes. Results show that Quito most likely experiences different air masses than San Cristobal and Paramaribo SHADOZ stations, both seen in the profiles collected on the same day (Figure 5.6), but also according to trajectories (Figures 5.15 and 5.22). The low values experienced by Quito might therefore be related to the ozone minimum as simulated by NorESM, but also observed by Bela et al. (2015) and Williams et al., 2016.

CHAPTER 8

Conclusion

The results show that there is no ozone minimum over the tropical Atlantic Ocean similar to that of the tropical West Pacific observed during the 2009 TransBrom campaign and published by Rex et al. (2014). Ozone volume mixing ratios over the tropical Atlantic were observed to be 45 ppb on average, ranging from 25 and 80 ppb throughout the troposphere during the SO287 CONNECT ship campaign. During this campaign, tropical, sub-tropical, and extra-tropical air masses were sampled by ozone-sondes, exhibiting characteristic from the regions. The ozone signatures in these Atlantic profiles indicate northern hemispheric origin when compared to nearby SHADOZ stations with cleaner and southern hemispheric signatures. Layers with elevated ozone values were sampled, and their possible origins are both biomass burning and stratospheric.

The attempt of sampling the same air mass twice, first during the SO287 CONNECT ship campaign and again by the Paramaribo SHADOZ station, was successful. Trajectories generated using GFS data within the HYSPLIT model suggest the air mass passed over both launch sites.

Ozone concentrations above the tropical Atlantic Ocean are higher compared to campaign data from the other tropical ocean basins. Observations from five different ship campaigns in four different tropical ocean basins also confirm the pattern of the tropospheric wave-one in ozone.

The NorESM including the chemistry addition of MOZART-TS1 is able to represent the expected patterns of surface ozone and wave-one. NorESM's wave-one pattern represents the main features of the observed wave-one by SHADOZ stations presented in Thompson et al. (2017), with some deviations. The tropospheric ozone peak most prominent in SON and JJA is shifted eastward. Comparisons to the observations conducted during the SO287 CONNECT campaign reveal that NorESM simulates the abrupt increase of ozone in the troposphere at too low altitudes, which is likely due to the coarse resolution in the upper troposphere and stratosphere.

8.1 Outlook

Further research on the factors that influence the background current of the ECC ozone sondes needs to be understood, so that a standard method for handling the current can be established, making ozone soundings more accurate and standardized. Such research is ongoing at f. e. WCCOS conducting the JOSIE experiments with the aim to investigate the performance of ECC ozone sondes in terms of precision, biases, and uncertainties. When such a standard method gets agreed upon, all existing ozone-sonde data needs to be post-processed to fit the new guidelines again.

The properties and origin of local ozone maximums or noses in ozone profiles can further be investigated by examining other tracers with longer lifetimes and therefore better fit to determine air mass origin. Such tracer can for example be CO, which has a lifetime of several months in the troposphere and is a marker of biomass burning.

In addition, NorESM with MOZART-TS1 would benefit from a higher vertical resolution, especially in the abrupt increase of ozone in the lower troposphere and stratosphere. Further validation of the model using ozone observations from other geographical places or other latitudes are needed to confirm the results of this thesis. Observations of other trace gases would also be beneficial to validate the representation of other tracers and reactions within the model. Analyzing daily NorESM model data may show more of the unique features like filaments, as the observations from ozone sondes. By using a nudged model run instead of a free-running atmosphere might improve the model's simulation of ozone. By using reanalysis data with assimilated ozone-sonde observations of the troposphere, the simulation of tropospheric ozone might improve.

Further work for investigating and isolating the impact of phenomenons like ENSO on tropospheric ozone, dynamical, chemical, and thermal by using both observations and models are needed to fully understand the contributing factors (Oman et al., 2011).

Appendices

APPENDIX A

Figures

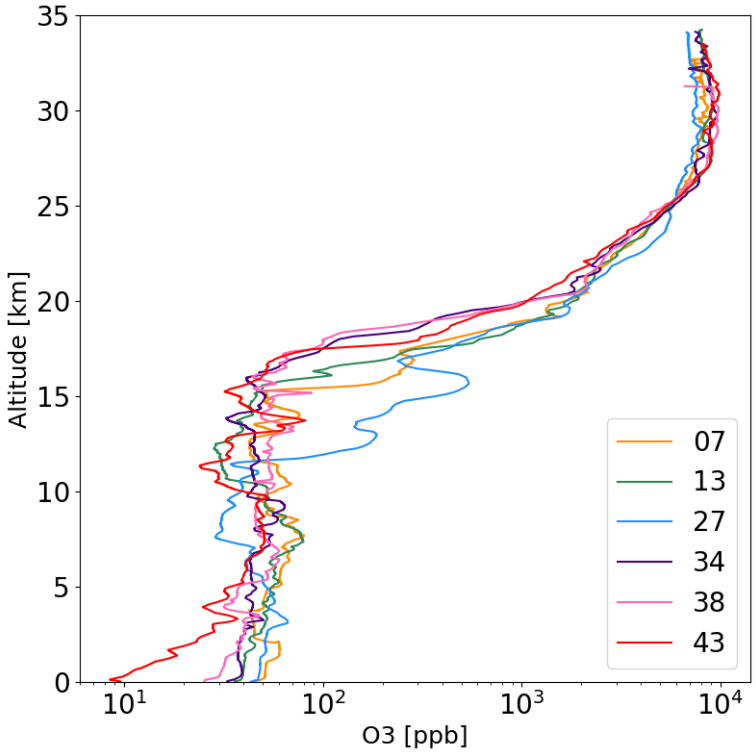

Figure A.1: SO287 CONNECT ozone sonde profile visilized on a logarithmic x-axis of ppb ozone.

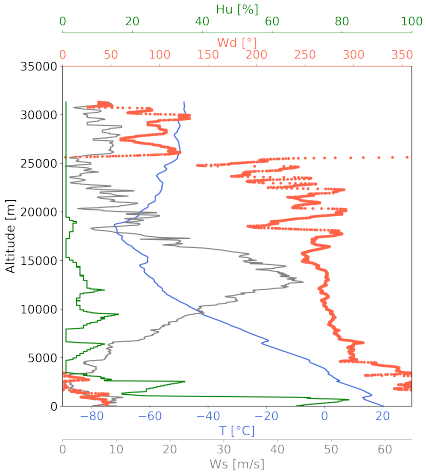

(a) Radiosonde 2

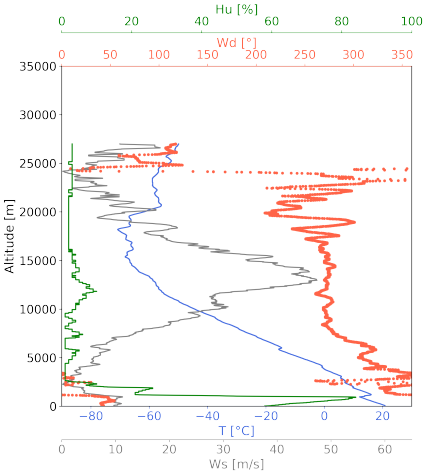

(b) Radiosonde 3

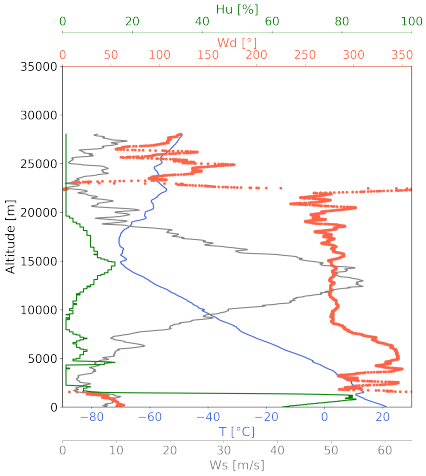

(c) Radiosonde 4

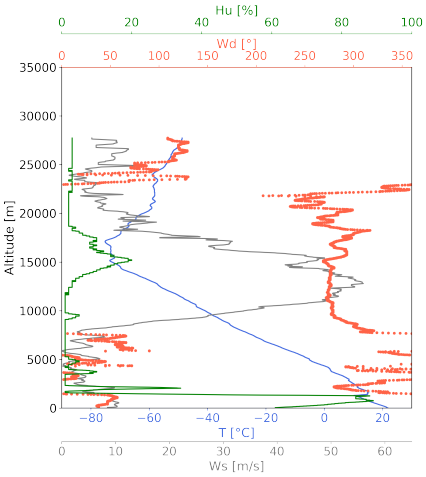

(d) Radiosonde 5

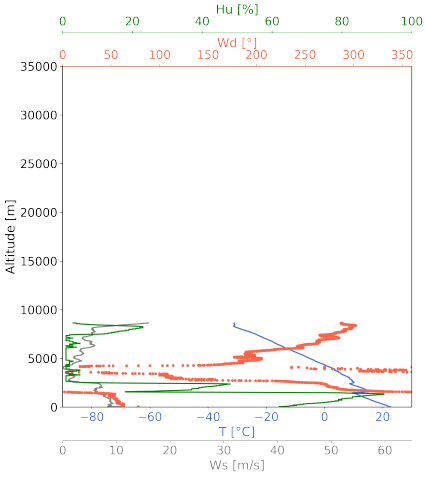

(e) Radiosonde 6

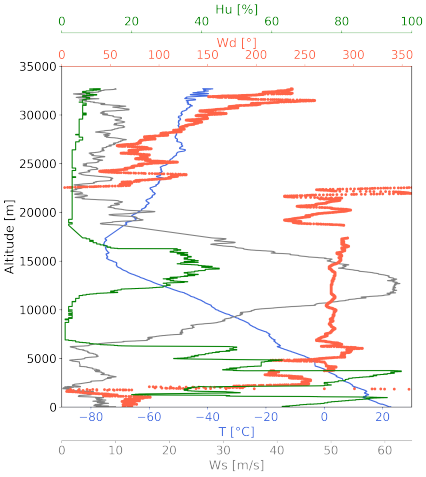

(f) Radiosonde 7

Figure A.2: Relative humidity [%], Wind speed [m/s], Wind direction [deg], Temperature [C].

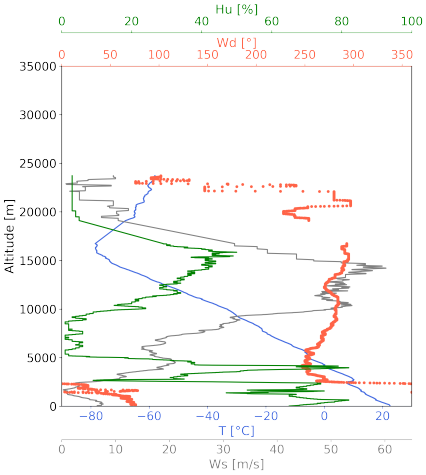

(a) Radiosonde 8

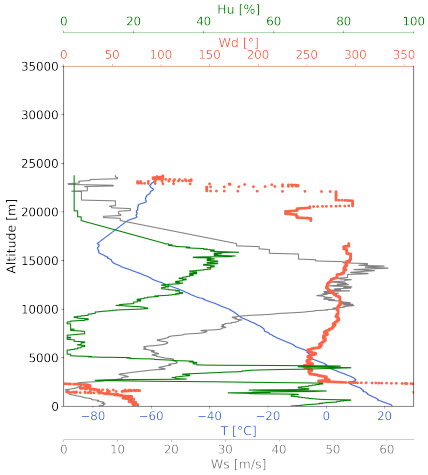

(b) Radiosonde 9

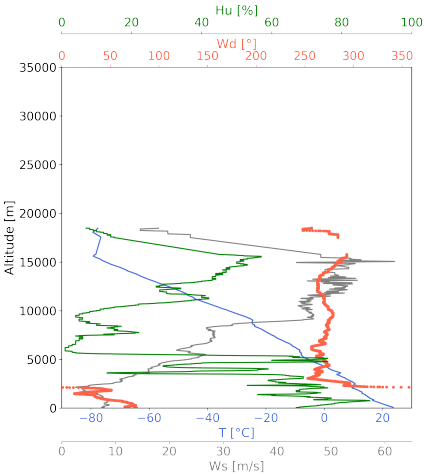

(c) Radiosonde 10

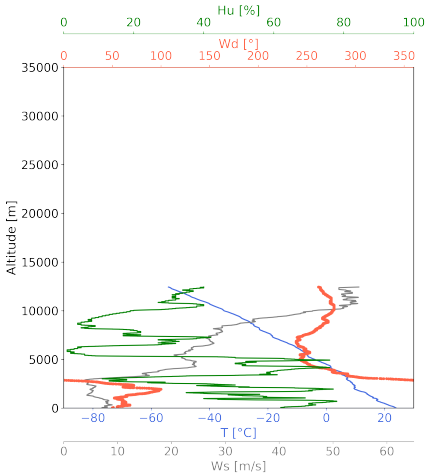

(d) Radiosonde 11

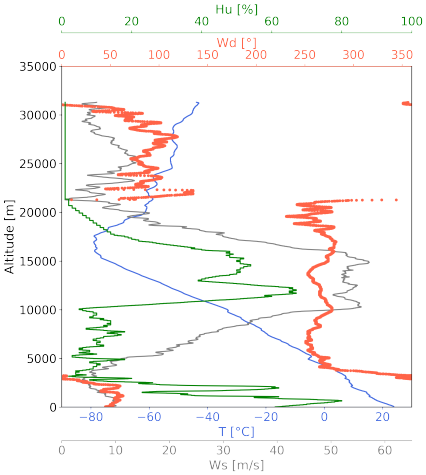

(e) Radiosonde 12

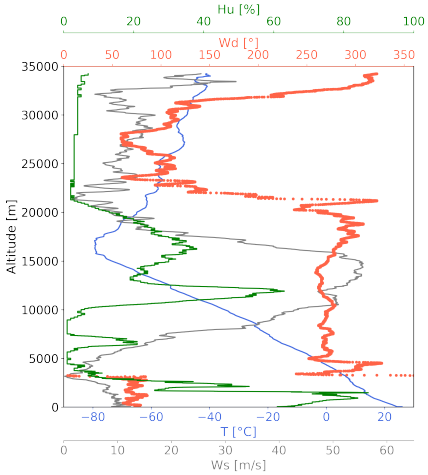

(f) Radiosonde 13

Figure A.3: Relative humidity [%], Wind speed [m/s], Wind direction [deg], Temperature [C].

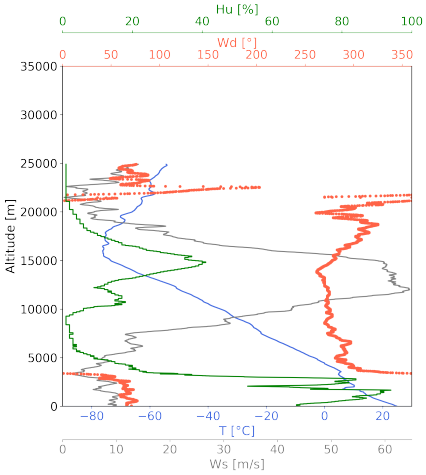

(a) Radiosonde 14

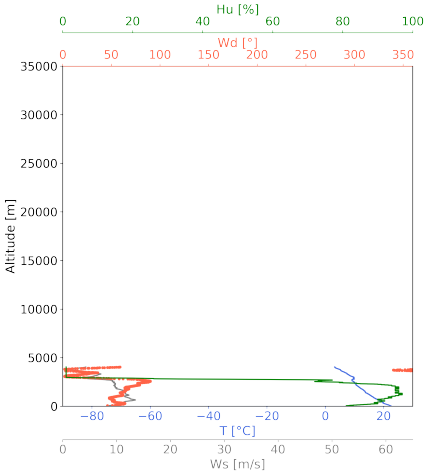

(b) Radiosonde 15

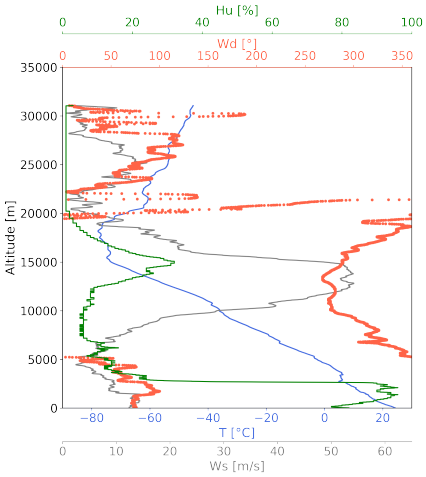

(c) Radiosonde 16

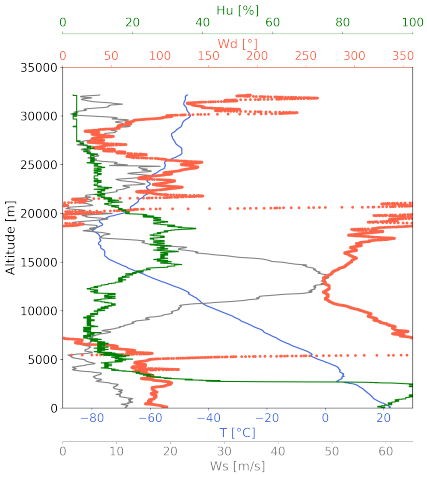

(d) Radiosonde 17

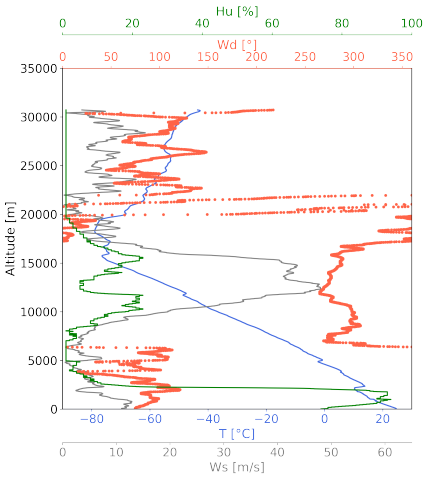

(e) Radiosonde 18

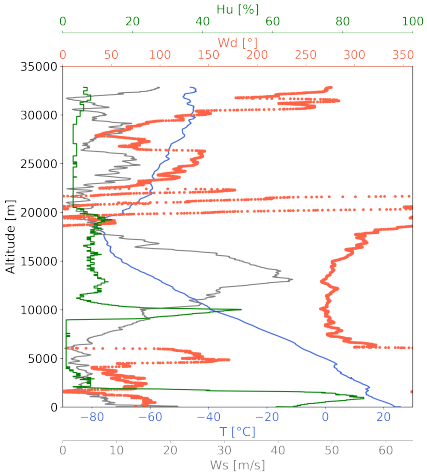

(f) Radiosonde 19

Figure A.4: Relative humidity [%], Wind speed [m/s], Wind direction [deg], Temperature [C].

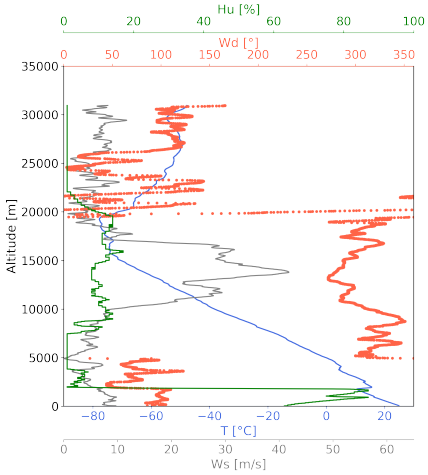

(a) Radiosonde 20

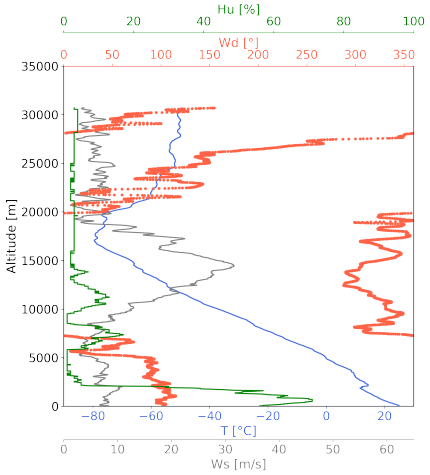

(b) Radiosonde 21

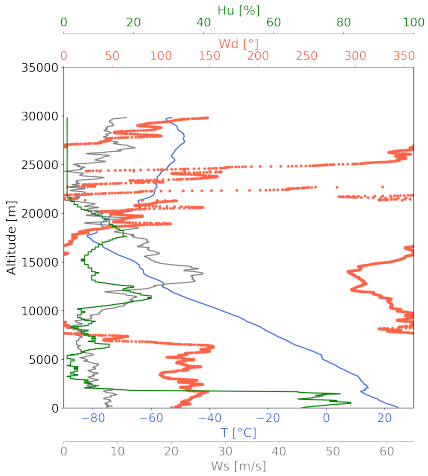

(c) Radiosonde 22

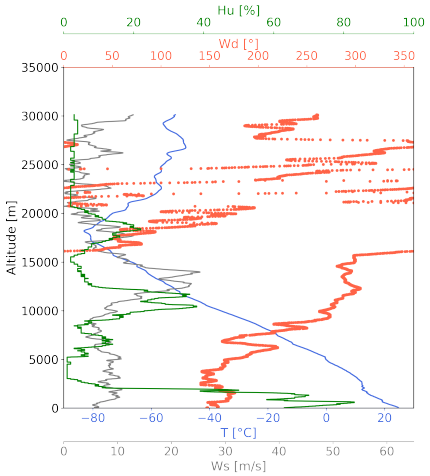

(d) Radiosonde 23

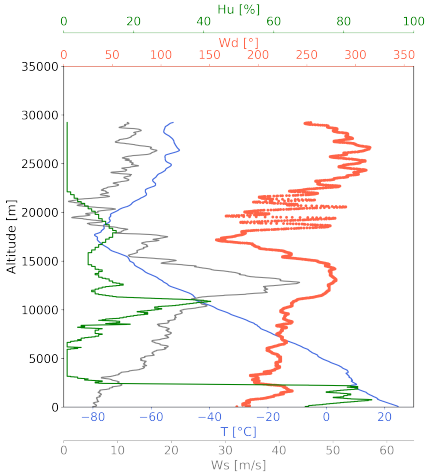

(e) Radiosonde 24

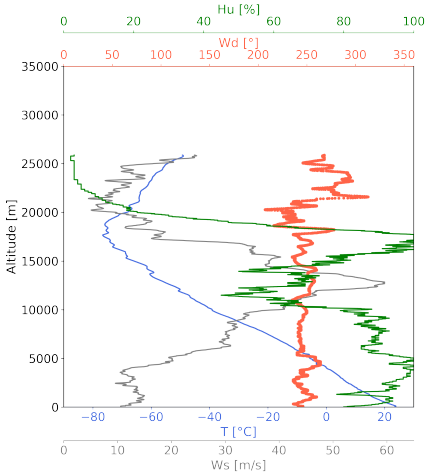

(f) Radiosonde 25

Figure A.5: Relative humidity [%], Wind speed [m/s], Wind direction [deg], Temperature [C].

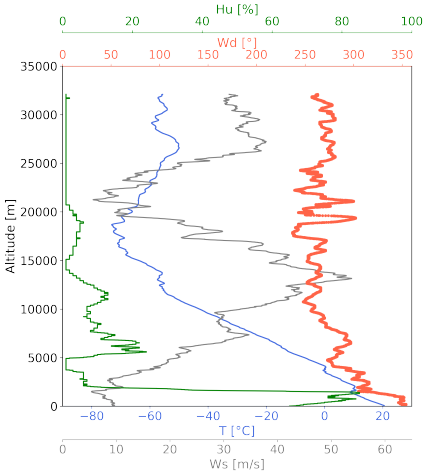

(a) Radiosonde 26

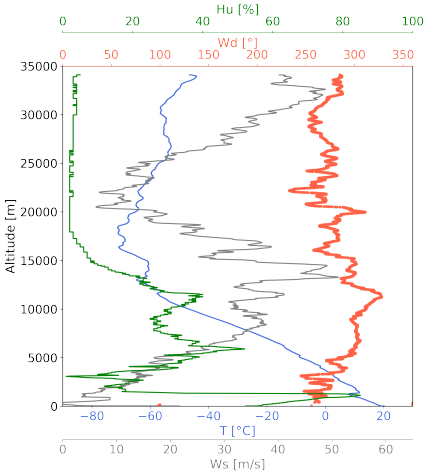

(b) Radiosonde 27

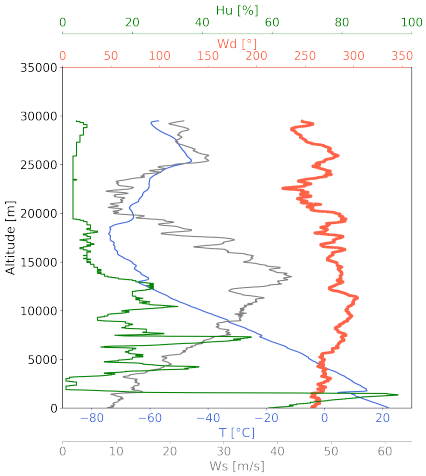

(c) Radiosonde 28

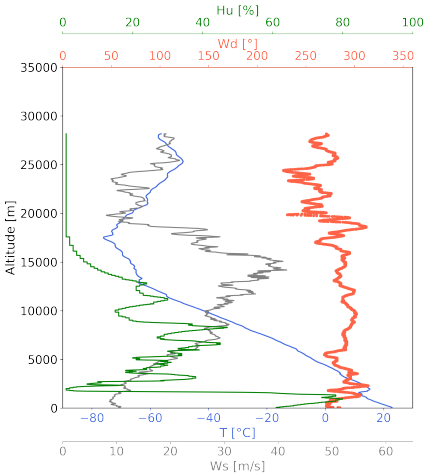

(d) Radiosonde 29

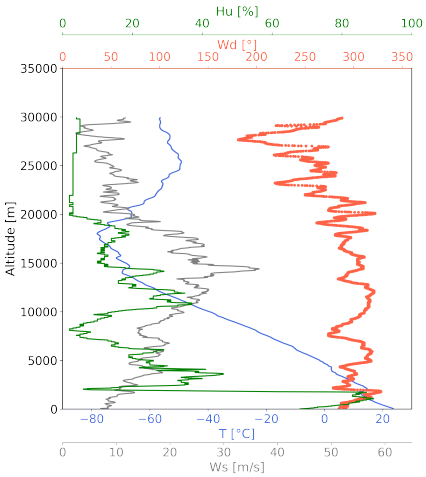

(e) Radiosonde 30

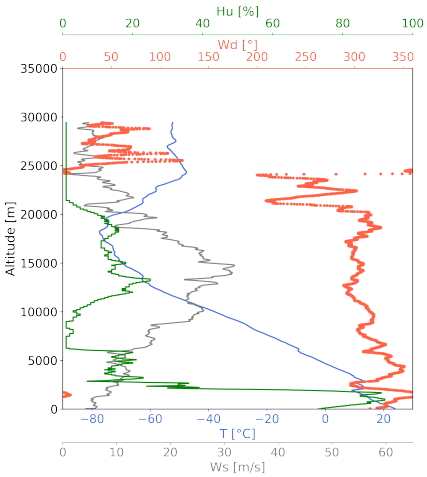

(f) Radiosonde 31

Figure A.6: Relative humidity [%], Wind speed [m/s], Wind direction [deg], Temperature [C].

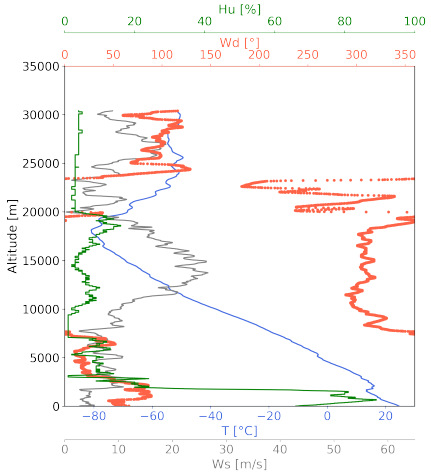

(a) Radiosonde 32

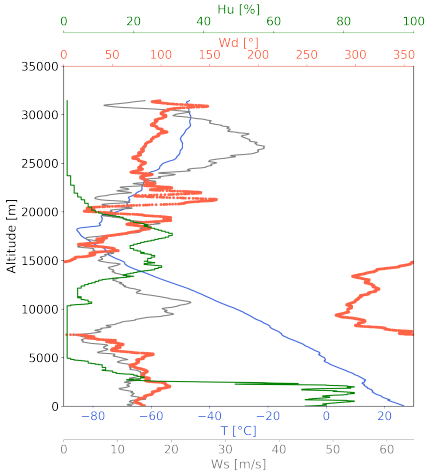

(b) Radiosonde 33

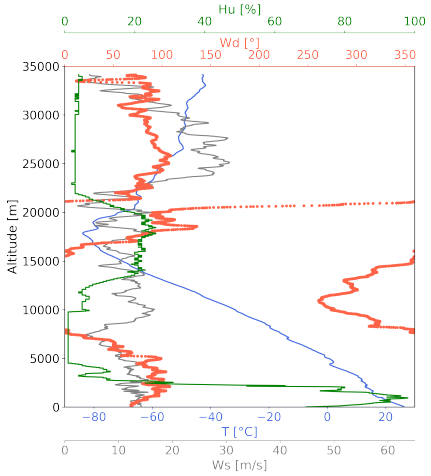

(c) Radiosonde 34

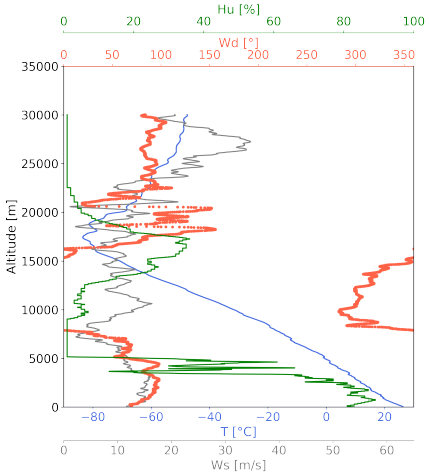

(d) Radiosonde 35

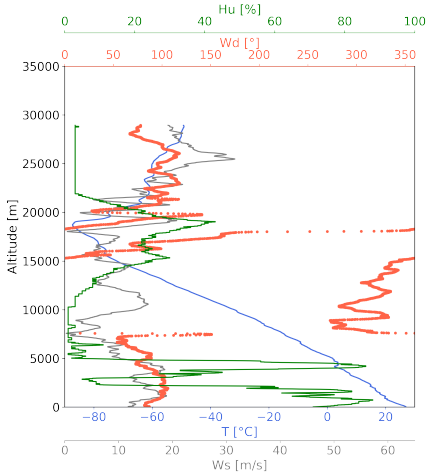

(e) Radiosonde 36

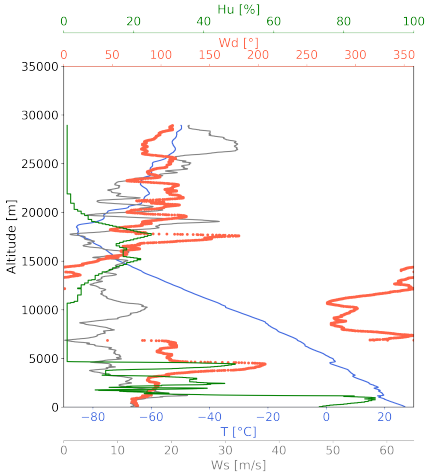

(f) Radiosonde 37

Figure A.7: Relative humidity [%], Wind speed [m/s], Wind direction [deg], Temperature [C].

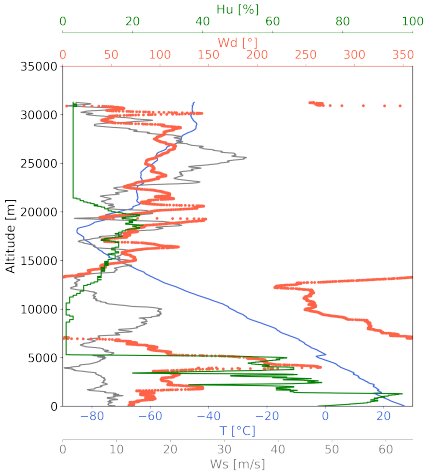

(a) Radiosonde 38

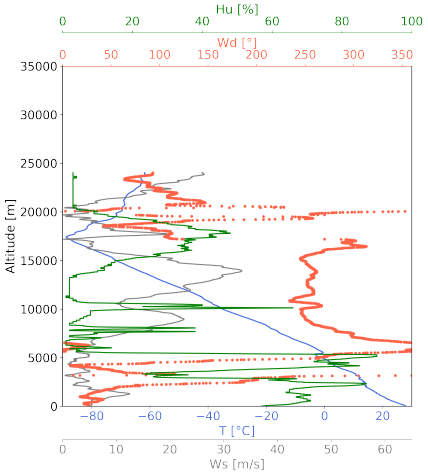

(b) Radiosonde 39

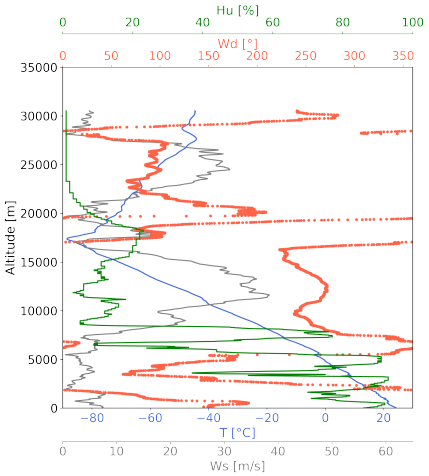

(c) Radiosonde 40

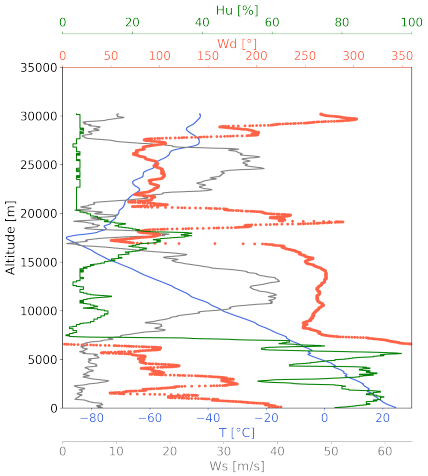

(d) Radiosonde 41

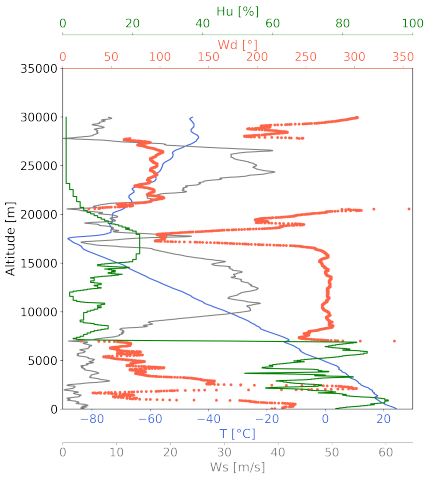

(e) Radiosonde 42

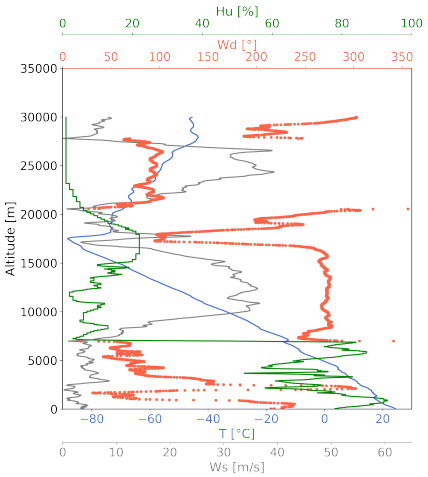

(f) Radiosonde 43

Figure A.8: Relative humidity [%], Wind speed [m/s], Wind direction [deg], Temperature [C].

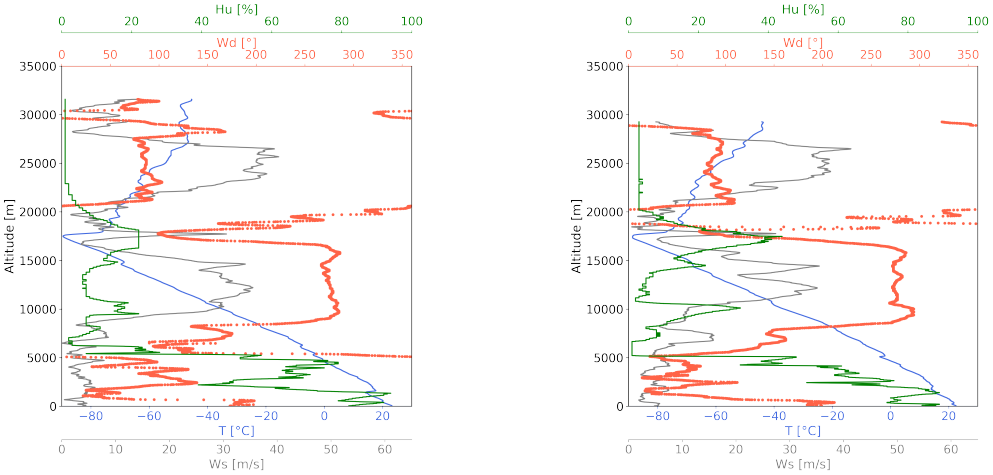

(a) Radiosonde 44

(b) Radiosonde 45

Figure A.9: Relative humidity [%], Wind speed [m/s], Wind direction [deg], Temperature [C]..

Bibliography

Ahrens, C. D., & Henson, R. (2016). *Essentials of Meteorology: An Invitation to the Atmosphere*. Cengage Learning.

Anderson, D. C., Nicely, J. M., Salawitch, R. J., Canty, T. P., Dickerson, R. R., Hanisco, T. F., Wolfe, G. M., Apel, E. C., Atlas, E., Bannan, T., Bauguitte, S., Blake, N. J., Bresch, J. F., Campos, T. L., Carpenter, L. J., Cohen, M. D., Evans, M., Fernandez, R. P., Kahn, B. H., … Weinheimer, A. J. (2016). A pervasive role for biomass burning in tropical high ozone/low water structures [Number: 1 Publisher: Nature Publishing Group]. *Nature Communications*, vol. 7no. 1, 10267. https://doi.org/10.1038/ncomms10267

Baldwin, M. P., Gray, L. J., Dunkerton, T. J., Hamilton, K., Haynes, P. H., Randel, W. J., Holton, J. R., Alexander, M. J., Hirota, I., Horinouchi, T., Jones, D. B. A., Kinnersley, J. S., Marquardt, C., Sato, K., & Takahashi, M. (2001). The quasi-biennial oscillation [_eprint: https://onlinelibrary.wiley.com/doi/pdf/10.1029/1999RG000073]. *Reviews of Geophysics*, vol. 39no. 2, 179–229. https://doi.org/10.1029/1999RG000073

Bela, M. M., Longo, K. M., Freitas, S. R., Moreira, D. S., Beck, V., Wofsy, S. C., Gerbig, C., Wiedemann, K., Andreae, M. O., & Artaxo, P. (2015). Ozone production and transport over the Amazon Basin during the dry-to-wet and wet-to-dry transition seasons. *Atmospheric Chemistry and Physics*, vol. 15no. 2, 757–782. https://doi.org/10.5194/acp-15-757-2015

Blake, N. J., Blake, D. R., Wingenter, O. W., Sive, B. C., McKenzie, L. M., Lopez, J. P., Simpson, I. J., Fuelberg, H. E., Sachse, G. W., Anderson, B. E., Gregory, G. L., Carroll, M. A., Albercook, G. M., & Rowland, F. S. (1999). Influence of southern hemispheric biomass burning on midtropospheric distributions of nonmethane hydrocarbons and selected halocarbons over the remote South Pacific. *Journal of Geophysical Research: Atmospheres*, vol. 104no. D13, 16213–16232. https://doi.org/10.1029/1999JD900067

Brasseur, G. P., & Jacob, D. J. (2017). *Modeling of Atmospheric Chemistry*. Cambridge University Press. https://doi.org/10.1017/9781316544754

Browell, E. V., Fenn, M. A., Butler, C. F., Grant, W. B., Ismail, S., Ferrare, R. A., Kooi, S. A., Brackett, V. G., Clayton, M. B., Avery, M. A., Barrick, J. D. W., Fuelberg, H. E., Maloney, J. C., Newell, R. E., Zhu, Y., Mahoney, M. J., Anderson, B. E., Blake, D. R., Brune, W. H., ... Talbot, R. W. (2001). Large-scale air mass characteristics observed over the remote tropical Pacific Ocean during March-April 1999: Results from PEM-Tropics B field experiment [_eprint: https://onlinelibrary.wiley.com/doi/pdf/10.1029/2001JD900001]. *Journal of Geophysical Research: Atmospheres*, vol. 106no. D23, 32481–32501. https://doi.org/10.1029/2001JD900001

Brune, W. H. (2020). 4.1 Atmospheric Composition | METEO 300: Fundamentals of Atmospheric Science. Retrieved May 21, 2023, from https://www.e-education.psu.edu/meteo300/node/534

Bunting, L., Espinoza, R., & Ramirez-Diaz, Z. (n.d.). tropopauseCalc. Retrieved March 1, 2023, from https://github.com/robertej09/tropopauseCalc

Butchart, N. (2014). The Brewer-Dobson circulation. *Reviews of Geophysics*, vol. 52no. 2, 157–184. https://doi.org/10.1002/2013RG000448

Emmons, L. K., Schwantes, R. H., Orlando, J. J., Tyndall, G., Kinnison, D., Lamarque, J.-F., Marsh, D., Mills, M. J., Tilmes, S., Bardeen, C., Buchholz, R. R., Conley, A., Gettelman, A., Garcia, R., Simpson, I., Blake, D. R., Meinardi, S., & Pétron, G. (2020). The Chemistry Mechanism in the Community Earth System Model Version 2 (CESM2). *Journal of Advances in Modeling Earth Systems*, vol. 12no. 4, e2019MS001882. https://doi.org/10.1029/2019MS001882

Eyring, V., Bony, S., Meehl, G. A., Senior, C. A., Stevens, B., Stouffer, R. J., & Taylor, K. E. (2016). Overview of the Coupled Model Intercomparison Project Phase 6 (CMIP6) experimental design and organization [Publisher: Copernicus GmbH]. *Geoscientific Model Development*, vol. 9no. 5, 1937–1958. https://doi.org/10.5194/gmd-9-1937-2016

Ferraro, R. R. (1997). Special sensor microwave imager derived global rainfall estimates for climatological applications. *Journal of Geophysical Research: Atmospheres*, vol. 102no. D14, 16715–16735. https://doi.org/10.1029/97JD01210

Fiehn, A., Quack, B., Hepach, H., Fuhlbrügge, S., Tegtmeier, S., Toohey, M., Atlas, E., & Krüger, K. (2017). Delivery of halogenated very short-lived substances from the west Indian Ocean to the stratosphere during the Asian summer monsoon [Publisher: Copernicus GmbH]. *Atmospheric Chemistry and Physics*, vol. 17no. 11, 6723–6741. https://doi.org/10.5194/acp-17-6723-2017

Fishman, J., & Larsen, J. C. (1987). Distribution of total ozone and stratospheric ozone in the tropics: Implications for the distribution of tropospheric ozone. *Journal of Geophysical Research: Atmospheres*, vol. 92no. D6, 6627–6634. https://doi.org/10.1029/JD092iD06p06627

Folkins, I., Loewenstein, M., Podolske, J., Oltmans, S. J., & Proffitt, M. (1999). A barrier to vertical mixing at 14 km in the tropics: Evidence from ozonesondes and aircraft measurements [_eprint: https://onlinelibrary.wiley.com/doi/pdf/10.1029/1999JD900404]. *Journal of Geophysical Research: Atmospheres*, vol. 104no. D18, 22095–22102. https://doi.org/10.1029/1999JD900404

Fueglistaler, S., Dessler, A. E., Dunkerton, T. J., Folkins, I., Fu, Q., & Mote, P. W. (2009). Tropical tropopause layer. *Reviews of Geophysics*, vol. 47no. 1. https://doi.org/10.1029/2008RG000267

Fuhlbrügge, S., Quack, B., Tegtmeier, S., Atlas, E., Hepach, H., Shi, Q., Raimund, S., & Krüger, K. (2016). The contribution of oceanic halocarbons to marine and free tropospheric air over the tropical West Pacific [Publisher: Copernicus GmbH]. *Atmospheric Chemistry and Physics*, vol. 16no. 12, 7569–7585. https://doi.org/10.5194/acp-16-7569-2016

Garrison, T. S. (2014). *Essentials of Oceanography*. Cengage Learning.

Hakim, G. J., & Patoux, J. (2018). *Weather: A Concise Introduction*. https://doi.org/10.1017/9781108264983

Highwood, E. J., & Hoskins, B. J. (1998). The tropical tropopause. *Quarterly Journal of the Royal Meteorological Society*, vol. 124no. 549, 1579–1604. https://doi.org/10.1002/qj.49712454911

Jacob, D. J. (1999). *Introduction to Atmospheric Chemistry*. Princeton University Press.

Kirkevåg, A., Grini, A., Olivié, D., Seland, Ø., Alterskjær, K., Hummel, M., Karset, I. H. H., Lewinschal, A., Liu, X., Makkonen, R., Bethke, I., Griesfeller, J., Schulz, M., & Iversen, T. (2018). A production-tagged aerosol module for Earth system models, OsloAero5.3 – extensions and updates for CAM5.3-Oslo [Publisher: Copernicus GmbH]. *Geoscientific Model Development*, vol. 11no. 10, 3945–3982. https://doi.org/10.5194/gmd-11-3945-2018

Krüger, K., & Quack, B. (2013). Introduction to special issue: The *TransBrom Sonne* expedition in the tropical West Pacific. *Atmospheric Chemistry and Physics*, vol. 13no. 18, 9439–9446. https://doi.org/10.5194/acp-13-9439-2013

Krüger, K., Tegtmeier, S., & Rex, M. (2009). Variability of residence time in the Tropical Tropopause Layer during Northern Hemisphere winter

[Publisher: Copernicus GmbH]. *Atmospheric Chemistry and Physics*, vol. 9no. 18, 6717–6725. https://doi.org/10.5194/acp-9-6717-2009

Krüger, K., Quack, B., & Marandino, C. (2014a). *RV SONNE Fahrtbericht / Cruise Report SO234-2 [SO234/2], 08.-20.07.2014, Durban, South Africa - Port Louis, Mauritius - SPACES OASIS Indian Ocean* (Report) [ISSN: 2193-8113]. GEOMAR Helmholtz-Zentrum für Ozeanforschung. Kiel, Germany. https://doi.org/10.3289/GEOMAR_REP_NS_20_2014

Krüger, K., Quack, B., & Marandino, C. (2014b). *RV SONNE Fahrtbericht / Cruise Report SO235, 23.07.-07.08.2014, Port Louis, Mauritius to Malé, Maldives* (Report) [ISSN: 2193-8113]. GEOMAR Helmholtz-Zentrum für Ozeanforschung. Kiel, Germany. https://doi.org/10.3289/GEOMAR_REP_NS_21_2014

Lee, S., Shelow, D. M., Thompson, A. M., & Miller, S. K. (2010). QBO and ENSO variability in temperature and ozone from SHADOZ, 1998–2005. *Journal of Geophysical Research: Atmospheres*, vol. 115no. D18. https://doi.org/10.1029/2009JD013320

L'Heureux, M., & LaJoie, E. (2021). CLIMATE PREDICTION CENTER, December 2021, climate diagnostic bulletin. https://www.cpc.ncep.noaa.gov/products/CDB/CDB_Archive_pdf/PDF/CDB.dec2021_color.pdf

L'Heureux, M., & LaJoie, E. (2022). CLIMATE PREDICTION CENTER, January 2022, climate diagnistic bulletin. https://www.cpc.ncep.noaa.gov/products/CDB/CDB_Archive_pdf/PDF/CDB.jan2022_color.pdf

Lu, X., Zhang, L., & Shen, L. (2019). Meteorology and Climate Influences on Tropospheric Ozone: A Review of Natural Sources, Chemistry, and Transport Patterns. *Current Pollution Reports*, vol. 5no. 4, 238–260. https://doi.org/10.1007/s40726-019-00118-3

Marandino, C. A. (2016). *RV SONNE SO243 Cruise Report / Fahrtbericht Guayaquil, Ecuador: 05. October 2015 Antofagasta, Chile: 22. October 2015 SO243 ASTRA-OMZ: AIR SEA INTERACTION OF TRACE ELEMENTS IN OXYGEN MINIMUM ZONES* (Report). GEOMAR Helmholtz Centre for Ocean Research Kiel. https://doi.org/10.3289/CR_SO243

Mohnen, V., Goldstein, W., & Wang, W.-C. (1993). Tropospheric Ozone and Climate Change. *Air & Waste*, vol. 43no. 10, 1332–1334. https://doi.org/10.1080/1073161X.1993.10467207

Montzka, S. A., Krol, M., Dlugokencky, E., Hall, B., Jöckel, P., & Lelieveld, J. (2011). Small Interannual Variability of Global Atmospheric Hydroxyl.

Science, vol. 331no. 6013, 67–69. https://doi.org/10.1126/science.1197640

Munchak, L. A., & Pan, L. L. (2014). Separation of the lapse rate and the cold point tropopauses in the tropics and the resulting impact on cloud top-tropopause relationships. *Journal of Geophysical Research: Atmospheres*, vol. 119no. 13, 7963–7978. https://doi.org/10.1002/2013JD021189

Müller, K. (2020). *Characterization of ozone and the oxidizing capacity of the tropical West Pacific troposphere* (Doctoral dissertation) [Accepted: 2021-02-25T09:38:27Z Publisher: Universität Bremen]. Retrieved April 21, 2023, from https://media.suub.uni-bremen.de/handle/elib/4666

Naik, V., Szopa, S., Adhikary, B., Artaxo Netto, P. E., Berntsen, T., Collins, W. D., Fuzzi, S., Gallardo, L., Kiendler-Scharr, A., Klimont, Z., Liao, H., Unger, N., & Zanis, P. (2021). Short-lived climate forcers. In V. Masson-Delmotte, P. Zhai, A. Pirani, S. L. Connors, C. Péan, S. Berger, N. Caud, Y. Chen, L. Goldfarb, M. I. Gomis, M. Huang, K. Leitzell, E. Lonnoy, J. B. R. Matthews, T. K. Maycock, T. Waterfield, Ö. Yelekcci, R. Yu & B. Zhou (Eds.), *Climate Change 2021: The Physical Science Basis. Contribution of Working Group I to the Sixth Assessment Report of the Intergovernmental Panel on Climate Change* (pp. 817–922). Cambridge University Press. https://doi.org/10.1017/9781009157896.001

Oltmans, S. J., Johnson, B. J., Harris, J. M., Vömel, H., Thompson, A. M., Koshy, K., Simon, P., Bendura, R. J., Logan, J. A., Hasebe, F., Shiotani, M., Kirchhoff, V. W. J. H., Maata, M., Sami, G., Samad, A., Tabuadravu, J., Enriquez, H., Agama, M., Cornejo, J., & Paredes, F. (2001). Ozone in the Pacific tropical troposphere from ozonesonde observations. *Journal of Geophysical Research: Atmospheres*, vol. 106no. D23, 32503–32525. https://doi.org/10.1029/2000JD900834

Oman, L. D., Ziemke, J. R., Douglass, A. R., Waugh, D. W., Lang, C., Rodriguez, J. M., & Nielsen, J. E. (2011). The response of tropical tropospheric ozone to ENSO. *Geophysical Research Letters*, vol. 38no. 13. https://doi.org/10.1029/2011GL047865

Pan, L. L., Honomichl, S. B., Bui, T. V., Thornberry, T., Rollins, A., Hintsa, E., & Jensen, E. J. (2018). Lapse Rate or Cold Point: The Tropical Tropopause Identified by In Situ Trace Gas Measurements [_eprint: https://onlinelibrary.wiley.com/doi/pdf/10.1029/2018GL079573]. *Geophysical Research Letters*, vol. 45no. 19, 10, 756–10, 763. https://doi.org/10.1029/2018GL079573

Quack, B. (2022). *Short Cruise Report RV SONNE, cruise SO287 : Las Palmas, Spain - Guayaquil, Ecuador 11.12.2021 - 11.01.202* (tech. rep.). Retrieved April 29, 2023, from https://digital.csic.es/handle/10261/268355

Quack, B., & Krüger, K. (2013). *RV SONNE Fahrtbericht / Cruise Report SO218 SHIVA 15.-29.11.2011 Singapore - Manila, Philippines Stratospheric Ozone: Halogens in a Varying Atmosphere Part 1: SO218- SHIVA Summary Report (in German) Part 2: SO218- SHIVA English reports of participating groups* (Report). GEOMAR Helmholtz-Zentrum für Ozeanforschung. Kiel, Germany. https://doi.org/10.3289/GEOMAR_REP_NS_12_2013

Reich, P. B., & Amundson, R. G. (1985). Ambient levels of ozone reduce net photosynthesis in tree and crop species. *Science (New York, N.Y.)*, vol. 230no. 4725, 566–570. https://doi.org/10.1126/science.230.4725.566

Rex, M., Wohltmann, I., Ridder, T., Lehmann, R., Rosenlof, K., Wennberg, P., Weisenstein, D., Notholt, J., Krüger, K., Mohr, V., & Tegtmeier, S. (2014). A tropical West Pacific OH minimum and implications for stratospheric composition [Publisher: Copernicus GmbH]. *Atmospheric Chemistry and Physics*, vol. 14no. 9, 4827–4841. https://doi.org/10.5194/acp-14-4827-2014

Rummel, U., Ammann, C., Kirkman, G. A., Moura, M. a. L., Foken, T., Andreae, M. O., & Meixner, F. X. (2007). Seasonal variation of ozone deposition to a tropical rain forest in southwest Amazonia [Publisher: Copernicus GmbH]. *Atmospheric Chemistry and Physics*, vol. 7no. 20, 5415–5435. https://doi.org/10.5194/acp-7-5415-2007

Schneider, T., Bischoff, T., & Haug, G. H. (2014). Migrations and dynamics of the intertropical convergence zone. *Nature*, vol. 513no. 7516, 45–53. https://doi.org/10.1038/nature13636

Schwela, D. (2000). Air Pollution and Health in Urban Areas [Publisher: De Gruyter]. *Reviews on Environmental Health*, vol. 15no. 1-2, 13–42. https://doi.org/10.1515/REVEH.2000.15.1-2.13

Seland, Ø., Bentsen, M., Olivié, D., Toniazzo, T., Gjermundsen, A., Graff, L. S., Debernard, J. B., Gupta, A. K., He, Y.-C., Kirkevåg, A., Schwinger, J., Tjiputra, J., Aas, K. S., Bethke, I., Fan, Y., Griesfeller, J., Grini, A., Guo, C., Ilicak, M., … Schulz, M. (2020). Overview of the Norwegian Earth System Model (NorESM2) and key climate response of CMIP6 DECK, historical, and scenario simulations. *Geoscientific Model Development*, vol. 13no. 12, 6165–6200. https://doi.org/10.5194/gmd-13-6165-2020

Shiotani, M., Fujiwara, M., Hasebe, F., Hashizume, H., Vömel, H., Oltmans, S. J., & Watanabe, T. (2002). Ozonesonde Observations in the Equatorial Eastern Pacific —the Shoyo-Maru Survey—. Vol. 80no. 4B, 897–909. https://doi.org/10.2151/jmsj.80.897

Smit, H. G. J., Gilge, S., & Kley, D. (1990). The Meridional Distribution of Ozone and Water Vapor Over the Atlantic Ocean between 30 °s and

52 °N in September/October 1988 (G. Restelli & G. Angeletti, Eds.). *Physico-Chemical Behaviour of Atmospheric Pollutants: Air Pollution Research Reports*, 630–637. https://doi.org/10.1007/978-94-009-0567-2_95

Smit, H. G. J. (2014). *Quality Assurance and Quality Control for Ozonesonde Measurements in GAW. GAW REPORT No. 201.* (tech. rep.). WMO. https://library.wmo.int/doc_num.php?explnum_id=7167

Smit, H. G. J., Straeter, W., Johnson, B. J., Oltmans, S. J., Davies, J., Tarasick, D. W., Hoegger, B., Stubi, R., Schmidlin, F. J., Northam, T., Thompson, A. M., Witte, J. C., Boyd, I., & Posny, F. (2007). Assessment of the performance of ECC-ozonesondes under quasi-flight conditions in the environmental simulation chamber: Insights from the Juelich Ozone Sonde Intercomparison Experiment (JOSIE). *Journal of Geophysical Research: Atmospheres*, vol. 112no. D19. https://doi.org/10.1029/2006JD007308

Smit, H. G. J., & Thompson, A. M. (2021). *GAW Report, 268. Ozonesonde Measurement Principles and Best Operational Practices : ASOPOS 2.0 (Assessment of Standard Operating Procedures for Ozonesondes) August 2021.* WMO.

Stein, A. F., Draxler, R. R., Rolph, G. D., Stunder, B. J. B., Cohen, M. D., & Ngan, F. (2015). NOAA's HYSPLIT Atmospheric Transport and Dispersion Modeling System. *Bulletin of the American Meteorological Society*, vol. 96no. 12, 2059–2077. https://doi.org/10.1175/BAMS-D-14-00110.1

Stevens, A. N. P. (2010). Introduction to the Basic Drivers of Climate | Learn Science at Scitable. https://doi.org/https://www.nature.com/scitable/knowledge/library/introduction-to-the-basic-drivers-of-climate-13368032/

Tegtmeier, S., & Krüger, K. (2022). *Chapter 8: Tropical Tropopause Layer* (tech. rep.). https://www.sparc-climate.org/wp-content/uploads/sites/5/2021/07/08_SRIP_Report_Ch08_EarlyOnlineRelease-2.pdf

Thompson, A. M., Doddridge, B. G., Witte, J. C., Hudson, R. D., Luke, W. T., Johnson, J. E., Johnson, B. J., Oltmans, S. J., & Weller, R. (2000). A tropical Atlantic Paradox: Shipboard and satellite views of a tropospheric ozone maximum and wave-one in January–February 1999 [_eprint: https://onlinelibrary.wiley.com/doi/pdf/10.1029/1999GL011273]. *Geophysical Research Letters*, vol. 27no. 20, 3317–3320. https://doi.org/10.1029/1999GL011273

Thompson, A. M., Witte, J. C., Oltmans, S. J., Schmidlin, F. J., Logan, J. A., Fujiwara, M., Kirchhoff, V. W. J. H., Posny, F., Coetzee, G. J. R.,

Hoegger, B., Kawakami, S., Ogawa, T., Fortuin, J. P. F., & Kelder, H. M. (2003). Southern Hemisphere Additional Ozonesondes (SHADOZ) 1998–2000 tropical ozone climatology 2. Tropospheric variability and the zonal wave-one. *Journal of Geophysical Research: Atmospheres*, vol. 108no. D2. https://doi.org/10.1029/2002JD002241

Thompson, A. M., Witte, J. C., Sterling, C. W., Jordan, A., Johnson, B. J., Oltmans, S. J., Fujiwara, M., Vömel, H., Allaart, M., & Piters, A. (2017). First Reprocessing of Southern Hemisphere Additional Ozonesondes (SHADOZ) Ozone Profiles (1998–2016): 2. Comparisons With Satellites and Ground-Based Instruments - Thompson - 2017 - Journal of Geophysical Research: Atmospheres - Wiley Online Library. https://doi.org/https://agupubs.onlinelibrary.wiley.com/doi/full/10.1002/2017JD027406

Trenberth, K. (2023). Nino SST Indices (Nino 1+2, 3, 3.4, 4; ONI and TNI). https://climatedataguide.ucar.edu/climate-data/nino-sst-indices-nino-12-3-34-4-oni-and-tni

UCAR, C. (n.d.). Introduction to Tropical Meteorology, Ch. 1: Introduction: Atmospheric Structure Temperature Profiles. Retrieved March 27, 2023, from https://ftp.comet.ucar.edu/memory-stick/tropical/textbook_2nd_edition/navmenu.php_tab_2_page_5.0.0.htm

Vaisala. (2019). *User guide, Ozone Sounding with Veisala Radiosonde RS41, M211486EN-E* (tech. rep.). https://www.vaisala.com/sites/default/files/documents/Ozone%20Sounding%20with%20Vaisala%20Radiosonde%20RS41%20User%27s%20Guide%20M211486EN-C.pdf

Vömel, H., & Diaz, K. (2010). Ozone sonde cell current measurements and implications for observations of near-zero ozone concentrations in the tropical upper troposphere [Publisher: Copernicus GmbH]. *Atmospheric Measurement Techniques*, vol. 3no. 2, 495–505. https://doi.org/10.5194/amt-3-495-2010

Vömel, H., Smit, H. G. J., Tarasick, D., Johnson, B., Oltmans, S. J., Selkirk, H., Thompson, A. M., Stauffer, R. M., Witte, J. C., Davies, J., van Malderen, R., Morris, G. A., Nakano, T., & Stübi, R. (2020). A new method to correct the electrochemical concentration cell (ECC) ozonesonde time response and its implications for "background current" and pump efficiency [Publisher: Copernicus GmbH]. *Atmospheric Measurement Techniques*, vol. 13no. 10, 5667–5680. https://doi.org/10.5194/amt-13-5667-2020

Wallace, J. M., & Hobbs, P. V. (2006). *Atmospheric Science (Second Edition)* (J. M. Wallace & P. V. Hobbs, Eds.). Academic Press. https://doi.org/10.1016/B978-0-12-732951-2.50006-5

Williams, J., Keßel, S., Nölscher, A., Yang, Y., Lee, Y., Yáñez-Serrano, A. M., Wolff, S., Kesselmeiner, J., Klüpfel, T., Leileveld, J., & Shao, M. (2016). Opposite OH reactivity and ozone cycles in the Amazon rainforest and megacity Beijing: Subversion of biospheric oxidant control by anthropogenic emissions - ScienceDirect. https://doi.org/https://doi.org/10.1016/j.atmosenv.2015.11.007

Witte, J. C., Thompson, A. M., Smit, H. G. J., Fujiwara, M., Posny, F., Coetzee, G. J. R., Northam, E. T., Johnson, B. J., Sterling, C. W., Mohamad, M., Ogino, S.-Y., Jordan, A., & da Silva, F. R. (2017). First reprocessing of Southern Hemisphere ADditional OZonesondes (SHADOZ) profile records (1998–2015): 1. Methodology and evaluation [_eprint: https://onlinelibrary.wiley.com/doi/pdf/10.1002/2016JD026403]. *Journal of Geophysical Research: Atmospheres*, vol. 122no. 12, 6611–6636. https://doi.org/10.1002/2016JD026403

WMO. (1957). *Annual Report of the World Meteorological Organization 1957* (tech. rep.). WMO. Geneva.

WMO. (2011). *Scientific Assessment of Ozone Depletion: 2010* (tech. rep.). Retrieved May 27, 2023, from https://library.wmo.int/index.php?id=5230&lvl=notice_display

Zell, H. (2015). Earth's Atmospheric Layers. *NASA*. https://doi.org/http://www.nasa.gov/mission_pages/sunearth/science/atmosphere-layers2.html

Zumdahl, S. S., & Zumdahl, S. A. (2013). *Chemistry*. Cengage Learning.